Trakya Üniversitesi
Mühendislik Bilimleri Dergisi

Cilt: 25 Sayı: 1 Haziran 2024

TRAKYA UNIVERSITY JOURNAL OF ENGINEERING SCIENCES

Volume: 25 Number: 1 June 2024

Trakya Univ J Eng Sci

http://dergipark.gov.tr/tujes
tujes@trakya.edu.tr

ISSN 2147-0308

Trakya Üniversitesi
Mühendislik Bilimleri Dergisi

Cilt: 25 **Sayı: 1** **Haziran** **2024**

Trakya University
Journal of Engineering Sciences

Volume: 25 **Number: 1** **June** **2024**

Trakya Univ J Eng Sci

http://dergipark.gov.tr/tujes
tujes@trakya.edu.tr

ISSN 2147-0308

ISSN 2147-0308

Dizgi / Design
Dr. Öğr. Üyesi Gökhan KOÇYİĞİT

İletişim Bilgisi / Contact Information
Address : Trakya Üniversitesi, Enstitüler Binası, Fen Bilimleri Enstitüsü, Balkan Yerleşkesi, 22030, Edirne / TÜRKİYE
Web site : http://dergipark.gov.tr/tujes E-mail : tujes@trakya.edu.tr
Tel : +90 284 2358230 Fax : +90 284 2358237

Baskı / Publisher
Trakya Üniversitesi Matbaa Tesisleri / Trakya University Publishing Centre

ISSN 2147-0308

İÇİNDEKİLER / CONTENTS

ARAŞTIRMA MAKALELERİ / RESEARCH ARTICLES

ISSN 2147-0308

Trakya University Journal of Engineering Sciences
http://dergipark.org.tr/tujes
ISSN 2147–0308

Research Article / Araştırma Makalesi
DOI : 10.59314/tujes.1404236

A MICROCONTROLLER-BASED SIGNAL GENERATOR WITH HIGH OUTPUT CURRENT

Ersoy MEVSİM[1]*, Reşat MUTLU[2]

[1]*Computer Technology Department, School of Vocational and Technical Sciences, Tekirdağ Namık Kemal University, Tekirdağ, Turkey*

[2]*Electronics and Communication Engineering Department, Çorlu Engineering Faculty, Tekirdağ Namık Kemal University, Tekirdağ, Turkey*

Makale Künye Bilgisi: Mevsim, E., Mutlu, R. (2024). A Microcontroller-based Signal Generator with High Output Current, *Trakya Üniversitesi Mühendislik Bilimleri Dergisi*. 25(1), 1-9.

Article Info

Article History:

Received:
December 13, 2023

Accepted:
April 5, 2024

Keywords:

Microcontroller-based circuit design;

Laboratory design;

Signal generation;

Direct Digital Synthesis.

Abstract

Signal generators play an important role in designing and testing circuits. These devices can supply various commonly used waveforms and can be designed using analog, digital, and Direct Digital Synthesis methods. Signal generators often have a low current output. In this paper, it is shown that a signal generator can be made using a cheap microcontroller board such as the Arduino Nano Klon V3.0 microcontroller. A power opamp TDA2030 is used to increase its output current. The signal generator can be operated up to 500 Hz Also, the signal generator can give an output current of up to 3 Amperes which is significantly higher than the ones sold in the market. The signal generator can be programmed to supply various common waveforms as well as any desired waveform considering its frequency limit.

Yüksek Çıkış Akımına Sahip Mikrodenetleyici Tabanlı Sinyal Jeneratörü

Makale Bilgileri

Makale Tarihçesi:

Geliş:
13 Aralık 2023

Kabul:
5 Nisan 2024

Anahtar Kelimeler:

Mikrodenetleyici tabanlı devre tasarımı;

Laboratuvar tasarımı;

Sinyal üretimi;

Doğrudan Sayısal Sentezleme.

Öz

Sinyal üreteçleri devrelerin tasarımında ve test edilmesinde önemli bir rol oynamaktadır. Bu cihazlar yaygın olarak kullanılan çeşitli dalga formlarını sağlayabilirler ve analog, sayısal ve doğrudan sayısal sentezleme yöntemleri ile tasarlanabilirler. Sinyal üreteçleri sıklıkla düşük akım çıkışına sahiptir. Bu makalede, Arduino Nano Klon V3.0 mikrodenetleyici gibi ucuz bir mikrodenetleyici kartı kullanılarak bir sinyal üretecinin yapılabileceği gösterilmiştir. Bu sinyal üretecinin çıkış akımını artırmak için bir güç opampı olan TDA2030 kullanılmıştır. Sinyal üreteci 500 Hz'e kadar çalıştırılabilmektedir. Ayrıca, bu sinyal üreteci, piyasada satılanlardan çok daha yüksek olan 3 Amper'e kadar çıkış akımı verebilmektedir. Sinyal üreteci, frekans limiti göz önünde bulundurularak çeşitli yaygın dalga biçimlerinin yanı sıra istenen herhangi bir dalga şeklini sağlamak üzere programlanabilir.

*Sorumlu Yazar: emevsim@nku.edu.tr

1. Introduction

Signal generators are important devices, which should be found in all electronics laboratories (Abdullah, Muhammed, Al-Helali, 2008, Electronic Signal Generators, 2023). They can be designed using analog or digital circuits (Schubert and Kim 2016, Boylestad and Nashelsky 2018). Nowadays, the Direct Digital Synthesis (DDS) Method is also commonly used to design signal generators. A digital waveform generator is presented in (Shoucheng, Aimin, and Xinke 2012). A memristor-based chaotic signal generator is made in (Arık and Kılıç 2014). An FPGA is used to make a Van der Pol-based chaotic signal generator in (Dursun and Kaşifoğlu 2018). In (Ding, An, and Gou 2012), an FPGA is used to make a digital signal generator. FPGAs are more expensive than microcontrollers. In (Gontean, Lucaciu, and Dan 2003), an SDA6000 microcontroller-based TV signal generator that can provide TV test signals is made. In (Bilgin, Üser, and Oktay 2016), a microcontroller-based Programmable Signal Generator is made with an At89s52 microcontroller providing common signals and controlled by a keypad. In (Mandaliya, Mankodi, and Makwana 2013), a PIC microcontroller is used to obtain square, sinus, and triangle waves with the DDS method. In (Castro, Olmo, Pérez, and Yúfera 2016), a sinusoidal voltage wave generator, which is based on the use of microprocessor digital signals with programmable duty cycles with application to real-time Electrical Cell-substrate Impedance Spectroscopy (ECIS) samples, is proposed. In (Hu 2014), having SCM STC89C52 and MAX038 integrated circuits and with a few peripheral devices, a function signal generator, that generates sine, square, and triangular wave signals, has been designed with adjustable frequency and amplitude. Therein, the MAX038 function generator generates the desired waveform, which then is input into the LM6361wideband voltage amplifier and a power amplifier as output. The DDS method is also used to design ECG, EEG, chaotic signal generators, and neuron emulators successfully (Yener, Barbaros, Mutlu, and Karakulak 2017, Usta, Tepeyurt, and Karakulak 2021). Microcontroller-based chaotic signal generators can be done due to the microcontroller's computing abilities and sufficiently high clock frequency. In (Yener, Barbaros, Mutlu, and Karakulak 2017), a memristive chaotic circuit is implemented using Arduino. In (Yener and Mutlu 2018), an ECG signal generator is made using the PWM output of the ARM microcontroller and experimental data. An H-R neuron model is implemented with a microcontroller to obtain its waveforms in (Yener and Mutlu 2019). A chaotic waveform source that is based on Lorenz Equations is made to obtain Lorenz variables as the outputs with a microcontroller (Yener, Mutlu, and Karakulak 2020). A hyperjerk system is emulated with a microcontroller (Karthikeyan, Çiçek, Pham, Akgül, and Duraisamy 2020). The famous Lotka-Volterra Equations are examined with a microcontroller-based signal generator in (Karakulak, Tan, and Mutlu 2021). A microcontroller-based synthetic ECG waveform generator is made in (Usta, Tepeyurt, and Karakulak 2021). An EEG Signal Generator Using Both the internal DAC and PWM Outputs of a microcontroller is made in (Karakulak 2022). An oscillator's output current is usually not very high, just in the order of milliamps [1, 3]. High-power signal generators can be designed using power electronics (Mohan, Undeland, and Robbins 2003). Power electronics design may require more time and it is more complex due to the power component devices and drivers (Çınar and Arseven 2021). Intermediate load powers or currents can be supplied with a power amplifier if the load requires it (Boylestad and Nashelsky 2018). The voltage requirement of the device in the study given in (Karakulak and Mutlu 2020) has been supplied with a power amplifier due to a voltage requirement that cannot be provided by an ordinary opamp. Such an opamp can also provide a current of 4 Amps. In this

study, it has been shown that a microcontroller-based signal generator (MBSG) with high current output can be made using a cheap microcontroller such as Arduino Nano Klon V3.0 and a Digital Analog Converter, and a power opamp TDA2030. The TDA2030 provides a cheap solution for the high current need. It can supply a current of up to 3 Amperes which is a lot higher than currents in the order of milliamperes common opamps can deliver. Accordingly, due to the high current output, the designed signal generator can provide a high current that the traditional signal generators cannot.

In this study, first, the signal waveform equations are derived, and then, the system's hardware and software are briefly explained. The signal generator's operation is verified with experiments.

The paper is arranged as follows. In the second section, it is explained how the waveforms are produced in the MBSG. In the third section, the MBSG topology is introduced. In the fourth section, the flowchart of the MBSG program is explained. In the fifth section, the experimental results of the circuit are given. The paper is finished with the conclusion section.

2. Waveform Production

In this section, it is described how to produce the waveforms.

2.1. Waveform Formulas in Continuous Time

The desired waveform equations are given in this section. Such equations can be found in related books such as (Oppenheim and Verghese 2017). A sinusoidal voltage can be expressed as

$$v(t) = V_m sin(\omega t) \tag{1}$$

where t is time, $\omega=2\pi/T$ is the angular frequency, T is the electrical period, and V_m is the maximum value of the sinusoidal voltage.

A triangular waveform can be given as

$$v(t) = \begin{cases} \frac{4V_m(t-T/2)}{T} + V_m, & 0 < t < T/2 \\ -\frac{4V_m\left(t-\frac{T}{2}\right)}{T} + V_m, & T/2 < t < T \end{cases} \tag{2}$$

where T is the electrical period and V_m is the maximum value of the triangular wave voltage.

A square waveform can be given as

$$v(t) = \begin{cases} V_p, & 0 < t < T/2 \\ -V_p, & ,T/2 < t < T \end{cases} \tag{3}$$

where T is the electrical period and V_p is the maximum value of the square wave voltage.

A Clock Pulse signal waveform can be given as

$$\boldsymbol{v(t)} = \begin{cases} \boldsymbol{V_p} & \boldsymbol{,0 < t < T_p} \\ \boldsymbol{0} & \boldsymbol{,T/2 < t < T} \end{cases} \tag{4}$$

where T_p and V_p are the length and peak value of the Clock pulse voltage, respectively.

Using the duty ratio D, the length of the pulse is calculated as

$$\boldsymbol{T_p = DT} \tag{5}$$

A sawtooth signal waveform with a rising slope can be given as

$$\boldsymbol{v[n]} = \left\{\frac{\boldsymbol{2V_p t}}{\boldsymbol{T}} - \boldsymbol{V_p}, \quad \boldsymbol{0 < t < T}\right. \tag{6}$$

where V_p is the maximum value of the sawtooth voltage.

All the waveforms are periodic, i.e.

$$\boldsymbol{v(t) = v(t+T)} \tag{7}$$

2.2. Waveform Formulas in Discrete Time

The signal waveforms are discretized in this section. A sinusoidal voltage in discrete time can be expressed as

$$\boldsymbol{v[n] = V_m sin(n\omega n T_s)} \tag{8}$$

where $v[n]$ is the nth discrete time value of the signal voltage, n is sample time, ω is the angular frequency, and V_m is the maximum value of the sinusoidal voltage.

A triangular waveform can be given as

$$\boldsymbol{v[n]} = \begin{cases} \frac{\boldsymbol{4V_m(nT_s - N/2)}}{\boldsymbol{T}} + \boldsymbol{V_m}, & \boldsymbol{0 \le n \le N/2} \\ -\frac{\boldsymbol{4V_m\left(nT_s - \frac{N}{2}\right)}}{\boldsymbol{T}} + \boldsymbol{V_m}, & \boldsymbol{\frac{N}{2} + 1 \le n \le N} \end{cases} \quad (9)$$

where $N = T/T_s$ is the electrical period in discrete time and V_m is the maximum value of the triangular wave voltage.

A square waveform can be given as

$$\boldsymbol{v[n]} = \begin{cases} \boldsymbol{V_p}, & \boldsymbol{0 \le n \le N/2} \\ \boldsymbol{-V_p}, & \boldsymbol{\frac{N}{2} + 1 \le t \le N} \end{cases} \quad (10)$$

where T is the electrical period and V_p is the maximum value of the square wave voltage.

A Clock Pulse signal waveform can be given as

$$\boldsymbol{v[n]} = \begin{cases} \boldsymbol{V_p} & \boldsymbol{0 \le n \le N_p} \\ \boldsymbol{0} & \boldsymbol{, N/2 + 1 \le t \le N} \end{cases} \quad (11)$$

where N_p is the length of the pulse in discrete time.

A sawtooth signal waveform with a rising slope can be given as

$$\boldsymbol{v[n]} = \boldsymbol{\{2V_p t/T - V_p}, \quad \boldsymbol{0 \le n \le N} \quad (12)$$

where V_p is the maximum value of the sawtooth wave voltage.

In discrete time domain, the periodicity condition is given as.

$$\boldsymbol{v[n]} = \boldsymbol{v[n + N]} \quad (13)$$

Due to the periodicity condition, the value of the desired voltage is calculated at the discrete times for a period and using a loop and/or a lookup table, the voltage values in the following periods are calculated.

3. Microcontroller-Based Signal Generator

The Proteus schematic of the MBSG circuit is shown in Figure 1. It consists of the Arduino Nano Klon V3.0 microcontroller, and a DAC, and the power opamp TDA2030. The microcontroller executes the lookup tables obtained using the method given in the previous section. The microcontroller reads the desired magnitude and frequency waveform, calculates the scaling factor, and sends the look-up table value through the digital ports to the DAC. At the output of the DAC, the desired waveform is obtained and amplified with the TDA2030. The signal at the output can be approximated as

$$\boldsymbol{v_{out}(t)} = \boldsymbol{v[n][u(t - (n+1)T_s) - u(t - nT_s)]} \quad (14)$$

where $u[n]$ is the unit step function.

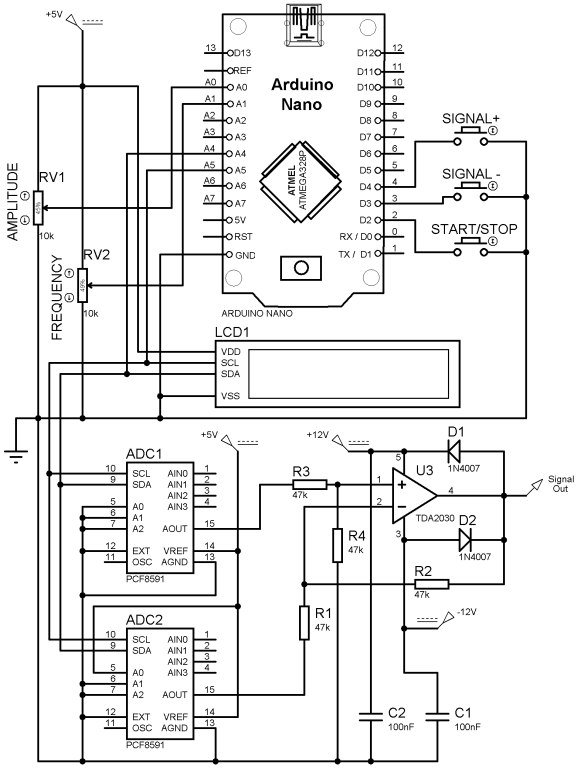

Figure 1. The circuit schematic was drawn in Proteus

4. The Circuit's Program

The microcontroller is programmed in C. The algorithm of the microcontroller program is given as the flowchart shown in Figure 2. The program takes the inputs such as which waveform is chosen. Then, the program starts calculating the discrete values of the desired waveform in a loop and keeps doing it until another waveform is chosen. When n equals N, n is reset to zero at the beginning of a new period. The

parameters required for the waveforms are adjusted by reading the ADC voltages.

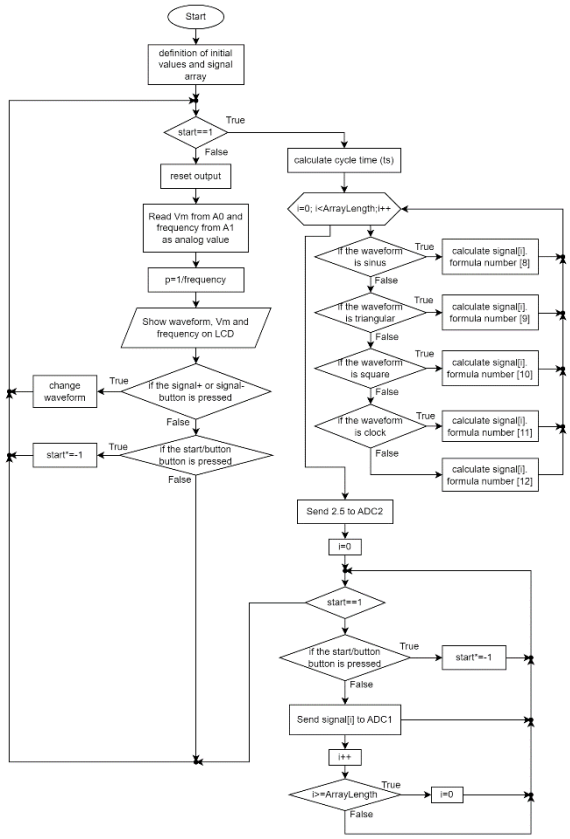

Figure 2. Flowchart of the VDPO Oscillator Program

5. Experimental Results of The Signal Generator

In this section, the experimental results of the MBSG circuit are given. The circuit whose photo is shown in Figure 3 has been assembled on a protoboard. The experimental voltage waveforms ($v_{out}(t)$) are acquired by a GW Instek GDS-1052-U 50 MHz digital oscilloscope. The experimental time domain waveforms are acquired in the periodic steady state and shown in Figures 4 and 5. The MBSG is able to produce all the waveforms up to 500 Hz and performs well. The effect of quantization on the waveforms can be seen in Figure 4. Increasing the DAC resolutions would result in decreasing the effect of quantization. At low frequencies of the output waveforms, the microcontroller can calculate more steps for the desired waveform in a period as can be seen in Figure 5. This results in smoother waveforms at lower frequencies than the ones in Figure 4.

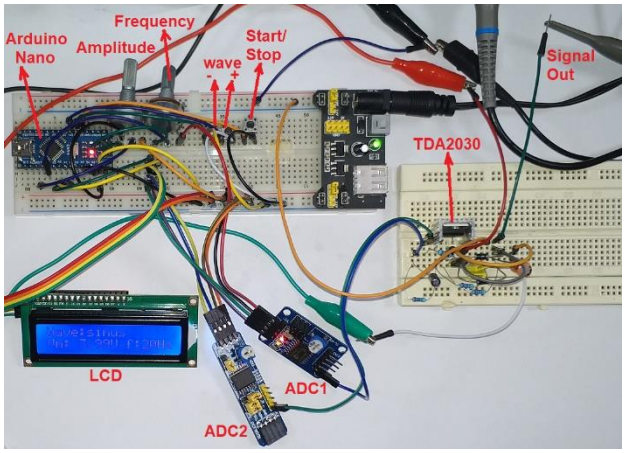

(a)

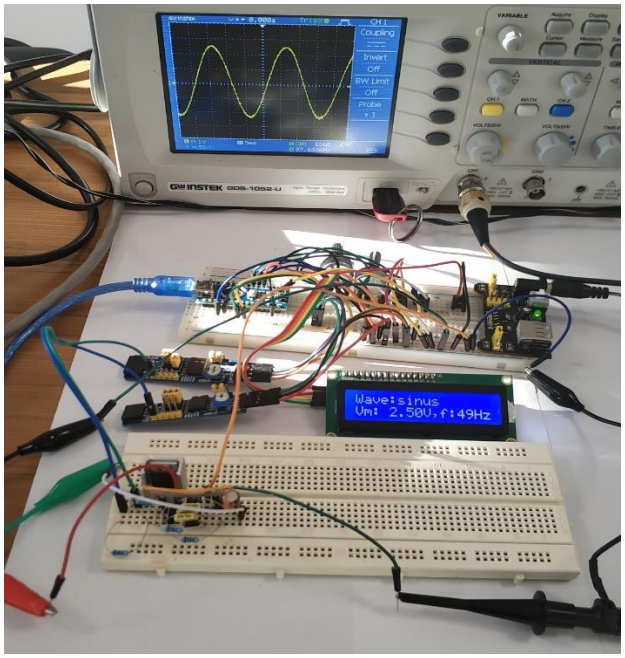

(b)

Figure 3. a) A photograph of the implemented circuit and b) The photograph taken during the mesurement of a sinusoidal signal for V_m=2.5 Volt and f=50 Hz.

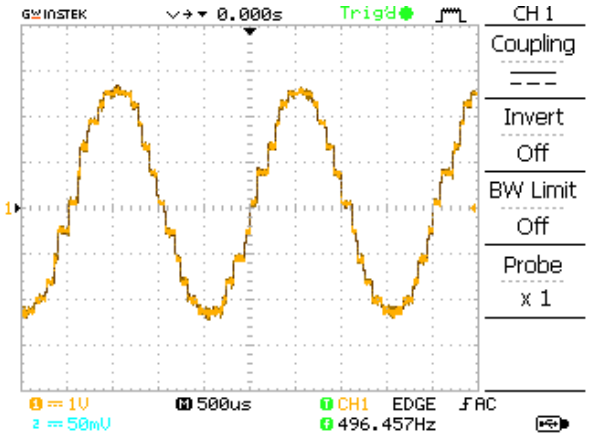

(a)

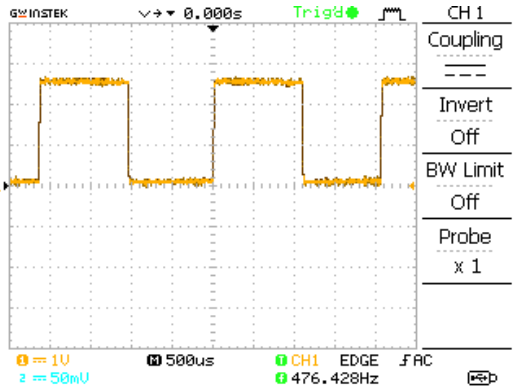

(b)

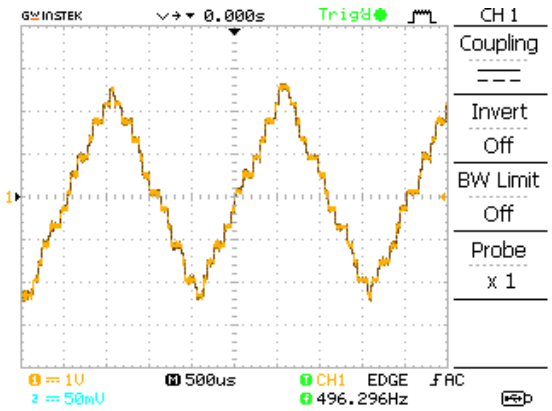

(c)

Figure 4. Experimental signal waveforms of microcontroller-based signal oscillator measured with an oscilloscope: a) a sinusoidal signal for V_m=2.5 Volt and f=499 Hz, b) a clock pulse signal for V_p=2.5 Volt and f=470 Hz, and c) a triangular waveform for V_m=2.5 Volt and f=484 Hz.

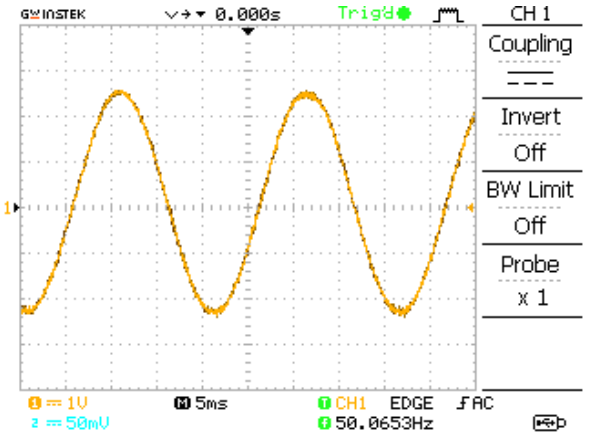

(a)

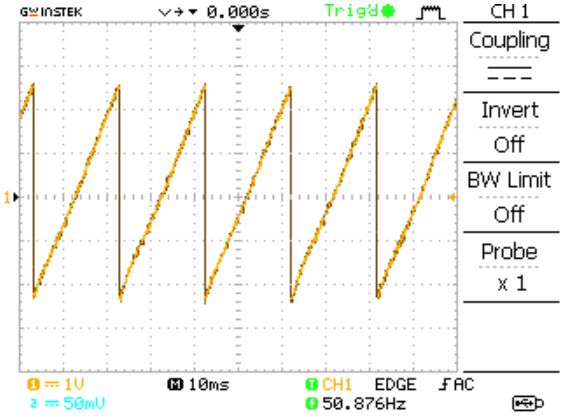

(b)

Figure 5. Experimental signal waveforms of microcontroller-based signal oscillator measured with an oscilloscope: a) a sinusoidal signal for V_m=2.5 Volt and f=50 Hz, and b) a sawtooth waveform for V_p=2.5 Volt and f=51 Hz.

5. Discussions

In the study, it has been seen that the resolution of the output voltage waveforms must be increased and this can be done using a DAC with a higher number of bits. The designed signal generator lacks an output filter and using a low-pass analog filter may help to reduce the resolution error and provide a low distorted output voltage waveform. The operation frequency of the designed signal generator was lower than that of the ones given in the introduction section. However, the output current of the designed signal generator is higher than that of the others reviewed in the introduction

section. The code of the designed signal generator can be optimized to increase its output frequency. If it is not enough, another microcontroller with a higher operation frequency can be used. Even in its current, the signal generator can be used for research and education purposes.

6. Conclusions

In this paper, a microcontroller-based high-current signal generator is designed. In this work, a cheap, rugged, easy-to-use microcontroller Arduino Nano Klon V3.0 microcontroller is preferred for this purpose. The device can supply a current of up to 3 Amperes because of having a power opamp while so many other signal generators can give a current less than 50 milliamperes. The signal generator has also its limitations defined by its electronic components. Its output current can be increased by using the power opamps in parallel if it is necessary. It can produce various waveforms. The experimental results have verified that the circuit performs well and produces waveforms with low distortion. Using a more advanced high-speed microcontroller such as ARM Microcontrollers, the signal generator that operates at higher frequencies can be made with a better performance. Also, using a better DAC with a bit number of 16 or higher, the resolution error in its output waveform can be reduced.

The device can also be programmed with new waveforms or use experimentally recorded waveforms. For example, it can also be used to produce experimentally recorded EKG waveforms done as in (Yener and Mutlu 2018) or be programmed to obtain chaotic waveforms similar to those in (Yener, Barbaros, Mutlu and Karakulak 2017, Yener, Mutlu and Karakulak 2020). In the literature, there is an increasing number of chaotic communication circuits and the signal generator can be found in usage in them. Such a circuit can also be used evaluate performance of the circuits such as fractional order filters and controllers.

The designed MBSG, which is a cheap off-the shelf solution to have a signal generator, can be used in circuit laboratories such as electronics and biomedical engineering laboratories for research and educational purposes. Also, it can be used in graduate projects. As a future work, it can also be optimized using effective programming techniques considering the hardware's specifications.

References

Arik, S., & Kilic, R. (2014). Reconfigurable hardware platform for experimental testing and verifying of memristor-based chaotic systems. Journal of Circuits, Systems, and Computers, 23(10), 1450145.

AL-Helali, R. A., Mohammed, I. A., & Abdullah, A. I. (2008). Microcontroller-based function generator. Al-Khwarizmi Engineering Journal, 4(1), 48-57.

Bilgin, S., Üser, Y., & Oktay, M. (2016). Low cost laboratory type signal generator using DDS method. International Journal of Engineering and Applied Sciences, 8(4), 59-65.

Boylestad, R. L., & Nashelsky, L. (2018). Electronic Devices and Circuit Theory 11th ed.

Castro, J. A., Olmo, A., Pérez, P., & Yúfera, A. (2016). Microcontroller-based sinusoidal voltage generation for electrical bio-impedance spectroscopy applications.

Çınar, S. M., & Arseven, B. (2021). Kısmi Gölgelenme Etkilerini Modelleyebilen Bir PV Emülatör Tasarımı. Journal of the Institute of Science and Technology, 11(2), 982-997.

Ding, Shoucheng, An, Aimin and Gou Xinke (2012). "Digital Waveform Generator Based on FPGA",

Research Journal of Applied Sciences, Engineering and Technology.

Dursun, M., Kaşifoğlu, E. (2018). "Design and implementation of the FPGA-based chaotic van der pol oscillator", International Advanced Researches and Engineering Journal, 2(3), 309-314.

Electronic Signal Generators, A Compilation, https://ntrs.nasa.gov/api/citations/19720004434/downloads/19720004434.pdf. (Access date: 01/12/2023).

Gontean, A., Lucaciu, L., & Dan, B. (2003). Microcontroller Based Programmable Signal Generator. IFAC Proceedings Volumes, 36(1), 105-108.

Hu, H. (2014). Design of a Functional Signal Generator based on MAX038 and Microcontroller. In Advanced Materials Research (Vol. 915, pp. 1167-1170). Trans Tech Publications Ltd.

Karakulak, E., Tan, R. K., & Mutlu, R. (2021). STM32F429 Discovery Board-Based Emulator for Lotka-Volterra Equations. Journal of the Institute of Science and Technology, 11(3), 1887-1895.

Karakulak, E (2022). ARM MCU-Based Experimental EEG Signal Generator Using Internal DAC and PWM Outputs. Gazi University Journal of Science, 1-1.

Karakulak, E., & Mutlu, R. (2020). The memristive system behavior of a diac. Journal of Computational Electronics, 19(3), 1344-1355.

Karthikeyan, R., Çiçek, S., Pham, V. T., Akgul, A., & Duraisamy, P. (2020). A class of unexcited hyperjerk systems with megastability and its analog and microcontroller-based embedded system design. Physica Scripta, 95(5), 055214.

Mandaliya, H., Mankodi, P., & Makwana, B. (2013). Microcontroller based DDS function generator. International Journal of Engineering Science and Innovative Technology (IJESIT), 2(1), 483-486.

Mohan, N., Undeland, T. M., & Robbins, W. P. (2003). Power electronics: converters, applications, and design. John wiley & sons.

Rahma, Fadhil (2014). "Analog Programmable Electronic Circuit-based Chaotic Lorentz System." Basrah Journal for Engineering Science14.1: 39-47.

Schubert Jr, T. F., & Kim, E. M. (2016). Fundamentals of electronics: Book 4 oscillators and advanced electronics topics. Synthesis Lectures on Digital Circuits and Systems, 11(2), 1-266.

Usta, B. N., Tepeyurt, B., & Karakulak, E. (2021). Simple Synthetic ECG Generation via PWM Output of Microcontroller. In 2021 5th International Symposium on Multidisciplinary Studies and Innovative Technologies (ISMSIT) (pp. 27-30). IEEE.

Yener, S. C., Barbaros, C., Mutlu, R., & Karakulak, E. (2017). Implementation of Microcontroller-Based Memristive Chaotic Circuit. Acta Physica Polonica A, 132(3), 1058-1061.

Yener, Ş.Ç., and Mutlu, Reşat (2018). "A microcontroller-based ECG signal generator design utilizing microcontroller PWM output and experimental ECG data." 2018 Electric Electronics, Computer Science, Biomedical Engineerings' Meeting (EBBT). IEEE.

Yener, Ş. Ç., & Mutlu, R. (2019). A Microcontroller Implementation Of Hindmarsh-Rose Neuron Model-Based Biological Central Pattern Generator. In 2019 1st International Informatics

and Software Engineering Conference (UBMYK) (pp. 1-4). IEEE.

Yener, Ş. Ç., Mutlu. R., & Karakulak. E. (2020). Implementation of a Microcontroller-Based Chaotic Circuit of Lorenz Equations. Balkan Journal of Electrical and Computer Engineering, 8(4), 355-360.

Oppenheim, A. V., & Verghese, G. C. (2017). Signals, systems & inference. London: Pearson.

Trakya University Journal of Engineering Sciences
http://dergipark.org.tr/tujes
ISSN 2147–0308

Research Article / Araştırma Makalesi
DOI : 10.59314/tujes.1432057

ASSESSING THE RELATIONSHIP BETWEEN COLOR CHANGE AND TENSILE STRENGTH IN THERMOPLASTIC POLYOLEFIN OUTER SHEATHS OF LOW-VOLTAGE POWER CABLES

Metin YURTSEVER[1], Avşin ÖZTAŞ[2], Reşat MUTLU[3*]

[1,2]*Unika Cable, Çerkezköy, Tekirdağ, Türkiye*
[3*]*Electronics and Communication Engineering Department, Çorlu Engineering Faculty, Tekirdağ Namık Kemal University, Çorlu, Tekirdağ, Türkiye*

Makale Künye Bilgisi: Yurtsever, M., Öztaş A., Mutlu, R. (2024). Assessing the Relationship between Color Change and Tensile Strength in Thermoplastic Polyolefin Outer Sheaths of Low-Voltage Power Cables, *Trakya Üniversitesi Mühendislik Bilimleri Dergisi*. 25(1), 11-19.

Article Info	**Abstract**
Article History: Received: February 5, 2024 Accepted: June 24, 2024 **Keywords:** Power Cables; Ultraviolet; UV Test; Cable Tests; Gray Scale Color Test; Insulation.	Power cables used outdoors age prematurely due to ultraviolet radiation. The mechanical strength of the cables may decrease and the color of the outer sheath of cable insulation changes when exposed to outdoor UV radiation. It is of great concern to know how the elongation strength of a cable varies with the exposure time to prevent cable break. The determination of the color of the cable insulator is also an important part of UV tests. In this study, Thermoplastic Polyolefin (TPO) insulation to be used in the outer sheath of low-voltage power cables is aged in a test chamber. 240-, 480-, and 720-hour test durations are chosen in the experiments. It has been found that the color change of TPO does not reflect the elongation at break and tensile strength value changes much and the elongation at break value of TPO is not a monotonous function of UV exposure time.

Alçak Gerilim Güç Kablolarının Dış Kılıfında Kullanılan Termoplastik Poliolefinin Renk Değişimi ile Gerilme Direnci Arasındaki İlişkinin Değerlendirilmesi

Makale Bilgileri	**Öz**
Makale Tarihçesi: Geliş: 5 Şubat 2024 Kabul: 24 Haziran 2024 **Anahtar Kelimeler:** Güç Kabloları; Ultraviyole; UV Testi; Kablo Testleri; Gri Tonlama Renk Testi; Yalıtım.	Açık havada kullanılan güç kabloları morötesi radyasyon nedeniyle erken yaşlanır. Dış mekânda mor ötesi ışınlarına maruz kaldığında kabloların mekanik mukavemeti azalabilir ve kablonun dış kablo kılıfının rengi değişir. Kablo kopmasını önlemek için bir kablonun uzama mukavemetinin maruz kalma süresine göre nasıl değiştiğini bilmek büyük önem taşımaktadır. Kablonun yalıtkanının renginin belirlenmesi UV testlerinin önemli bir parçasıdır. Bu çalışmada alçak gerilim güç kablolarının kılıfında kullanılacak Termoplastik Poliolefin (TPO) yalıtkanının bir test odasında yaşlandırılması yapılmıştır. Deneylerde 240, 480 ve 720 saatlik test süreleri seçilmiştir. TPO'nun renk değişiminin kopma uzamasını ve gerilme direncinin değişimini fazla yansıtmadığı ve Kopma uzamasının morötesi maruziyet zamanının monoton bir fonksiyonu olmadığı ve tespit edilmiştir.

[*]**Sorumlu Yazar: rmutlu@nku.edu.tr**

1. Introduction

The cable insulations age when exposed to heavy thermal, electrical, environmental, chemical, and mechanical stresses (Thue, 2017, Dang et al., 1996, Shwehdi et al., 2003). Reviews of electrical insulation aging models can be found in the literature (Dang et al., 1996, Choudhary et al., 2022). Insulators of outdoor power cables are exposed to sunlight, ultraviolet, (UV) light, and humidity and that's why the power cables used outdoors age quickly (Arora et al., 2004, Karhan M., 2021, İlhan et al., 2004). UV test chambers are commonly made to examine their mechanical and electrical behaviors (Zhu et al., 2023). Xenon light test chambers are expensive but they can emulate sunlight and UV exposure very well, and that's why they are commonly used in aging experiments (Hedir et al. 2016). In this test, a UV chamber, which was illuminated artificially with a Xenon light lamp (Liu et al., 2021, Pandey, 2008), is used to age the insulators for a predetermined amount of duration described with standards such as IEEE 1580:2021 and UL 2556 (IEEE 1580-2021, 2021, UL 2556, 2021). The aged insulator pieces are cut as dump bells, they are aged in the chamber, and, then, their electrical and mechanical strength is tested (Hedir et al., 2020, Alghamdi et al., 2020, Shwehdi et al., 2003). Elongation at break is one of the commonly made mechanical tests (Alghamdi et al., 2020, Tan et al, 2023). Exposure to sunlight or such an artificial lamp also causes the insulator to change its color (Amin et al., 2011). A gray scale is used to determine the unaged and aged insulators' colors. Thermoplastic polyolefin (TPO) insulation is used in low-voltage power cables (Amin et al., 2011, Ismail et al., 2018). The mechanism of polyolefin photodegradation has been reported (Guillet, 1980). Geussens (2021) has provided a review on it. Degradation studies of polyolefins incorporating transparent nanoparticulate zinc oxide UV stabilizers were conducted by (Ammala et al., 2002). The reactions causing degradation during weathering and photo-oxidation of polyolefins are reviewed comprehensively (Grause et al., 2020). To the best of our knowledge, there are not any studies examining the time-dependent relationship between color change and the mechanical strength of TPO material. This study aims to determine whether the color change implies the mechanical strength of the aged TPO material or not. For this purpose, thermoplastic polyolefin dump-bell pieces are aged in a Q-SUN Xenon light test chamber for three different test durations determined according to UL 2556 (IEEE 1580-2021, 2021), the tensile strength and Elongation at Break values of the unaged and the aged TPO samples are measured as described in UL 2556 (UL 2556, 2021), and their colors are defined using a gray scale tool (Bide, 2010).

2. Material and Method

2.1 UV Ageing Test of the Thermoplastic Polyolefin

The explanation of the experimental procedure of the Ultra Violet test is presented in IEEE 1580:2021 (IEEE 1580-2021, 2021). The flowchart of the test process is presented in Figure 1. The endpoint of the test properties for Thermoplastic polyolefin material is selected as 80 % Elongation at break and Tensile strength in this study whose monitoring is made according to the standard IEEE 1580:2021 (IEEE 1580-2021, 2021).

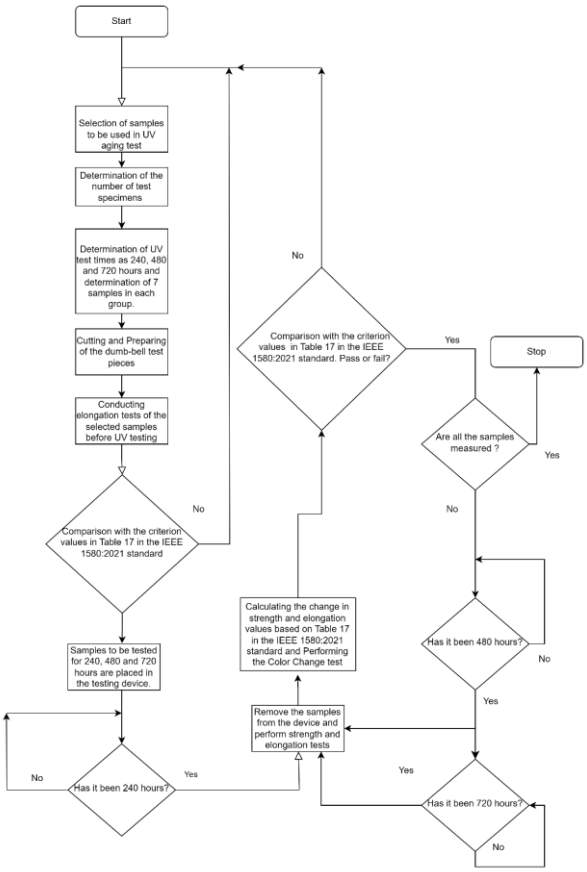

Figure 1. The flowchart of the UV aging experiment

The exposure durations are selected according to standard IEEE 1580-2021 (IEEE 1580:2021, 2021).

12]. Dumb-bell test pieces are prepared with dimensions according to Standard IEC 60811-501 as seen in Figure 2 (IEC 60811-501, 2011).

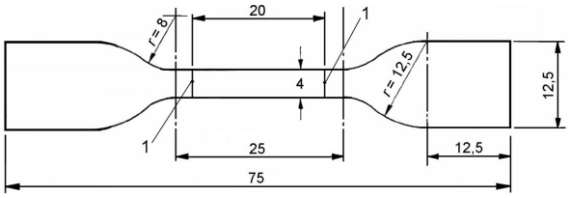

Figure 2. Dimensions of the Dumb-bell test pieces prepared according to Standard IEC 60811-501 (IEC 60811-501, 2011).

2.2. Experimental Results

Thermoplastic polyolefin used in the experiments is made with raw material produced by Avient. The thermoplastic polyolefin dumb-bell pieces are cut with a tensile testing machine and are shown in the photograph given in Figure 3. A total of 28 dumbbell samples were used in the experiments. The Q-SUN Xenon light test chamber used in the tests can be seen in Figure 4 (Q-SUN Xenon light test chamber). The dumb-bell pieces are placed in the Q-SUN Xenon light test chamber as shown in Figure 5.

Figure 3. The thermoplastic polyolefin dumb-bell pieces prepared.

Figure 4. The Q-SUN Xenon light test chamber used for the UV aging test.

Figure 5. The thermoplastic polyolefin dumb-bell test pieces placement in the Q-SUN Xenon light test chamber.

The prepared samples or dumb-bell pieces should be tested for the specified time in the Xenon-arc test

chambers, providing that the pH of the water is between 4.5-8.0 and surfaces exposed to the light source should not be polished, stripped, or planed. Impression marks should be applied after conditioning. For comparison purposes, the unaged samples are also prepared in the same manner. Each cycle of the Xenon-Arc apparatus consists of 102 minutes of lighting and 18 minutes of lighting besides water spraying. The samples should be properly mounted in the Xenon-arc apparatus according to the manufacturer's instructions. Following the exposure, the samples are maintained in the testing apparatus and stagnant air under ambient room temperature conditions for not less than 16 hours and not more than 96 hours at atmospheric pressure. The dumbbell samples were tested in a UV tester according to UL2556 standard with reference to ASTM G155 Cycle 1 method (ASTM G155, 2021). After the UV exposure, a photograph of the aged pieces is shown in Figure 6. In general, it has been observed in UV experiments that the strength of the material increases and elongation decreases at the same temperature and after an aging time defined in the standard. This is the case for HFFR (Halogen Free, Flame Retardant) materials.

(a)

(b)

Figure 6. The Dumb-bell Test Pieces a) Before UV Aging Test and b) After a 720 h UV Aging Test

The elongation at break and Tensile strength tests were performed according to international standard IEC 60811-501. A Zwick/Roell Z010 10kN ProLine machine is used for this purpose. and a photo taken during an elongation at break test is shown in Figure 7. A photograph taken during the evaluation of the test results of the broken thermoplastic polyolefin pieces is shown in Figure 8. The average value of the measurement results obtained from each experiment is used to evaluate the experimental results. The average values of the elongation at break and the tensile strength obtained with the UV exposure test and the UV exposure times are presented in Table 1.

Figure 7. The elongation at break test with a Zwick/Roell Z010 10kN ProLine 739384.

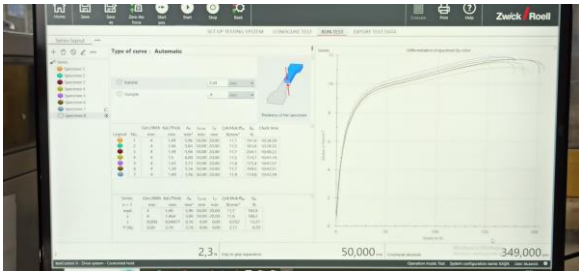

Figure 8. The screen of the Zwick/Roell machine interface program showing the test results of the thermoplastic polyolefin dumb-bell pieces after the tensile strength test.

The tool known as gray scale is based on 5 major and 4 intermediate step gradations and is used to visually evaluate and compare the color loss of a sample. The rating consists of matches of gray swatches, from 5 best to 1 poorest. Each pairing shows the difference in shade between a tested sample and a control sample corresponding to a numbered rating. The gray scale tool shown in Figure 9 is used to evaluate the colors of the test pieces. The color of the samples after being tested in the UV chamber for 240, 480, and 720 hours can be seen in Figure 10. The color of the material has varied from dark gray to light gray. The assessed color codes can be found in Table 1.

Figure 9. The gray scale tool used in this study.

Table 1. Test Results

Test Duration or Exposure Time (h)	0	240	480	720
Tensile Strength (N/mm2)	11.47	11.69	12.52	15.35
Elongation at Break (%)	204.25	183.85	162.38	165.76
Grayscale color code	5	4/5	4	3/4

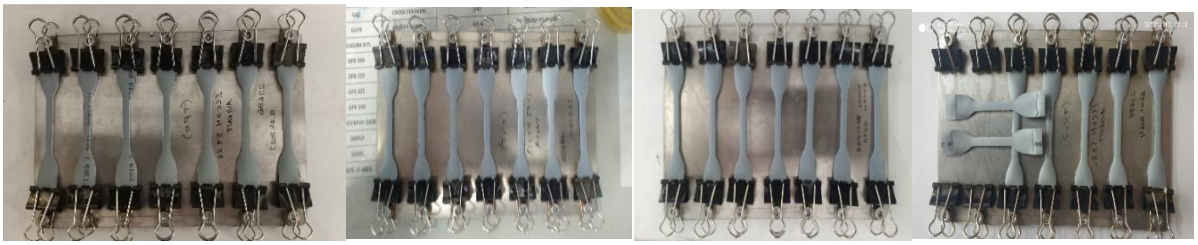

(a) (b) (c) (d)

Figure 10. Appearance changes of the dumb-bell test pieces with a UV exposure time of a) 0 h (unaged), b) 240 h, c) 480 h, and d) 720 h.

3. Results and Discussion

The elongation at break and Tensile strength values of the samples are shown in Figure 11. The elongation at break has decreased by %18,84 and the tensile strength has only increased by %33,83 after the UV exposure. This indicates that UV exposure increases the tensile strength and the color change does not always indicate the mechanical strength loss. Considering the experimental exposure times, the tensile strength increases monotonously. However, the elongation at break with respect to exposure time decreases first and starts increasing again. It is found that the elongation at break as a function of exposure time can be expressed as the following cubic polynomial:

$$\varepsilon = a_3 t^3 + a_2 t^3 + a_1 t + a_0 \quad (1)$$

where ε is the elongation at break and t is the exposure time.

The parameters of the polynomial of the curve fitted elongation at break are found as $a_1 = -0.046771$, $a_2 - 0.00023429$, $a_3 = 3.125\text{e} - 07$, and $a_0 = 204.25$. Norm of residuals of the elongation at break function is pretty low and equal to 1.3024e-13.

The tensile strength as a function of exposure time can be expressed as the following cubic polynomial:

$$\sigma = p_3 t^3 + p_2 t^3 + p_1 t + p_0 \quad (2)$$

where σ is the tensile strength.

The parameters of the polynomial of the curve fitted tensile strength are calculated as $p_1 = 0.0015764$, $p_2 = -6.7708\text{e} - 06$, $p_3 = 1.6758\text{e} - 08$, and $p_0 = 11.47$. Norm of residuals of the tensile strength function is pretty low and equal to 8.1403e-15.

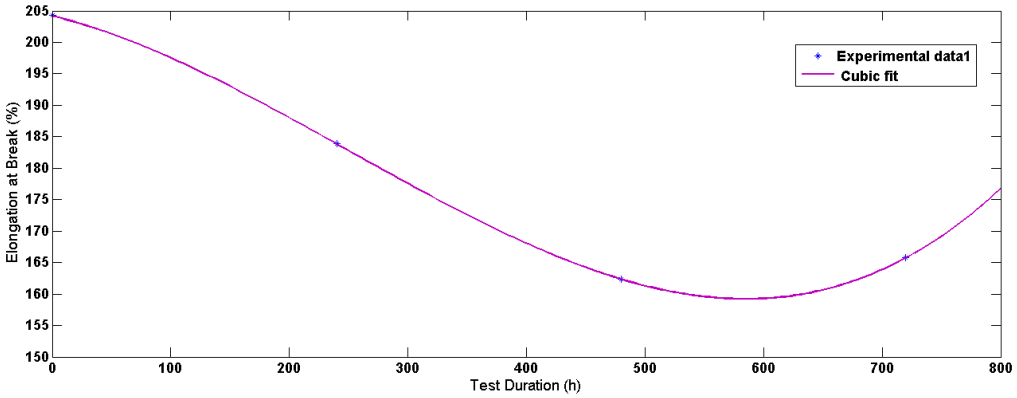

(a)

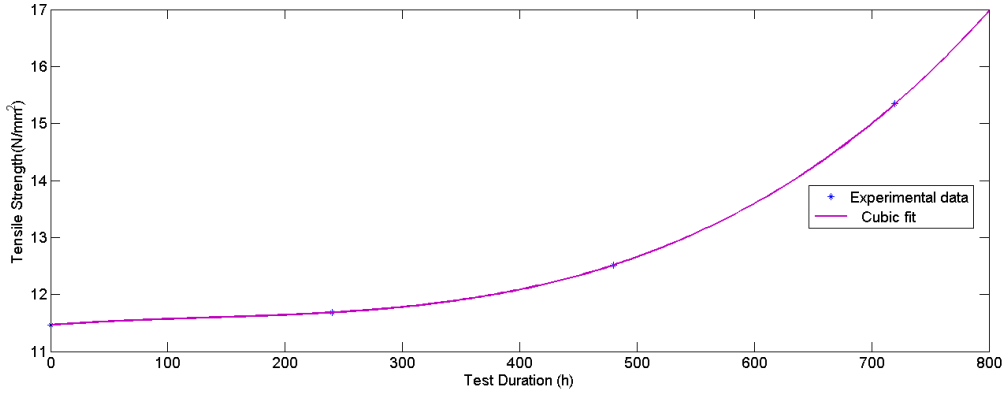

(b)

Figure 11. Effect of Accelerated ageing on a) Elongation at break and b) Tensile strength of the Thermoplastic Polyolefin İnsulator pieces prepared.

4. Conclusion

UV radiation can induce color changes on the surface or within polymers, and its impact on mechanical strength has been explored in the literature (Harris, R. M., 1999). Some studies indicate that prolonged UV exposure can adversely affect mechanical properties, leading to reductions in tensile strength and increased material brittleness (Lu et al., 2018). However, other research highlights the complexity of directly linking color changes caused by UV radiation to mechanical

strength. Color changes often occur on the polymer surface or in superficial layers, whereas mechanical strength largely depends on the material's internal structure and chemical composition. Therefore, surface color changes may not necessarily correlate with significant impacts on mechanical strength (Wypych, 2020).

In this study, a UV aging test of thermoplastic polyolefin polymer to be used in a low-voltage power cable is made according to UL 2556. It has been shown that UV exposure whitens thermoplastic polyolefin polymer, the surface of the thermoplastic polyolefin polymer material under investigation changes color in the first step of aging and then remains almost unchanged in the later stages of aging, and the color of the material has changed from dark gray to light gray. Considering the values of the elongation at break and the tensile strength, the elongation at break's value has dropped by %18.84 and the tensile strength's value has increased by %33.83, suggesting an enhancement in the material's mechanical strength at the end of the UV aging test. While not all polymers exhibit increased tensile strength upon UV exposure, thermoplastic polyolefin polymer does. The effect depends on the specific polymer composition, additives, and the presence of crosslinking agents or functional groups that can participate in UV-induced crosslinking reactions (Wypych, 2020). UV exposure increasing the tensile strength of thermoplastic polyolefin polymer can be attributed to UV-induced crosslinking, where UV light initiates chemical reactions leading to the formation of crosslinks between polymer chains, thereby strengthening the material over time.

The results of the tests show that color change due to aging does not indicate a tensile strength loss for thermoplastic polyolefin polymer. It is also interesting that Elongation at break for thermoplastic polyolefin polymer is not a monotonous function of exposure time. These experimental results may mean that it is possible to use the thermoplastic polyolefin polymer in low-voltage outdoor power cables which are exposed to considerably more UV light than indoor cables. Also, the color change of polyolefin polymer does not mean the tensile strength loss since it is monotonously increasing, and a decrease in Elongation at break since it first falls and starts increasing again concerning the experimental exposure times in this study. These results underscore the importance of understanding the specific composition and additives within polymers used in outdoor power cables, as well as their susceptibility to UV-induced reactions. The findings from this study provide valuable insights for the development and selection of materials that are resilient to UV degradation, particularly in applications requiring prolonged outdoor exposure.

Author Contributions

Formal analysis –Reşat Mutlu (RM), Metin Yurtsever (MY); Investigation – RM, MY; Experiments – Avşin Öztaş (AÖ); Processing – MY, RM, AÖ; Literature review – RM, MY, AÖ; Writing –RM, AÖ, Review and editing – RM, MY, AÖ.

Declaration of Competing Interest

The authors declared no conflicts of interest concerning the research, authorship, and/or publication of this article.

Acknowledgments

This study has been supported through the project UPN-2206 funded by the research and development center of Ünika Üniversal Kablo Sanayi ve Tic. A.Ş. The researchers are thankful to Kaan Önder and Fatih Yerişenoglu for their assistance.

References

Alghamdi, A. S., & Desuqi, R. K. (2020). A study of expected lifetime of XLPE insulation cables working at elevated temperatures by applying accelerated thermal ageing. *Heliyon*, *6*(1).

Amin, S., & Amin, M. (2011). Thermoplastic elastomeric (TPE) materials and their use in outdoor electrical insulation. *Rev. Adv. Mater. Sci*, *29*(1), 15-30.

Ammala, A., Hill, A. J., Meakin, P., Pas, S. J., & Turney, T. W. (2002). Degradation studies of polyolefins incorporating transparent nanoparticulate zinc oxide UV stabilizers. *Journal of Nanoparticle Research*, *4*(1), 167-174.

Arora, R., & Tripathi, V. (2004, September). Effect of ultra violet irradiation on low voltage cable insulation. In *Conference Record of the 2004 IEEE International Symposium on Electrical Insulation* (pp. 358-361). IEEE.

Bide, M. (2010). Colour measurement and fastness assessment. In *Colour Measurement* (pp. 196-217). Woodhead Publishing.

Choudhary, M., Shafiq, M., Kiitam, I., Hussain, A., Palu, I., & Taklaja, P. (2022). A review of aging models for electrical insulation in power cables. *Energies*, *15*(9), 3408.

Dang, C., Parpal, J. L., & Crine, J. P. (1996). Electrical aging of extruded dielectric cables: review of existing theories and data. *IEEE transactions on dielectrics and electrical insulation*, *3*(2), 237-247.

Geussens, T. (2021). Thermoplastics for cables. *The Global Cable Industry: Materials, Markets, Products*, 21-55.

Grause, G., Chien, M. F., & Inoue, C. (2020). Changes during the weathering of polyolefins. *Polymer degradation and stability*, *181*, 109364.

Guillet, J. E. (1980). Studies of the mechanism of polyolefin photodegradation. *Pure and Applied Chemistry 19th*, *52*(2), 285-294.

Harris, R. M. (1999). *Coloring technology for plastics*. William Andrew.

Hedir, A., & Moudoud, M. (2016). Effect of ultraviolet radiations on medium and high voltage cables insulation properties. *International Journal of Engineering and Technology*, *8*(5), 2308-2317.

Hedir, A., Bechouche, A., Moudoud, M., Teguar, M., Lamrous, O., & Rondot, S. (2020). Experimental and predicted XLPE cable insulation properties under UVRadiation. *Turkish Journal of Electrical Engineering and Computer Sciences*, *28*(3), 1763-1775.

İlhan, S., & Özdemir, A. (2004, December) Elektriksel Yalıtım Sistemlerinde Yaşlanma, Yaşlanma Modelleri Ve İstatistiksel Veri Analizi, In *Elektrik-Elektronik Ve Bilgisayar Mühendisliği Sempozyumu ELECO 2004 (ELECO 2004).*

International Standard. (2011). IEC 60811- 501. *Electric and Optical Fibre Cables – Test Methods for Non-metallic Materials - Part 501: Mechanical Tests – Tests for Determining the Mechanical Properties of Insulating and Sheathing Compounds*, IEC Central Office. https://webstore.iec.ch/publication/3551. Retrieved 03.02.2021.

Ismail, N. H., & Mustapha, M. (2018). A review of thermoplastic elastomeric nanocomposites for high voltage insulation applications. *Polymer Engineering & Science*, *58*(S1), E36-E63.

Karhan, M. (2021). Dielektrik Malzemelerin Yüzeyleri için Islanabilirlik ve Buharlaşma Hızının Analizine Yönelik Ayrık Kosinüs Dönüşümü Tabanlı Bir Yaklaşım. *Gazi Mühendislik Bilimleri Dergisi*, *7*(2), 160-168.

Liu, G., Ning, J., Gu, Z., & Wang, Z. (2021, March). Stability Test on Power Supply to the Xenon

Lamp of Solar Simulator. In *Journal of Physics: Conference Series* (Vol. 1820, No. 1, p. 012142). IOP Publishing.

Lu, T., Solis-Ramos, E., Yi, Y., & Kumosa, M. (2018). UV degradation model for polymers and polymer matrix composites. *Polymer degradation and stability*, *154*, 203-210.

Pandey, K. K., & Vuorinen, T. (2008). Comparative study of photodegradation of wood by a UV laser and a xenon light source. *Polymer Degradation and Stability*, *93*(12), 2138-2146.

Q-SUN Xenon light test chamber Model Xe-1 / https://www.q-lab.com/tr-tr/products/q-sun-xenon-arc-test-chambers/, Retrieved 03.02.2021.

Shwehdi, M. H., Morsy, M. A., & Abugurain, A. (2003, October). Thermal aging tests on XLPE and PVC cable insulation materials of Saudi Arabia. In *2003 Annual Report Conference on Electrical Insulation and Dielectric Phenomena* (pp. 176-180). IEEE.

Standard, A. (2005). *ASTM Standard G155 standard practice for operating xenon arc light Apparatus for exposure of non-metallic materials*. ASTM International. https://cdn.standards.iteh.ai/samples/42608/1e37cd07634b4c579d12b3b1d4ad376a/ASTM-G155-05.pdf. Retrieved 03.02.2021.

Standard, IEEE. (2021). IEEE 1580-2021. *IEEE Recommended Practice for Marine Cable for Use on Shipboard and Fixed or Floating Facilities*. IEEE. https://standards.ieee.org/ieee/1580/7228/, Retrieved 03.02.2021.

Standard, UL. (2021). *UL 2556 UL Standard for Safety Wire and Cable Test Methods*, Underwriters Laboratories Inc. (UL), 5th Edition. https://global.ihs.com/doc_detail.cfm?document_name=UL%202556&item_s_key=00467382, Retrieved 03.02.2021.

Tan, R. K., Önder, K., Yerişenoğlu, F., & Mutlu, R. (2023). Usage of an Excel Spreadsheet for a Thermal Endurance Test Report. *European Journal of Engineering and Applied Sciences*, *6*(2), 91-97.

Thue, W. A. (2017). *Electrical power cable engineering* (Vol. 1). Crc Press.

Wypych, G. (Ed.). (2020). *Handbook of UV degradation and stabilization*. Elsevier.

Zhu, J., Jin, L., & Li, C. (2023, October). Research and design of a wireless calibration device for measuring irradiance in solar aging test chambers. In *Fifth International Conference on Artificial Intelligence and Computer Science (AICS 2023)* (Vol. 12803, pp. 573-577). SPIE.

Trakya University Journal of Engineering Sciences
http://dergipark.org.tr/tujes
ISSN 2147–0308

Research Article / Araştırma Makalesi
DOI : 10.59314/tujes.1464575

EFFICIENT SOIL MOISTURE MONITORING WITHOUT IN-SITU PROBES: LSTM-BASED BLUETOOTH SIGNAL STRENGTHS ANALYSIS

Selçuk YAZAR[1]*, Deniz TAŞKIN[2], Erdem BAHAR[3]

[1]*Kirklareli Üniversitesi, Mühendislik Fakültesi Yazilim Mühendsiliği Bölümü*
[2]*Trakya Üniversitesi, Mühendislik Fakültesi Bilgisayar Mühendisliği Bölümü*
[3]*T.C. Tarim ve Orman Bakanliği, Gelibolu İlçe Müdürlüğü*

Makale Künye Bilgisi: Yazar, S., Taşkın, D., Bahar, E. (2022). Efficient Soil Moisture Monitoring Without In-Situ Probes: Lstm-Based Bluetooth Signal Strengths Analysis, *Trakya Üniversitesi Mühendislik Bilimleri Dergisi*, 25(1), 21-38.

Highlights

- Monitoring soil moisture levels by tracking changes in Bluetooth signal strength over time, eliminating the need for in-situ probes or specialised sensors.
- Utilising artificial intelligence techniques from the LSTM architecture, this research achieves a remarkable level of accuracy in predicting soil moisture content changes.
- This study presents a method that enables the use of Bluetooth signals, traditionally used in wireless communication, as a means to non-invasively measure soil moisture content.

Article Info

Article History:
Received:
April 11, 2023
Accepted:
July 18, 2023

Keywords:
Bluetooth Low Energy;
Active microwaves;
Long Short-Term Memory;
Deep learning;
Soil moisture.

Abstract

Measuring soil moisture without damaging the soil structure is important in agriculture. Electrical conductivity and microwaves are widely used for this purpose. Recently, there has been increasing interest in using artificial neural networks and time series forecasts to determine soil moisture content. This study investigates the possibility of determining soil moisture content, especially for soil samples with different pH values, using neural network architecture and Bluetooth signal power values with a transmission power of 0.001 Watt. The aim is to assess the soil moisture change state directly using Bluetooth signal levels without an in-situ probe. In an experimental study, a machine learning model based on Bluetooth signal strengths from alkaline soil samples was used to estimate the soil moisture content change with a root-mean-square error of 15%. This method eliminates the need for a dedicated sensor, as soil moisture can be measured reliably by monitoring signal level changes over time.

Yerinde Problar Olmadan Etkili Toprak Nemi İzleme: LSTM Tabanlı Bluetooth Sinyal Gücü Analizi

Makale Bilgileri

Makale Tarihçesi:
Geliş:
11 Nisan 2023
Kabul:
18 Temmuz 2023

Anahtar Kelimeler:
Bluetooth Düşük Enerji;
Derin öğrenme;
Uzun-Kısa Süreli Bellek;
Aktif mikrodalgalar;
Toprak nemi

Öz

Toprak yapısına zarar vermeden toprak nemi ölçümü tarımda önemlidir. Elektriksel iletkenlik ve mikrodalgalar bu amaçla yaygın olarak kullanılmaktadır. Son zamanlarda, toprak nem içeriğini belirlemek için yapay sinir ağları ve zaman serisi tahminlerinin kullanılmasına olan ilgi artmaktadır. Bu çalışmada, bir yapay sinir ağı mimarisi ve 0,001 Watt iletim gücüne sahip Bluetooth sinyal güç değerleri kullanılarak, özellikle farklı pH değerlerine sahip toprak örnekleri için toprak nem içeriğinin belirlenme olasılığı araştırılmaktadır. Amaç, toprak nem değişim durumunu yerinde bir prob olmadan doğrudan Bluetooth sinyal seviyelerini kullanarak değerlendirmektir. Yapılan deneysel bir çalışmada, alkali toprak örneklerinden elde edilen Bluetooth sinyal güçlerine dayalı bir yapay öğrenme modeli kullanılarak toprak nem içeriği değişimi %15'lik bir kök-ortalama-kare hata (RMSE) değeri ile tahmin edilmiştir. Bu yöntem, toprak nemi zaman içindeki sinyal seviyesi değişiklikleri izlenerek güvenilir bir şekilde ölçülebildiğinden, özel bir sensör ihtiyacını ortadan kaldırmaktadır.

*Sorumlu Yazar: selcukyazar@klu.edu.tr

1. Introduction

Soil moisture retrieval methods which are frequently used today to measure the amount of water in the soil is a critical element that should be known mainly in agricultural production. In addition to agricultural production, the amount of water in the soil is important information for hydrological applications, disaster prediction, and environmental monitoring. There are many remote and proximal detection methods for calculating this value. All these measurement techniques used today have been developed primarily considering the chemical and physical properties of the soil. Different variables, including vegetation, need to be taken into account to determine the moisture content of the soil. Characterization and monitoring of soil characteristics are necessary to perform site-specific farming practices that are important for matching human activities with local environmental requirements.

Measuring the water content has a great interest in many disciplines, especially in porous environments such as soil. Although gravimetric sampling is the best way to measure the water content in the soil, samples must be removed from a soil mass. The methods used in the '50s and '60s to measure soil water content were mostly radioactive (Gardner and Kirkham 1952; Reginato and Bavel 1964). These methods were quite accurate and harmful to the soil; however, they required special care to avoid calibration and potential health hazards for each soil sample. A novel and innovative technique for quantifying the moisture content in soil without causing any damage or alteration was devised by employing Time Domain Reflectometry (TDR) as the primary means of measurement (Davis and Chudobiak 1975). TDR determines the dielectric constant of an object using simple electrodes placed on the sample in which moisture content is to be measured (Topp et al. 1980) proposed an empirical relationship between the dielectric constant of the soils with various tissues and the volumetric water content. One advantage of TDR is that the water content and collective electrical conductivity of the soil are measured simultaneously with a single probe. The methods which are used to determine the hydrological properties of the soil are in two main titles. Reference sampling methods or TDR at small scales such as (0.1 m) passive microwave radiometry or active radar method used in large scales such as (> 10 m and 100 m) (Lambot et al. 2010).

Small-scale techniques are often invasive, sometimes require drilling holes, and they may not represent soil characteristics on a management scale. Electrical drilling of the soil, which is an invasive method, can be done with conventional geoelectric or electromagnetic induction techniques (Carriere et al. 2021). However, the electrical conductivity of the soil is highly variable depending on the water content, water salinity, texture, and structure at the same time (Noborio 2001). For large-scale techniques, the characterization in the measured area is limited with the first few centimeters of soil and the temporal resolution is relatively poor. Non-invasive field scale techniques are required for applications involving agricultural water management, soil and water conservation, and to close the existing scale gap between ground accuracy measurements and remote sensing.

One of the most often measured soil parameters is soil reaction, or pH, which has an impact on a variety of chemical, biological, and physicochemical soil processes. Nutrient availability, root development, microbial activity, mineral solubility, and adsorption phenomena are a few examples of these activities. Despite how simple it is to measure a pH meter's output; it can be challenging to ascertain the true pH of the soil or soil solution. Because it influences many chemical and microbiological activities as well as plant growth, soil pH is a crucial factor. Valdez et al. show that it is crucial to understand that pH is a dynamic variable that is influenced by a variety of

circumstances. In irrigated soils and soils that experience wetting and drying in natural ecosystems, significant fluctuations in pH are expected to happen throughout wetting/drying cycles (Zarate-Valdez, 2006). Cycles of wet and dry weather are likely to cause changes in the pH of the soil. Some other articles (Gascho, Parker, Gaines,1996; Scheberl et al., 2019) shows a relationship with pH value and soil moisture. In those papers for all soil textures and moisture contents, it was discovered that the glass electrode sensors could measure soil pH very precisely and substantially. The relationship between some specific water solutions and soil pH levels was statistically determined.

Outside of the traditional methods used for measurement, a variety of machine learning techniques, such as the K-neighbors Regressor (KNR), Random Forest Regressor (RFR), Gradient Boosting (GB), Multi-layer Perceptron Regressor (MLPR), and Stochastic Gradient Descent Regressor (SGDR), have shown to be very beneficial for assessing soil moisture content. In a paper (Manfreda et al, 2023), the authors examined accurate global surface soil moisture (SSM) data, which is vital for hydrological and climatological needs. Machine learning (ML) techniques using various data sources were used to estimate daily SSM. Eight ML algorithms and ten ensemble models were tested. Gradient Boosting (GB), Multi-layer Perceptron Regressor (MLPR), Stochastic Gradient Descent Regressor (SGDR) and RFR showed promise in multiple climates. In particular, ensemble models combining KNR, RFR, and XB have demonstrated their potential in water management and crop yield forecasting by improving forecast accuracy.

Some other research (Pekel, 2020) discusses the development of a hybrid method that combines particle swarm optimization (PSO) and artificial neural network (ANN) for estimating soil moisture (SM) in different parameters such as air temperature, time, relative humidity, and soil temperature. The PSO algorithm is used to change the weights of the ANN in order to optimize the estimation process. The proposed hybrid PSO-ANN method shows promise in accurately estimating soil moisture, which can have implications for agriculture and climate research.

Furthermore, several Artificial Neural Networks (ANN) (Zonghan 2023; Singh and Gaurav 2023; Luo et al. 2023; Mu et al. 2022; Batchu et al. 2023) are commonly used inversion techniques for soil moisture retrieval. In the literature, several studies have been done using machine-learning-based inversion models. For instance (Ma et al. 2023) proposed a soil moisture prediction neural network guided by the water transport driving mechanism, which reduced the need for large datasets and training capability while achieving high accuracy. (Singh and Gaurav 2023) developed a fully connected feed-forward artificial neural network model to estimate surface soil moisture using satellite images, outperforming other machine learning algorithms. (Luo et al. 2023) introduced a back propagation neural network model to determine the relationship between characteristic bands/indices and soil moisture measurements, achieving high accuracy and applicability. (Mu et al. 2022) developed a nonlinear Erf-BP neural network method using multiple-resource remote-sensing data, which improved the accuracy of soil moisture estimation compared to linear models. (Batchu et al., 2023) developed a deep learning convolutional-regression model that estimated soil moisture using various predictors, achieving high correlation and accuracy.

The aim of this study is the possibility of determine soil moisture content using Long Short-Term Memory (LSTM) neural network architecture and Bluetooth Low Energy (BLE) signal strengths with a maximum transmission power of 1 mW. Here, the pH values of soil samples have been used as distinctive features. Our study will contribute to soil moisture detection by

presenting a novel technique based on neural networks with satisfactory efficiency. With our method, we have shown that the moisture of the soil can be measured directly with BLE signals without using a special sensor.

2. Material and Method

2.1 Microwave Sensing

Microwaves are now frequently employed to study the structure of objects in a variety of domains, including astronomy and food (Martin et al. 2022). Energy is reflected, transmitted, or absorbed by the substance when microwaves are directed at it. Microwaves also scatter in soil and rocks due to various factors such as roughness, water content, polarization, and angle of incidence. These three types of energy ratios are referred to as material properties (Nguyen and S. Songsermpong 2022). The fundamental variables that describe how materials interact with electromagnetic fields like microwaves are dielectric constant and permeability. Diverse frequency regions of a material's dielectric profile are studied. The dielectric constant of materials can be measured at microwave frequencies using a variety of non-resonance and resonant techniques, such as transmission lines, free space, coaxial probes, and cavities. The permeability of microwaves in soil measurements has been discovered to be influenced by several factors. These factors include not only frequency, but also density, water content, sampling depth, mineral composition, grain size distribution, porosity, boundary conditions, vegetation canopies, and geographical conditions. Some of these parameters, especially the last few have very typical features. Remote measurements with microwaves can be grouped as active and passive microwave remote sensing. Images of some devices used in active and passive microwave soil water moisture measurements are shown in Figure1.

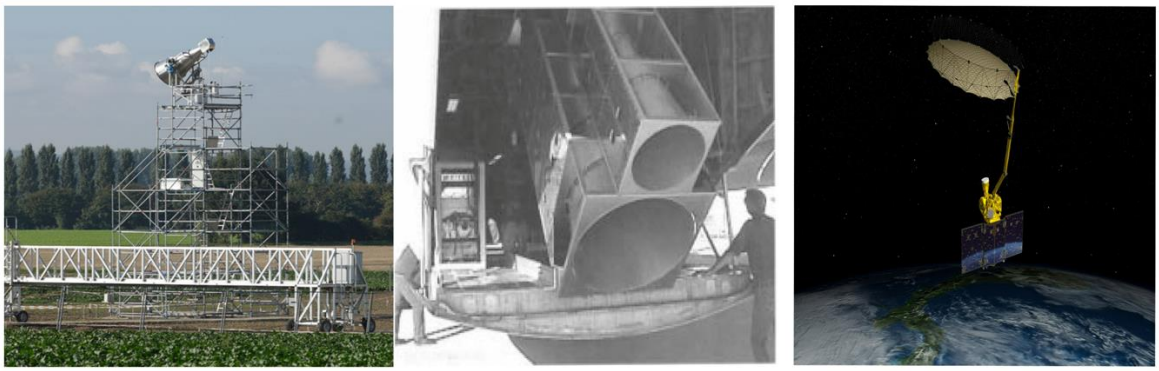

(a) (b) (c)

Figure 1. (a, b). Passive microwave sensors at performing at sites, (c) SMAP satellite launch in January 2015, for both active and passive microwave earth sensing.2.2 Dielectric measurements

Dielectric permeability is a measure of the change in the electric charge distribution caused by the electric field applied to any material. It is often expressed in relation to free space and for these reasons, it is called as complex relative permeability and is expressed as ε_r. ε_r describes the behavior of the material in the electric field as shown in Equation 1. The value shown as ε_r' in the same equation is called the dielectric constant. The second part, ε_r'', is called the loss factor. The value of ε_r varies between 2.5 for dry soil and 25 for very moist soil (Newman 1964).

$$\varepsilon_r = \varepsilon_r' - j\varepsilon_r'' \quad (1)$$

In addition, these properties differ accordingly soil density and texture. The ε_r value in Eq.(1) affects variables such as the grain size of the soil and water content in the spaces between them. The sand and clay content of the soil should also add more empirical expressions to dielectric constant.

The loss factor represents the loss of electric field energy in the material, whereas the dielectric constant represents a material's capacity to hold electrical energy. The loss tangent, as described in equation (2), is another widely used parameter. It is the ratio of the loss factor to the dielectric constant.

$$\tan\delta = {\varepsilon_r''}\Big/{\varepsilon_r'} \qquad (2)$$

Soil as a general definition can be defined as the main material in which land plants grow in the world, providing a natural environment. In the process of soil formation, it is subjected to climatic and genetic changes, and as a result, an altered material emerges with the effects of micro and macro-organisms. The content of this material is effective to a particular extent in determining its properties.

Microwaves, which are used to determine the moisture properties of the soil, can penetrate the vegetation and soil deeply. For dry vegetation and dry soil, microwave penetration

depth is larger. With an increase in vegetation and soil moisture content, penetration declines. The power of the waves will weaken as they travel through the soil due to this characteristic of microwaves. This is brought on by the dry material's variable dielectric constant in the presence of water. At ambient temperature, pure water has a dielectric constant of between 80 and 1 GHz (Calla 2002). Therefore, by computing the soil's dielectric constant using these microwave properties, the moisture content in the soil can be determined. The electromagnetic (EM) properties of the soil are impacted not only by frequency dependence but also by the dependency on density and water content. Surface soil moisture, which is an important component especially in drought studies and agricultural activities, is the water content of the top 10 cm of the soil (Dong et al. 2016). Knowing the moisture value at this depth provides the necessary information in the decision-making stages for the studies to be carried out.

2.3 Long-Short Term Memory

For many learning issues involving sequential input, recurrent neural networks with long short-term memory (LSTM) have proven to be an efficient and scalable solution. LSTM was originally designed by Hochreiter and Schmidhuber in 1997 (Hochreiter and Schmidhuber 1997). Deep learning techniques have led to the recent rediscovery of this kind of neural network. Many conventional methods for deep learning can be replaced with LSTM-based neural networks, which excel at predicting and categorizing temporal sequences. A memory cell with the ability to maintain its status over time and nonlinear door units that control the flow of information into and out of the cell make up the core of the LSTM architecture. The three different types of gates found in each LSTM block the input gate, output gate, and forget gate perform writing, reading, and resetting to the cell memory, respectively. These gates are not binary, but they are analogical (usually mapped in [0, 1], representing 0 total inhibition and 1 total activation) are managed by a sigmoidal activation function.

These gates make it possible for LSTM cells to retain information indefinitely. The cell keeps its prior state if the input gate protects it on the activation threshold, and if the current state is activated, it is coupled with the entry value. The output gate determines whether or not the value in the cell will be carried out, while the forget gate, as the name suggests, resets the present state of the cell when its value is cleared to 0.

All repetitive neural networks have the shape of a chain of the network's repetitive modules. This repeating module in conventional RNNs has a fairly straightforward structure similar to a single tanh layer. Although the repeated module of LSTMs also has a chain-like structure, it is structured differently. Four layers interact in a highly unique way instead of just one, like in a neural network. Figure 2 depicts a typical LSTM cell's general structure.

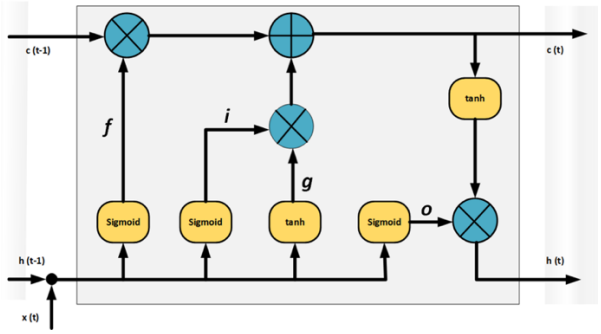

Figure 2: Sample diagram of standard LSTM cell and contents

The line shown above Figure 2 is c, which indicates the status of an LSTM cell and represents the internal memory of the unit. The technique that works around the gradient problem of LSTM is the hidden state, and it uses the i, f, o, and g gates. The parameters for these gates are learned by the LSTM during the recurrent neural network's training. i, f, and o are the input, forget, and output gates in Figure 2. The same equations are used to calculate them, but with different parameter matrices. The output vector is utilized to specify how much of the second vector can travel through the first since the sigmoid function modulates the output of these gates between zero and one. During this process, another vector can multiply the output element. Briefly, we can explain how LSTM works as follows.

The forget-gate equation (3) defines how much of the previous case h (t-1) you want to pass.

$$f = \sigma\left(W_f h_{t-1} + U_f x_t\right) \quad (3)$$

The input gate, an essential component within the architecture of a recurrent neural network, determines the degree to which the recently computed state for the present entry x(t) shall be considered, while the exit output, another crucial element, denotes the extent of the internal state that one desires to exhibit to the subsequent layer in the network.

$$i = \sigma(W_i h_{t-1} + U_i x_t) \quad (4)$$

$$o = \sigma(W_o h_{t-1} + U_o x_t) \quad (5)$$

The internal hidden state g shown in Figure 2 is calculated based on the current entry x (t) and the previously hidden state h (t-1).

$$g = tanh\left(W_g h_{t-1} + U_g x_t\right) \quad (6)$$

Equation (6) is the same as the SimpleRNN cell used in recurrent neural network methods, but in this case, its output is modulated by the output of the input gate i. Considering i, f, o and g, the cell state at any time t are expressed in c (t). Here, c(t) value can be calculated as the sum of c(t-1) multiplied by forget-gate and g value multiplied by input-gate during the training of the neural network in equation (7).

$$c_t = (c_{t-1} \otimes f) \oplus (g \otimes i) \quad (7)$$

This method is essentially a technique for merging the significance of the preceding memory and the fresh input when it comes to the learning process of the network. By assigning a value of 0 to the forget-gate, the previous memory is disregarded, while setting the input-gate to 0 results in the disregard of the newly computed state. Ultimately, the hidden-state h(t) at any given time t is obtained through the multiplication of the memory value c (t) by the output-gate.

$$h_t = \tanh(c_t) \otimes o \quad (8)$$

On the other hand, LSTMs are effective in catching long-term temporal dependencies in general. Optimization problems encountered in Simple Recurrent Networks (SRN) (Gao et al. 2020; Allen-Zhu, Li, and Song 2019) do not appear here, and thanks to these features, they have provided new approaches to solve many difficult problems. Some of these problems can be listed as handwriting recognition and production (Carbune et al. 2019; Paul et al. 2019; Ren and Ganapathy 2019), language modeling and translation (Adate and Tripathy 2019), speech acoustic modeling (Zia and Zahid 2019), speech synthesis (Hanzlíček, Vít, and Tihelka 2019), protein secondary structure prediction (Hu et al. 2019), the analysis of audio (Ertam 2019) and video data (Hussain et al. 2019), indoor based location (Zhang, Qu, and Wang 2020).

2.4 Bi-directional LSTM and Gated Recurrent Unit

In general behavior, RNN's are unidirectional and move along the directions of the original time series data. However, in some applications, capturing ordered information in reversed series greatly improves prediction. RNN structures like this that use both forward and backward pass-through improves the ability of the network to capture memory over long ranges and are called bi-directional (Schuster and Paliwal 1997). Bi-directional LSTM also acts on the time series with the same logic.

The so-called gated recurrent unit (GRU) method is quite similar to LSTM, and compared to LSTM, which has three gates, the GRU has only two processing gates. It does not have the output gate and internal memory found in LSTM. The update gate in the GRU determines how the previous memory is combined with the available memory and combines the functionality achieved by the LSTM's input and forget gates. Combining the effect of the previous memory with the effect of the current input, the reset gate is applied directly to the previous memory. Despite a few differences in how memory is transmitted across the data series within the time series, the gate mechanisms in both LSTM and GRU aim to learn long-range dependencies in the data. On the other hand, GRU has the advantage of less trainable weights compared to LSTM. Tuning model hyperparameters, such as the dimensionality of hidden units, improves the predictions of both. GRU has more advantages in situations with less training data as it requires fewer trainable weights (Cho et al. 2014).

2.4 Bluetooth Low Energy

Bluetooth Low Energy (BLE), commercially known as Bluetooth Smart which, is a low power wireless technology evolves for short-range communication. BLE operates on the 2.4 GHz Industrial Scientific Medicine (ISM) band. Since the main feature of BLE technology is lower power consumption, it is very suitable for systems running on small batteries (Darroudi, Caldera-Sànchez, and Gomez 2019). That is the reason why devices operating on BLE have the ability to utilize a coin cell as a source of power and function continuously for many years. The advantageous attributes of BLE, including its low power consumption and economical cost, render it an optimal selection for sensor devices that require power sensitivity. Furthermore, BLE can be seamlessly integrated into a diverse range of applications, such as efficient monitoring of environmental and health conditions (Ghori, Wan, and Sodhy 2019; Al Mamun and Yuce 2019; Wu, Wu, and Yuce 2019), smart home automation (Ali and Ali 2019), indoor localization (Nagarajan et al. 2020), as well as labeling and services based on proximity. It is also used in combination with other close-range communication protocols such as Near Field Communication (NFC) or RFID (Wang et al. 2019). In BLE applications, multiple BLE slave devices known as advertisers can be connected to the master BLE devices known as scanners.

There are three class devices in BLE with radio transmission power specified as 100mW (20dBm), 2.5mW (4dBm) and 1mW (0dBm). For Class 3 devices with 0dBm radio transmission power, the communication range exceeds 10 meters, and for 20dBm, the communication range exceeds 100 meters. Bluetooth power classes shown in Table 1.

Table 1: Bluetooth power classes.

Power Class	Maximum Output Power (mW)	Range (m)
1	100	100
2	2.5	15
3	1	10

In this study, the signals produced by the simple advertiser BLE beacon device were used. The devices that used are in the 3rd power class and their transmitter power is maximum 1mW.

2.4 Soil Samples Preparation

The soil samples used in this study were prepared in the laboratories of Kırklareli Agricultural Research Institute. Soil samples were prepared for analysis by drying, beating and sieving and their reactions were examined using purified water. The pH determination method here is based on potentiometric measurement of the amount of hydrogen ions in the medium created by mixing the soil with deionized purified water using a pH meter. No measurements were made for moisture during soil sample preparation but moisture measurements made during experiment. Soil samples were prepared at the institute, brought to the laboratory of Trakya University for the experiments and the measurement system was installed there.

3. Experiment

During this study, we used soil samples with pH values of 4.47, 5.31, 6.64, and 7.52 to determine the soil water content. We did not make a special selection study for properties such as texture, hardness except pH value that can be found in soil samples. We placed beacons with Texas Instruments CC2541 BLE chip in plastic containers where we put soil samples. We placed the transmitting devices at a depth of 15 cm and in the horizontal plane. Beacon devices that we use BLE chips have antennas in the "inverted F" format and produce an approximately spherical electromagnetic field. The BLE receiver is the BLE receiver on the RaspberryPi card. We recorded the Received Signal Strength Indicator (RSSI) values of beacons at 15 seconds intervals, to a database over the network with a scanner application running on Raspberry Pi device. Soil samples and plastic containers are shown in Figure 3.

In our experiment, for 8 weeks, we added 200 ml of water to each soil sample with the different pH properties on Mondays. We assumed that all soil samples were found in the same atmospheric conditions since the containers with the samples were open-mouthed. During this process, we constantly recorded the values of Beacon devices.

BLE receiver software is developed by Python with pyBluez, the Python port of the Bluez protocol stack, and the basic Python libraries, which transform each BLE node into a container based virtual nodes. The Python port of the Bluez protocol stack is preferred due to its flexibility and ease of use in implementing Bluetooth-based systems. Additionally, the Bluez protocol stack, offers direct access to the Host Controller Interface (HCI) layer, reducing overhead from higher layers and enabling efficient data transfer operations. The Python application scans and receives RSSI information from beacon devices.

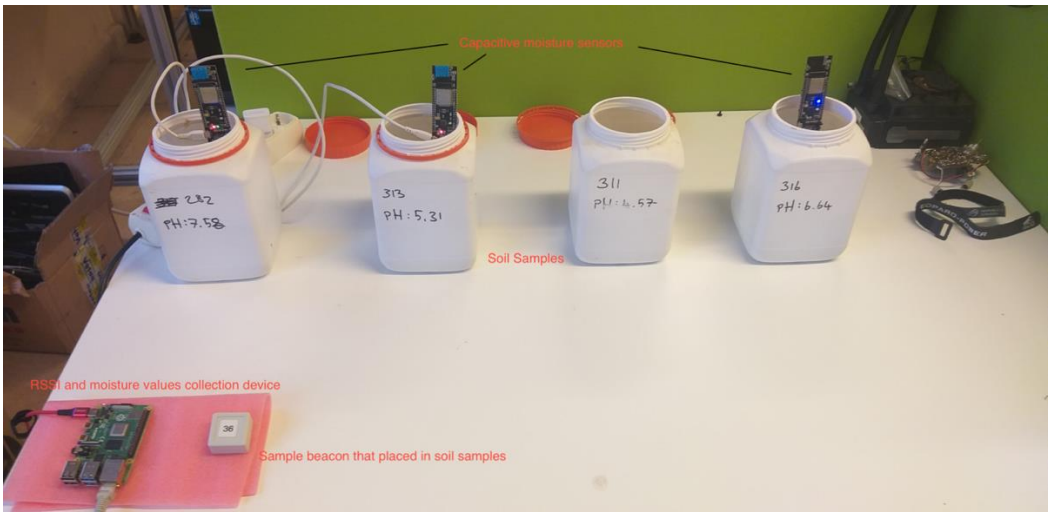

Figure 3: Setup of sample soils for BLE for RSSI and moisture values collecting.

4. Results and Discussion

First, we reduced the signal strength data we collected in our experiment to 30 minutes intervals. We reduced the number of data we collected at intervals of 15 seconds to a reasonable level. Before creating the artificial intelligence model for the collected RSSI data, we examined the mean values of this information according to the days of the week. The mean values we obtained are shown in Table 2.

Table 2: Table of calculated mean values of daily measurements based on the pH value of the soil samples.

Weekdays / Means of RSSI values	pH 4.47	pH 5.31	pH 6.64	pH 7.52
1	-80.997520	-79.096771	-73.359802	-80.034737
2	-80.539352	-80.437500	-76.238426	-82.134262
3	-79.851852	-81.171295	-75.680557	-82.004631
4	-78.689812	-80.858795	-72.793983	-80.821762
5	-78.392250	-78.968521	-72.450363	-79.595642
6	-77.174477	-79.648438	-71.059898	-80.125000
7	-79.463539	-79.473961	-70.554688	-78.958336

When we examine the data in Table 2, we found that the rate of change of RSSI values based on days of the week is closer to each other in alkali soil samples. To see this result better, we graphically analyzed the mean values we obtained. The results are shown in Figure 4. According to the results shown in Figure 4, we have seen that the means of RSSI values are close to each other as the pH value of the soil samples increases. When we pay particular attention to the graphics (c) and (d), we observed a similar change in RSSI levels from the first day of the week when we added water to soil samples with pH 6.64 and pH 7.52. This shows that in our experiment, we can use BLE signals to estimate soil moisture value/level.

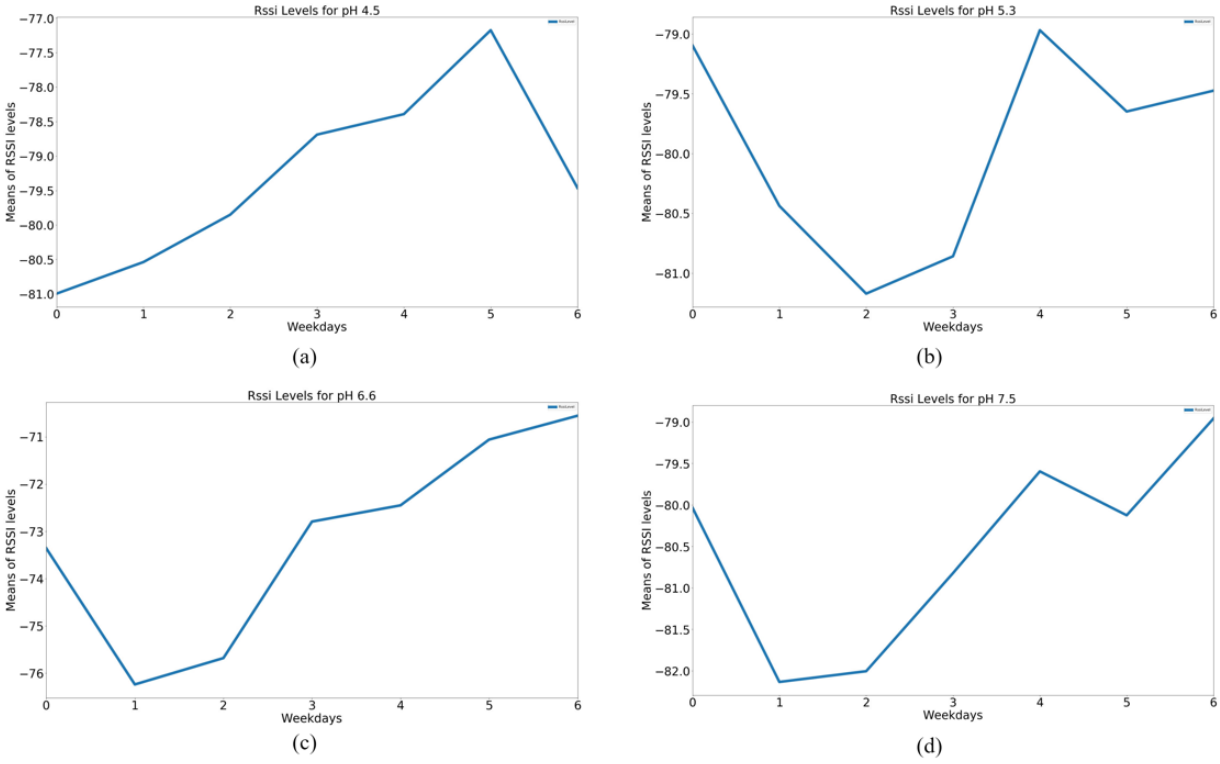

Figure 4: (a) RSSI levels for pH 4.5 daily manner, (b) RSSI levels for pH 5.3 daily manner, (c) RSSI levels for pH 6.6 daily manner, (d) RSSI levels for pH 7.5 daily manner, Graphs showing the change of RSSI levels of all soil samples on days of the week (0:Monday, 6:Sunday).

We aimed to develop an artificial neural network model where we can estimate the RSSI values here based on time, especially since we observed the gradual change in the soil at pH 7.52. While creating the artificial neural network, we chose to send the time-bound BLE signals to the 1D convolution layer before sending them to the LSTM cells for higher performance. One dimensional convolution artificial neural network layer is used especially in time series analysis. In our studies, we have achieved the most successful result of the prediction models we have created to find the lowest RMSE value for four different pH soil samples, thanks to the model shown in Figure 5.

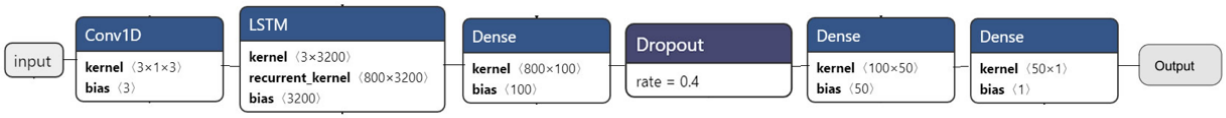

Figure 5: Artificial Neural Network model for predicting for RSSI values.

In the model we have developed, there are 800 time steps in the LSTM layer we feed after the first convolution layer. In this study, the total data set size that we use for the training of the neural network is 2880 BLE signal data. The filter that we set here as 1x3x1, is moved by a stride of the one-time unit over the on data set. Thus, 1 x 3 feature maps are created. The rest of the time steps are calculated similarly. We used an approach equivalent to the third degree autoregressive model training using a 1 x 3 convolution filter. We also added a 40% drop out layer to our model to prevent over-fitting of training data. This style of approach produces features on short-term subsets of time series. Progress of filter shown in Figure 6.

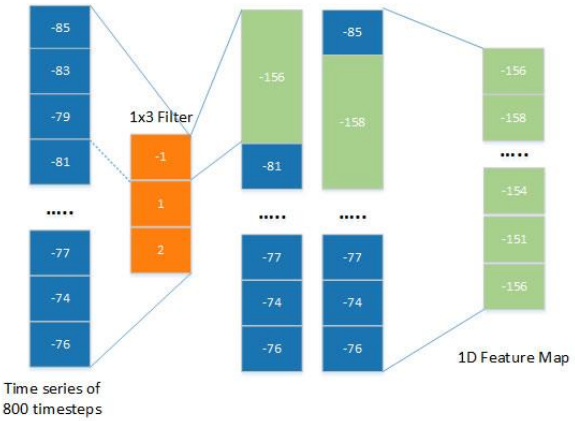

Figure 6: Illustration of 1D convolution.

In the LSTM layer, we preferred hyperbolic tangent (tanh) as the activation function. We used the 3200-dimensional vector we obtained from the LSTM layer to feed 100, 50 and 1 dimensional fully connected layers, respectively. In this way, we tried to predict BLE signal strength values we obtained with 30 minutes intervals. By running this model for 100 epochs, we compared the results for all different pH values. In the model training, no significant change was observed for more than 100 epochs, and to avoid overfitting, an optimum number of 100 was found to be appropriate. A lower value was found to be insufficient considering the frequency of signal recording.

During the training of the artificial neural network, we used the Mean squared Error function for the loss function and the adaptive momentum (ADAM) approach to optimize the Loss function. We also set the value of batch size to 256. The training and prediction results of the soil sample at pH 7.52 with the lowest RMSE value we obtained are shown in Figure 7. As seen here, even though the train and predict values of our artificial intelligence model do not fully capture the signal levels, we have seen that the RSSI values are close to the peak values generated over time with a certain offset difference.

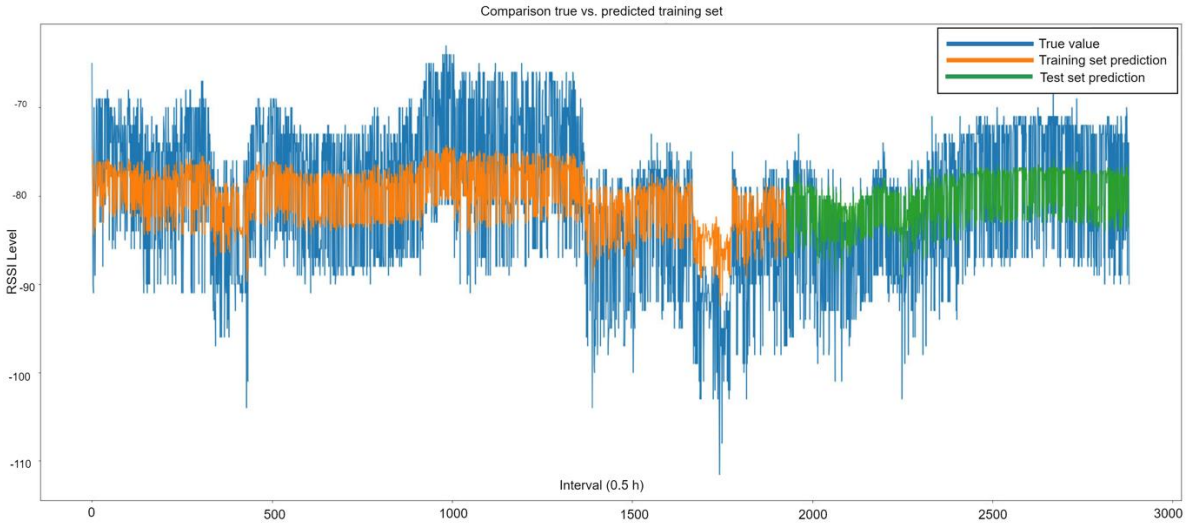

Figure 7: Best train and prediction results for pH 7.52 soil sample

Also, as seen in Figure 7, there is a technical artifact that we think our dataset originates in measurement devices between 1500 –2000 values. However, this distortion did not make any difference to the mean values we calculated at the signal levels. The model results that we obtained for all different pH values are shown in Table 3. Considering the results in Table 3, it is seen that the GRU and the Bi-directional LSTM methods give very good results in soils at the acidity limit. But the other values in the table also show that the method used works well.

Table 3: RMSE results for all soil samples with other LSTM types

Soil pH value	RMSE value with LSTM	RMSE value with GRU	RMSE value with Bi-directional LSTM
4.47	8.42	8.61	8.59
5.31	8.12	7.75	7.79
6.64	8.75	8.82	8.73
7.52	8.01	0.15	0.20

Another metric used in regression estimation such as LSTM is the R2 value. R2, also known as the coefficient of determination, is a statistical measure of the proportion of variance in the dependent variable that can be estimated from the independent variables in a regression model. R2 is a scale-free score, meaning that its value is always less than one, regardless of how big or tiny the values are. The calculation of R2 is shown in equation (9).

$$R^2 = 1 - \frac{\sum(y_i - \hat{y})}{\sum(y_i - \bar{y})} \qquad (9)$$

Table 4 shows the R2 values of the measured RSSI values. Again, the highest and consistent values were obtained in the alkaline soil sample, confirming the RMSE results. In terms of R2 and RMSE relationship, the prediction made with GRU unit for the sample with a pH value of 7.52 fits the data better than other models.

Table 4: R2 results for all soil samples with other LSTM types

Soil pH value	R^2 value with LSTM	R^2 value with GRU	R^2 value with Bi-directional LSTM
4.47	0.06432	0.08620	0.086182
5.31	0.04050	0.04041	0.04048
6.64	-1.6210	0.08264	0.09006
7.52	0.08626	0.08625	0.08624

During the experiments, RSSI values were measured periodically but not frequently with a capacitive moisture meter. This device measures the moisture in the soil in % value. This value, which is found by proportioning two discrete values defined as dry and wet, is used to determine the moisture content in the soil in simple applications. On device sensor there is a

capacitor and when the capacitor is charged, it begins to discharge. The duration of this process is measured by the sensor. The variance of the moisture values we obtained during the study period is shown in Table 5.

Table 5: Variance of moisture sensor values

Soil pH value	Variance of moisture sensor values
4.47	1.06122449
5.31	1.346938776
6.64	1.530612245
7.52	1.204081633

As can be seen in Table 5, the variance of the change between the measured values increases gradually in alkaline samples. Although the variation of soil moisture is not related to pH in terms of certain minerals, the result seen here is that moisture values change visibly. The distinctive properties of the soil samples were determined only on the basis of pH and other components were not taken into account. Therefore, although it is not clear whether this change is due to other characteristics of the samples, there is a significant change. Different pH values were used here as a distinguishing feature of the four different soil samples. The effects of pH values in relation to water or various salts have been studied in many studies. However, this study did not set up a setup to directly examine these relationships.

In our study, we observed that the results of the artificial intelligence model and it also gave good results in clay soils, even if we did not take into account the clay rate in soil samples.

Considering Fig. 4.b, although the change in RSSI values here occurs later than acidic soil samples, the RMSE values obtained as a result of the artificial intelligence model are closer to the alkali soil sample (pH 7.52). Under normal conditions, water diffusion in clay soils is slow due to the very small gaps in the clay (Haria et al. 1994). Our model results support this fact. Another result is that the clay rate in the soil increases and behaves similarly to acidic properties. The prediction of the RSSI values of the clay soil sample at pH 5.31 is shown in Figure 8.

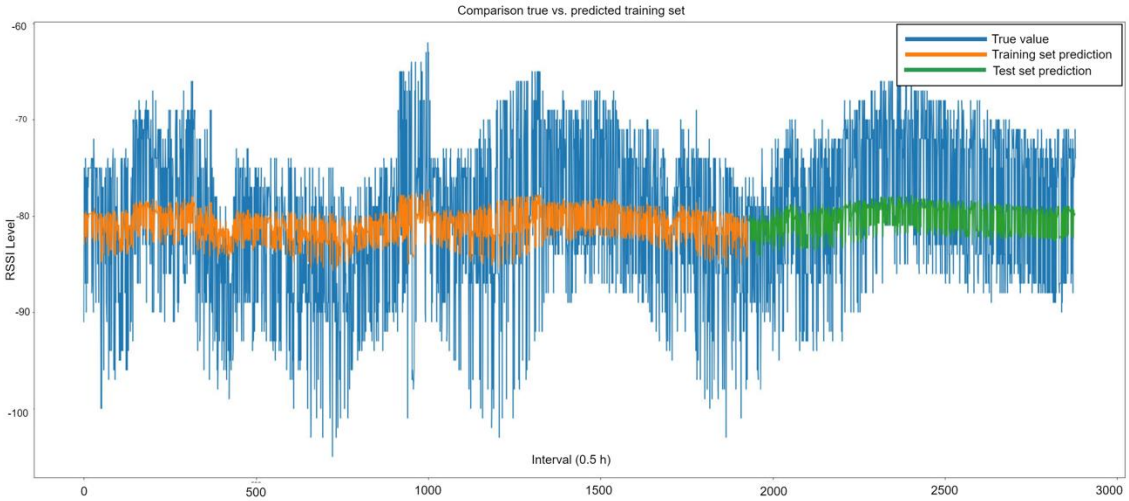

Figure 8: Train and prediction results for pH 5.3 clay soil sample

Here, it was seen that the offset difference between the measured signals and the predicted values found during the training of the model was higher. This difference is due to the fact that the 1D feature map values are lower than the measured RSSI values. However, the results of the artificial intelligence model still follow the pattern of the signal levels.

Numerous theoretical, empirical and semi-empirical methods have been developed to detect the moisture level of soil with active and passive microwave remote

sensing technics. In particular, assimilation of frequently referenced Radiometry and Synthetic Aperture Radar (SAR) data is a new technique used in soil moisture measurements, and there is a lot of research on this subject. The equipment in this type of works is quite large and energy-consuming devices. Today, researchers are constantly developing studies with active and passive microwaves. It can be said that these have some advantages and disadvantages compared to each other. A summary of the advantages and disadvantages of the different methods is available in Table 6.

Table 6: Passive and active microwave sensing methods comparation

Studies	Method	Power	Advantages	Disadvantages
(De Jeu et al. 2014)	Passive Microwave	300 kW	Can penetrate through different objects. Not limited by clouds, dust and daytime conditions, etc.	The energy level being emitted is quite low.
(Sun et al. 2019)		400W		
(Panciera et al. 2014)	Active Microwave	500 W	Detailed spatial resolution, not limited by clouds, dust and daytime conditions, etc.	Complicated analysis, cost-intensive.
(Abdel-Wahab et al. 2019)		10W		
Our Proposal	Active Microwave (BLE)	1mW	Low Power, Low Cost Devices. In-situ detection. Not limited by clouds, dust and daytime conditions, etc.	Low spatial resolution. Best results for acidic soils.

5 Conclusion

In this paper, we have presented the soil moisture content prediction method using LSTM recurrent neural networks. It has shown promising results on acidic soil samples and clay soil sample. We believe that using BLE signal strengths predicting soil moisture content proposed method has contributed to environmental and agricultural improvement. We foresee that the artificial intelligence solution applied in this study will make the method of obtaining information about the soil more widespread with the help of easily accessible and cheap devices.

Today, passive microwave measurements that used to determine soil moisture content are made at wavelengths called L-Band. These measurements are usually carried out via satellites. However, many factors should be taken into account during the remote sensing of soil moisture content. These factors can be listed as soil content, surface hardness, vegetation, backscattering angle of microwaves. There are theoretically and empirically constantly developed approaches to explain the effects of all these components. Even though there are effects to be neglected, even the effects of dipole moment, which will occur by the interaction of water molecules and microwaves in the soil, should be examined to determine the exact value in the measured sites. In this study, we tried to find the water content by the machine learning method by examining the BLE signal behavior in acidic soils without ignoring the importance of all these physical effects. Our results show that the artificial neural

network method we created is feasible.

On the other hand, BLE signals are similar to microwaves defined as L and S bands in satellite measurement systems, which are used frequently today. Although the transmission power of BLE signals is lower than the L and S bands, we think that the applications to be carried out using these signals will vary depending on the water content of the soil in the long term by the method of temporal analysis. With BLE signals, an estimate of water moisture content can also bring economic gain. The market prices of these BLE devices that are incomparable degree with similar microwave radar and measuring devices and methods are quite low. The properties of BLE and other L, S-band microwaves are shown in Table 7 (Sengupta and Liepa 2005).

Table 7: Frequency and wavelength values for L, S microwave bands and simple BLE signal values

Microwave Bands	Frequency Range (GHz)	Wavelength (cm)
L	1 – 2	30 – 15
S	2 – 4	15 – 7.5
BLE	2.4	~12

References

Abdel-Wahab, W., Al-Saedi, H., Ehsandar, A., Palizban, A., Raeis-Zadeh, M., & Safavi-Naeini, S. (2019). Efficient integration of scalable active-phased array antenna based on modular approach for MM-wave applications. Microwave and Optical Technology Letters, 61(5), 1333–1336. https://doi.org/10.1002/mop.31744

Adate, A., & Tripathy, B. K. (2019). S-LSTM-GAN: Shared Recurrent Neural Networks with Adversarial Training. In A. J. Kulkarni, S. C. Satapathy, T. Kang, & A. H. Kashan (Eds.), Proceedings of the 2nd International Conference on Data Engineering and Communication Technology (Vol. 828, pp. 107–115). Singapore: Springer Singapore. https://doi.org/10.1007/978-981-13-1610-4_11

Allen-Zhu, Z., Li, Y., & Song, Z. (2019). On the convergence rate of training recurrent neural networks. In Proceedings of the 33rd International Conference on Neural Information Processing Systems (pp. 6676–6688). Red Hook, NY, USA: Curran Associates Inc.

Batchu, V., Nearing, G., & Gulshan, V. (2023). A Deep Learning Data Fusion Model Using Sentinel-1/2, SoilGrids, SMAP, and GLDAS for Soil Moisture Retrieval. Journal of Hydrometeorology, 24(10), 1789–1823. https://doi.org/10.1175/JHM-D-22-0118.1

Calla, O. P. N. (2002). Application of Microwave Remote Sensing In Ocean Studies. 2, 623–632. Kochi, India: Allied Publishers.

Carbune, V., Gonnet, P., Deselaers, T., Rowley, H. A., Daryin, A., Calvo, M., … Gervais, P. (2020). Fast multi-language LSTM-based online handwriting recognition. International Journal on Document Analysis and Recognition (IJDAR), 23(2), 89–102. https://doi.org/10.1007/s10032-020-00350-4

Carrière, S. D., Martin-StPaul, N. K., Doussan, C., Courbet, F., Davi, H., & Simioni, G. (2021). Electromagnetic Induction Is a Fast and Non-Destructive Approach to Estimate the Influence of Subsurface Heterogeneity on Forest Canopy Structure. Water, 13(22), 3218. https://doi.org/10.3390/w13223218

Cho, K., van Merrienboer, B., Gulcehre, C., Bahdanau, D., Bougares, F., Schwenk, H., & Bengio, Y. (2014, September 2). Learning Phrase Representations using RNN Encoder-Decoder for Statistical Machine Translation. arXiv. Retrieved from http://arxiv.org/abs/1406.1078

Darroudi, S., Caldera-Sànchez, R., & Gomez, C. (2019). Bluetooth Mesh Energy Consumption: A Model. Sensors, 19(5), 1238. https://doi.org/10.3390/s19051238

Davis, J. L., & Chudobiak, W. J. (1975). In Situ Meter for Measuring Relative Permittivity of Soils. 75-1A. https://doi.org/10.4095/104349

De Jeu, R. A. M., Holmes, T. R. H., Parinussa, R. M., & Owe, M. (2014). A spatially coherent global soil moisture product with improved temporal resolution. Journal of Hydrology, 516, 284–296. https://doi.org/10.1016/j.jhydrol.2014.02.015

Dong, J., Steele-Dunne, S. C., Ochsner, T. E., & Van De Giesen, N. (2016). Determining soil moisture and soil properties in vegetated areas by assimilating soil temperatures. Water Resources Research, 52(6), 4280–4300. https://doi.org/10.1002/2015WR018425

Ertam, F. (2019). An effective gender recognition approach using voice data via deeper LSTM networks. Applied Acoustics, 156, 351–358. https://doi.org/10.1016/j.apacoust.2019.07.033

Gao, T., Gong, X., Zhang, K., Lin, F., Wang, J., Huang, T., & Zurada, J. M. (2020). A recalling-enhanced recurrent neural network: Conjugate gradient learning algorithm and its convergence analysis. Information Sciences, 519, 273–288. https://doi.org/10.1016/j.ins.2020.01.045

Gardner, W., & Kirkham, D. (1952). DETERMINATION OF SOIL MOISTURE BY NEUTRON SCATTERING: Soil Science, 73(5), 391–402. https://doi.org/10.1097/00010694-195205000-00007

Gascho, G. J., Parker, M. B., & Gaines, T. P. (1996). Reevaluation of suspension solutions for soil pH. Communications in Soil Science and Plant Analysis, 27(3–4), 773–782. https://doi.org/10.1080/00103629609369594

Ghori, M. R., Wan, T.-C., & Sodhy, G. C. (2020). Bluetooth Low Energy 5 Mesh Based Hospital Communication Network (B5MBHCN). In M. Anbar, N. Abdullah, & S. Manickam (Eds.), Advances in Cyber Security (Vol. 1132, pp. 247–261). Singapore: Springer Singapore. https://doi.org/10.1007/978-981-15-2693-0_18

H. Ali, M., & K. Ali, N. (2019). IoT based security system and intelligent home automation multi monitoring and control systems. IAES International Journal of Robotics and Automation (IJRA), 8(3), 205. https://doi.org/10.11591/ijra.v8i3.pp205-210

Han, Q., Zeng, Y., Zhang, L., Cira, C.-I., Prikaziuk, E., Duan, T., … Su, B. (2023). Ensemble of optimised machine learning algorithms for predicting surface soil moisture content at global scale [Preprint]. Earth and space science informatics. https://doi.org/10.5194/gmd-2023-83

Hanzlíček, Z., Vít, J., & Tihelka, D. (2019). LSTM-Based Speech Segmentation for TTS Synthesis. In K. Ekštein (Ed.), Text, Speech, and Dialogue (Vol. 11697, pp. 361–372). Cham: Springer International Publishing. https://doi.org/10.1007/978-3-030-27947-9_31

Haria, A. H., Johnson, A. C., Bell, J. P., & Batchelor, C. H. (1994). Water movement and isoproturon behaviour in a drained heavy clay soil: 1. Preferential flow processes. Journal of Hydrology, 163(3–4), 203–216. https://doi.org/10.1016/0022-1694(94)90140-6

Hochreiter, S., & Schmidhuber, J. (1997). Long Short-Term Memory. Neural Computation, 9(8), 1735–1780. https://doi.org/10.1162/neco.1997.9.8.1735

Hu, H., Li, Z., Elofsson, A., & Xie, S. (2019). A Bi-LSTM Based Ensemble Algorithm for Prediction of Protein Secondary Structure. Applied Sciences, 9(17), 3538. https://doi.org/10.3390/app9173538

Hussain, T., Muhammad, K., Ullah, A., Cao, Z., Baik, S. W., & De Albuquerque, V. H. C. (2020). Cloud-Assisted Multiview Video Summarization Using CNN and Bidirectional LSTM. IEEE Transactions on Industrial Informatics, 16(1), 77–86. https://doi.org/10.1109/TII.2019.2929228

Lambot, S., Slob, E., Minet, J., Jadoon, K. Z., Vanclooster, M., & Vereecken, H. (2010). Full-Waveform Modelling and Inversion of Ground-Penetrating Radar Data for Non-invasive Characterisation of Soil Hydrogeophysical Properties. In R. A. Viscarra Rossel, A. B. McBratney, & B. Minasny (Eds.), Proximal Soil Sensing (pp. 299–311). Dordrecht: Springer Netherlands. https://doi.org/10.1007/978-90-481-8859-8_25

Luo, D., Wen, X., & He, P. (2023). Surface Soil Moisture Estimation Using a Neural Network Model in Bare Land and Vegetated Areas. Journal of Spectroscopy, 2023, 1–10. https://doi.org/10.1155/2023/5887177

Ma, Z., Wu, B., Chang, S., Yan, N., & Zhu, W. (2023). Developing a physics-guided neural network to predict soil moisture with remote sensing evapotranspiration and weather forecasting [Other]. pico. https://doi.org/10.5194/egusphere-egu23-10597

Mamun, M. A. A., & Yuce, M. R. (2019). Sensors and Systems for Wearable Environmental Monitoring Toward IoT-Enabled Applications: A Review. IEEE Sensors Journal, 19(18), 7771–7788. https://doi.org/10.1109/JSEN.2019.2919352

Martín, F., Vélez, P., Muñoz-Enano, J., & Su, L. (2023). Planar microwave sensors. Hoboken, New Jersey: Wiley-IEEE Press.

Mu, T., Liu, G., Yang, X., & Yu, Y. (2022). Soil-Moisture Estimation Based on Multiple-Source Remote-Sensing Images. Remote Sensing, 15(1), 139. https://doi.org/10.3390/rs15010139

Nagarajan, B., Shanmugam, V., Ananthanarayanan, V., & Bagavathi Sivakumar, P. (2020). Localization and Indoor Navigation for Visually Impaired Using Bluetooth Low Energy. In A. K. Somani, R. S. Shekhawat, A. Mundra, S. Srivastava, & V. K. Verma (Eds.), Smart Systems and IoT: Innovations in Computing (Vol. 141, pp. 249–259). Singapore: Springer Singapore. https://doi.org/10.1007/978-981-13-8406-6_25

Newman, A. L. (1964). Soil Survey (Vol. 17). US Department of Agriculture, Soil Conservation Service.

Nguyen, T. P., & Songsermpong, S. (2022). Microwave processing technology for food safety and quality: A review. Agriculture and Natural Resources, 56(1), 57–72. Retrieved from https://li01.tci-thaijo.org/index.php/anres/article/view/253973

Noborio, K. (2001). Measurement of soil water content and electrical conductivity by time domain reflectometry: a review. Computers and Electronics in Agriculture, 31(3), 213–237. https://doi.org/10.1016/S0168-1699(00)00184-8

Panciera, R., Walker, J. P., Jackson, T. J., Gray, D. A., Tanase, M. A., Ryu, D., … Hacker, J. M. (2014). The Soil Moisture Active Passive Experiments (SMAPEx): Toward Soil Moisture Retrieval From the SMAP Mission. IEEE Transactions on Geoscience and Remote Sensing, 52(1), 490–507. https://doi.org/10.1109/TGRS.2013.2241774

Paul, I. J. L., Sasirekha, S., Vishnu, D. R., & Surya, K. (2019). Recognition of handwritten text using long short term memory (LSTM) recurrent neural network (RNN). 030011. Kurdistan, Iraq. https://doi.org/10.1063/1.5097522

Pekel, E. (2020). EVALUATION OF ESTIMATION PERFORMANCE FOR SOIL MOISTURE USING PARTICLE SWARM OPTIMIZATION AND ARTIFICIAL NEURAL NETWORK. Ömer Halisdemir Üniversitesi Mühendislik Bilimleri Dergisi. https://doi.org/10.28948/ngumuh.529418

Reginato, R. J., & Van Bavel, C. H. M. (1964). Soil Water Measurement with Gamma Attenuation. Soil Science Society of America Journal, 28(6), 721–724. https://doi.org/10.2136/sssaj1964.03615995002800060014x

Ren, G., & Ganapathy, V. (2019). Recognition of Online Handwriting with Variability on Smart Devices. ICASSP 2019 - 2019 IEEE International Conference on Acoustics, Speech and Signal Processing (ICASSP), 7605–7609. Brighton, United Kingdom: IEEE. https://doi.org/10.1109/ICASSP.2019.8682706

Scheberl, L., Scharenbroch, B. C., Werner, L. P., Prater, J. R., & Fite, K. L. (2019). Evaluation of soil pH and soil moisture with different field sensors: Case study urban soil. Urban Forestry & Urban Greening, 38, 267–279. https://doi.org/10.1016/j.ufug.2019.01.001

Schuster, M., & Paliwal, K. K. (1997). Bidirectional recurrent neural networks. IEEE Transactions on Signal Processing, 45(11), 2673–2681. https://doi.org/10.1109/78.650093

Sengupta, D. L., & Liepa, V. V. (2005). Applied Electromagnetics and Electromagnetic Compatibility (1st ed.). Wiley. https://doi.org/10.1002/0471746231

Singh, A., & Gaurav, K. (2023). Deep learning and data fusion to estimate surface soil moisture from multi-sensor satellite images. Scientific Reports, 13(1), 2251. https://doi.org/10.1038/s41598-023-28939-9

Sun, H., Cai, C., Liu, H., & Yang, B. (2019). Microwave and Meteorological Fusion: A method of Spatial Downscaling of Remotely Sensed Soil Moisture. IEEE Journal of Selected Topics in Applied Earth Observations and Remote Sensing, 12(4), 1107–1119. https://doi.org/10.1109/JSTARS.2019.2901921

Topp, G. C., Davis, J. L., & Annan, A. P. (1980). Electromagnetic determination of soil water content: Measurements in coaxial transmission lines. Water Resources Research, 16(3), 574–582. https://doi.org/10.1029/WR016i003p00574

Wang, T., Zhou, J., Wang, W., Zhang, G., Huang, M., & Lai, Y. (2019). A personal local area information interaction system based on NFC and Bluetooth technology. International Journal of High Performance Computing and Networking, 13(4), 455. https://doi.org/10.1504/IJHPCN.2019.099268

Wu, F., Wu, T., & Yuce, M. (2018). An Internet-of-Things (IoT) Network System for Connected Safety and Health Monitoring Applications. Sensors, 19(1), 21. https://doi.org/10.3390/s19010021

Zárate-Valdez, J. L., Zasoski, R., & Läuchli, A. (2006). SHORT-TERM EFFECTS OF MOISTURE CONTENT ON SOIL SOLUTION pH AND SOIL EH. Soil Science. Retrieved from https://www.semanticscholar.org/paper/SHORT-TERM-EFFECTS-OF-MOISTURE-CONTENT-ON-SOIL-pH-Z%C3%A1rate-Valdez-

Zasoski/ba3aba909b76ba66b9be0cc8bfec3c897ae25f32

Zhang, Y., Qu, C., & Wang, Y. (2020). An Indoor Positioning Method Based on CSI by Using Features Optimization Mechanism With LSTM. IEEE Sensors Journal, 20(9), 4868–4878. https://doi.org/10.1109/JSEN.2020.2965590

Zia, T., & Zahid, U. (2019). Long short-term memory recurrent neural network architectures for Urdu acoustic modeling. International Journal of Speech Technology, 22(1), 21–30. https://doi.org/10.1007/s10772-018-09573-7

Trakya University Journal of Engineering Sciences
http://dergipark.org.tr/tujes
ISSN 2147–0308

Research Article / Araştırma Makalesi
DOI : 10.59314/tujes.1504510

EVALUATION OF TREATMENT PERFORMANCE OF DIFFERENT METHODS ON WHEAT STRAW COMPOSITES

Ümit HÜNER[1*]

[1]*Kırklareli Üniversitesi, Mühendislik Fakültesi, Makine Mühendisliği Bölümü, Kırklareli, TÜRKİYE*

Cite this article as: Hüner, Ü. (2024)**.** Evaluation of Treatment Performance of Different Methods On Wheat Straw Composites, *Trakya Üniversitesi Mühendislik Bilimleri Dergisi*, 25(1), 39-51.

Highlights

- Treatment methods are essential to ensure compatibility with the matrix
- The morphological form of the roughness after treatment affects wetting and mechanical interlocking
- Since microwave breeding is an energy-based process, it fulfills its application purpose through many molecular mechanisms

Article Info

Article History:
Received:
May 25, 2024

Accepted:
June 26, 2024

Keywords:
Wheat straw;
Microwave;
Alkali;
Composite

Abstract

The objective of this research is to evaluate the impact of both traditional and innovative techniques on the qualities of wheat straw, as well as the mechanical performance of epoxy composites which use wheat straw as a reinforcing material. Two different methods were used for treatment: Alkali treatment (AlT) was carried out using NaOH at concentration of 5% w/v for 1 hour at 25°C, Microwave irradiation (MwT) aws performed at 300 W for 20 minutes. It was found that Alkali and microwave treatment both changed the surface morphology of wheat straw. Microwave treatment provided further improvement in the mechanical properties of the composite materials, enabling a 37% increase in tensile strength and 62% increase in flexural strength. Microwave reclamation, which is cleaner and performs better than chemical reclamation, shows promising performance for more sensitive material application areas.

Buğday Sapı Kompozitlerde Farklı Yöntemlerin Islah Performanslarının Değerlendirilmesi

Makale Bilgileri

Makale tarihçesi:
Geliş:
25 Mayıs 2024

Kabul:
26 Haziran 2024

Anahtar Kelimeler:
Buğday sapı;
Mikrodalga;
Alkali;
Kompozit

Öz

Bu araştırmanın amacı hem geleneksel hem de yenilikçi tekniklerin buğday samanının nitelikleri üzerindeki etkisini ve buğday samanını takviye malzemesi olarak kullanan epoksi kompozitlerin mekanik performansını değerlendirmektir. İşlem için iki farklı yöntem kullanılmıştır: Alkali işlem (AlT) 25°C'de 1 saat süreyle %5 w/v konsantrasyonda NaOH kullanılarak, Mikrodalga ışınlama (MwT) ise 20 dakika süreyle 300 W'da gerçekleştirilmiştir. Alkali ve mikrodalga işlemlerinin her ikisinin de buğday samanının yüzey morfolojisini değiştirdiği bulunmuştur. Mikrodalga işlemi, kompozit malzemelerin mekanik özelliklerinde daha fazla iyileşme sağlayarak çekme mukavemetinde %37 ve eğilme mukavemetinde %62 artış sağlamıştır. Kimyasal ıslahtan daha temiz olan ve daha iyi performans gösteren mikrodalga ıslahı, daha hassas malzeme uygulama alanları için umut verici bir performans göstermektedir.

[*]**Sorumlu Yazar: umithuner@klu.edu.tr**

1. Introduction

The growing concern for the environment has necessitated a shift in perspective when it comes to engineering materials and their design. There is now a renewed interest in natural materials that are obtained from safe, renewable, and sustainable sources, as they show great potential in meeting industrial demands. These materials can be used in their natural form, or in forms such as powders, fibers, straws, or husks that are obtained as harvest residues. Lignocellulosic natural resources, in particular, offer exceptional advantages over traditional synthetic materials, owing to their inherent properties such as light weight, low cost, renewability, and sustainability. Among these, cereal straw has emerged as a highly promising natural ingredient, which is widely used as waste biomass in various industrial applications, owing to its impressive characteristics.

Wheat straw is a by-product of wheat production in agriculture. In Turkey, for instance, the production of wheat in 2016 amounted to 20.6 million tons, which, considering the wheat-to-wheat straw ratio of 3:1 (Talebnia, Karakashev, Angelidaki, 2010), results in approximately 7.4 million tons of wheat straw produced at the end of the process. While most of the wheat straw is utilized as animal feed, the remaining amount is either left on the ground or burned. Unfortunately, burning the straw leads to environmental pollution and reduced soil productivity. In recent years, several studies have been conducted to address these issues and increase the utilization of this value-added by-product in various industrial and technical applications.

Recent studies have highlighted the potential use of wheat straw as a natural reinforcement in polymer-based composite production, owing to its lightweight, low cost, and relatively high thermal stability. However, wheat straw contains different components such as lignin, silica, carbohydrates, wax, silica, cutin, and some lipophilic substances, both on its interior and exterior surfaces. This structural difference between the two surfaces of wheat straw presents a significant challenge in composite production, as it creates incompatibility between the straw and polymer matrix (Xu, Minzhi, Xiaoyan, 2017). The lipophilic substances on the exterior surface cause strong adhesion forces and superficial adherence to the matrix, while the hydrophilic heteropolysaccharides containing hydroxyl (OH) and carboxylic acid (COOH) groups lead to weak adhesion forces and poor interfacial bonding (Mengeloglu, Karakus, 2008; Vaisanen et al., 2016). These factors inhibit the penetration of the hydrophobic matrix into the cellular structure of the wheat straw, leading to the formation of micro void spaces and insufficiently wet regions within the composite, resulting in impaired stress transfer from the matrix to wheat straw. Moreover, the compatibility between wheat straws and polymer matrices is not only influenced by interfacial attraction, but also by surface properties such as porosity, roughness, hydrophilicity/hydrophobicity, and functional groups (Xu, 2017). In addition, large-scale composite production with wheat straw for outdoor applications can be challenging due to their tendency to absorb moisture and poor dimensional stability caused by micro-cracking of the matrix around the swollen reinforcements.

In composite material manufacturing and various industrial applications (such as biofuel production, component extraction, or reinforcement), numerous physical (Zou, Shah, Yiqi, 2010), thermal, and chemical treatment methods have been employed to address the incompatibility stemming from the substrates present in wheat straw (both on the surface and within the biomass). These treatment applications aim to enhance compatibility between the reinforcement and the matrix by altering the proportion of structural components in the reinforcement or by introducing functional groups on the surface, as well as

by creating a suitable topographical texture. Chemical treatments, ion bombardments (plasma), microwave irradiation (as reviewed), and heat treatment play integral roles in this process. They function by either reacting with intrinsic hydroxyl groups to eliminate them or by forming new functional groups with a greater bonding tendency to the matrix material. These reactions also lead to a reduction in the proportions of wax, lignin, and hemicellulose present in the natural structure. Consequently, changes in surface characteristics, including topography, hydrophilicity, and surface free energy, become inevitable. In this context, the enhancement of mechanical interlocking between the matrix and the reinforcement becomes apparent. This is primarily attributed to the rougher surfaces resulting from the removal of irregularities or the formation of new functional groups through interactions and reactions.

Treatment mechanisms act in various ways on the reinforcement structure. Chemical treatments, such as alkali treatment, result in the partial removal of hemicellulose, lignin, and pectin content by dissolving the primary cell wall of the fiber structure. This process increases the number of potential bond-forming reactions due to the lack of OH groups on the fiber surface (Alemdar, Mohini,2008; Huner et al. 2017). Alkaline treatment also enhances the amorphous cellulose content on the fiber surface, exposing short-length crystals through cellulose depolymerization. This exposure facilitates interactions between the OH groups, imparting hydrophilicity to the cellulose molecule and enhancing its interaction with alkali chemical agents (Mohanty, Misra, Drzal, 2001). Subsequently, substitution reactions form fiber-cell-O-Na groups between cellulose molecular chains, reducing hydrophilic OH groups and increasing the wettability between the fiber and the hydrophobic matrix (Kabir, wang,Lau, Cardona, 2012, Väisänen et al. 2016). Microwave irradiation treatment, predominantly used as a pre-treatment method to improve fermentation (Li et al, 2016) and biofuel efficiency (Satpathy et al, 2014), acts as a heating process in the treatment of natural reinforcement materials (Sgriccia, Hawley,2007). Depending on microwave power and processing time, it can have various effects on wheat straw. Microwave irradiation induces weight loss by removing water, low-molecular-weight organic volatiles, and pyrolyzing internal straw (Sgriccia, 2007 and Zhao, 2014). Additionally, it enhances hydrophobic characteristics, reducing moisture uptake and decreasing atomic H/C and O/C ratios associated with hydrophilicity due to volatile removal (Satpathy et al, 2014). Cross-linking occurs through covalent interactions between polymer molecular chains and the reinforcement surface. Notably, the physical, chemical, or irradiation treatment studies can lead to different directions in terms of surface hydrophilicity (more hydrophilic or more hydrophobic), depending on the intensity and application time. Physically, the treatment expands the microporous structure of the straw surface, increasing the interaction (wetting) area of the interface with the matrix material. Overall, these changes contribute to improvements in mechanical properties such as internal bond strength, modulus of elasticity, and modulus of rupture (Li et al, 2016 and Xu et al,2017]. It is noteworthy that no research has compared the effects of different treatment methods under the same study. There is a need for studies that broaden the perspective on both the methods used and the utilization of wheat straw as reinforcement in composite production.

This study was carried out in order to investigate the effects of the treatment with simple chemical, microwave irradiation on the wheat straw and the reflections of these changes on the epoxy based composite material. It has been noticed that quite a few studies have been conducted using different treatments to improve the physical and mechanical properties of the wheat straw. The results of this study will contribute to remedy deficiencies by providing detailed information.

2. Materials and Method

2.1 Materials

Wheat straw was sourced from the Thrace region in Turkey and subjected to natural drying under sunlight for one month to eliminate surface water post-harvest in 2019. The resulting dry matter content of the wheat straw was 94.2 wt%. Before treatment, the wheat straws were precision-cut to sizes of 10-12 cm using a razor blade and then further dried under vacuum conditions at 70 °C for 24 hours. The polymer matrix utilized in the study was MGS LR 160 (Hexion), a commercial epoxy resin obtained from Dost Kimya Ltd. The technical characteristics of the epoxy resin, as provided by the manufacturer, are outlined in our previous study [reference]. Additionally, MGS LH 160 (Epikure) served as the curing agent in the epoxy, applied at a concentration of 0.40 w/w. The epoxy's properties, as per the manufacturer's data sheet, include a density of 1.17 g/cm^3, viscosity of 800 MPas, tensile strength of 55 MPa, tensile modulus of 13 GPa, flexural strength of 125 MPa, and flexural modulus of 15 GPa. For alkaline treatments, sodium hydroxide (NaOH) and acetic acid (CH3COOH, glacial, ≥ 99.85%) were procured from Sigma-Aldrich (St. Louis, MO, USA). High purity water, with a conductivity less than 0.5 µS cm^{-1}, was obtained from a PURELAB® Option-Q (ELGA LabWater, UK) unit.

2.2 Alkali treatment

The wheat straws underwent alkalization by exposure to 5% w/v NaOH aqueous solution. To facilitate this process, the straws were immersed in NaOH solutions for 1 hour at 25±1 °C to eliminate irregularities. Subsequently, the treated straws were thoroughly cleansed with distilled water and neutralized using an acetic acid solution (10 mL in 1 L water). This was followed by multiple washes with fresh distilled water until complete removal of NaOH. Finally, the straws were dried in an oven at 80 °C for 5 hours and then cooled in a desiccator. The alkali-treated wheat straws, denoted by specific codes in Table 1, were securely stored in a vacuum-sealed plastic bag to prevent atmospheric moisture contamination. This precaution was taken in anticipation of composite preparation and subsequent analyses.

2.3 Microwave treatment

The wheat straws were processed using a Kenwood Microwave Oven (Model MW587, London, UK) in a household setting, operating at a power intensity ranging from 0 to 1400 W and a frequency of 2.45 GHz. This apparatus is equipped with a glass turntable plate, a digital power control panel, and a time control panel. Initially, the samples were positioned at the center of the glass turntable plate. Subsequently, the microwave power was set to 300 W and the straws were exposed for 20 minutes. Following the microwave treatment, the treated samples (refer to Table 1) were stored using the previously mentioned method.

Table 1. Sample codes for the untreated and treated wheat straws

Untreated wheat straws		Alkali treated wheat straws			Microwave treated wheat straws		
Int.	Ext.	NaOH concent. (%)	Int.	Ext.	Exposure power-time	Int.	Ext.
Unt-IWS	Unt-EWS	5	5AlT-IWS	5AlT-EWS	300W-20min	300:20MwT-IWS	300:20MwT-EWS

Int: Interior surface, Ext: Exterior surface

2.4 Preparation of Composite Samples

Composite samples were fabricated employing the hand lay-up technique with vacuum assistance. The epoxy resin was meticulously prepared by blending it with the recommended curing agent at a manufacturer-specified ratio of 100:32. To ensure optimal homogeneity, the mixture underwent thorough stirring with a glass rod, eliminating any potential bubbling, and was further subjected to 30 minutes of sonication. The molds, featuring dimensions in accordance with ASTDM D 3039 and ASTM D 790 standards, were constructed using glass and transparent PMMA. To prevent adhesion, a mold release agent was applied, and each straw was carefully immersed in the epoxy, with placement into the mold facilitated by hand and forceps to ensure comprehensive wetting. The fiber volume fraction (Vf) for all composites consistently fell within the range of 0.45–0.47. Subsequently, the molds were subjected to a vacuum, facilitated by a bag, for a duration of 6 hours under pressure. The ensuing step involved post-curing at 50°C for an additional 6 hours. Wheat straw reinforced epoxy composites were denoted by codes in Table 2.

Table 2. Sample codes for the untreated and treated wheat straws reinforced composites

Untreated wheat straws r-comp.	Alkali treated wheat straws r-comp.	Microwave treated wheat straws r-comp.
UWSc	AlTWSc	MWTWSc

2.5 Water absorption test

The water absorption test was conducted in accordance with ASTM D-570-98. The test specimens were rectangular bars measuring 76.2 mm in length, 25.4 mm in width, and 3.2 mm in thickness. The dry weights of the samples (Wd) were determined using a precise balance (Sartorius, Model Ed 224s, Gottingen, Germany, accuracy ± 0.0001) at room temperature. Subsequently, the samples were immersed in a water bath (Memmert, Model WBN 22, Germany) set at temperatures of 25 and 90 °C for a duration of 24 hours. Weight measurements were recorded at 1, 2, 3, 4, 5, 6, 12, and 24 hours for each sample. At regular intervals, the samples were removed from the water, and any excess water on the surfaces was carefully wiped off using blotting paper. The wet weights (Ww) were then measured. The percentage of water absorption was determined by calculating the weight difference using Equation (1). The results were reported as the average of three replicate measurements. Additionally, the normalized water absorption (WA/WA_0) was defined as the ratio of water absorption values to the initial values of water absorption

$$\text{Water absorption (WA, \%)} = \frac{Ww-Wd}{Ww} x100 \qquad (1)$$

Where, *Wd* is the initial dry weight of the samples (g) and *Ww* is the weight of the samples after exposure to water (g).

2.6 Atomic Force Microscopy and Scanning Electron Microscopy

The surface topographies of the untreated and treated wheat straws were investigated by atomic force microscopy (AFM, Nano Magnetics Instruments, Ankara, Turkey) using in contact mode. The roughness of the samples was quantified as the root mean square (Sq), derived from an average of five independent measurements over a scan area of 10 µm x 10 µm. The silicon nitride (Si3N4) probe employed in the analysis featured a curvature radius of 10 nm, as specified by the manufacturer. A cantilever spring constant (k) of approximately 0.02 N/m was selected due to the high force gradient in air. The calibration of cantilever spring constants was performed using a reference cantilever with a precisely controlled force constant. The scan rate in the force channel was set at 6 Hz.

The morphology of the composite surfaces and the fractured composite samples were examined using a Quanta™ FEG 250 scanning electron microscope (Oregon, USA) with an acceleration voltage of 2 kV and a large field low vacuum SED (LFD) detector.

2.7 Fourier transform infrared spectroscopy (FTIR)-attenuated total reflectance (ATR)

The differences in chemical composition of untreated and treated wheat straws were examined with Fourier transform infrared (FTIR) spectrophotometer (Perkin-Elmer spectrum BX, Perkin- Elmer, Woodbridge, Canada) equipped with a horizontal attenuated total reflectance (ATR) system (Perkin-Elmer spectrum BX, Perkin- Elmer, Woodbridge, Canada). All spectra were recorded in a range of 4000–400 cm^{-1} at a resolution of 4 cm^{-1} with 64 scans.

2.8 Mechanical Characterization

Mechanical properties of untreated and treated wheat straw reinforced composites were determined by tensile and bending tests. Mechanical tests were performed with an Instron Model 8501 (UK) (5 kN). The tensile test was carried out according to the ASTM D638 method at a crossing speed of 5 mm/min and a gauge length of 50 mm. The flexural test was carried out at 5 mm/min in accordance with ASTM D790 method. Three samples of each sample were tested for tensile and bending tests and the average results reported.

3. RESULTS and DISCUSSION

3.1 Water absorption results

Understanding and manipulating the polarity fraction of cellulosic materials can be crucial in designing materials with specific water absorption properties for diverse applications ranging from textiles and packaging to biomedical devices. It involves a balance between hydrophilic and hydrophobic components to achieve the desired performance characteristics. Higher polarity fraction generally leads to increased hydrophilicity (gaffar, 2016 and Gaffar, Mizi, 2017). Within the scope of the study, the water absorption test results of composite samples containing treated and untreated wheat straws are shown in Figure 1.

Hydrophilic groups, such as hydroxyl (-OH) groups in cellulose, can form hydrogen bonds with water molecules, making the material more capable of absorbing water. Additionally, wheat straw has a porous structure, and its fibers create a network that can absorb and retain water.

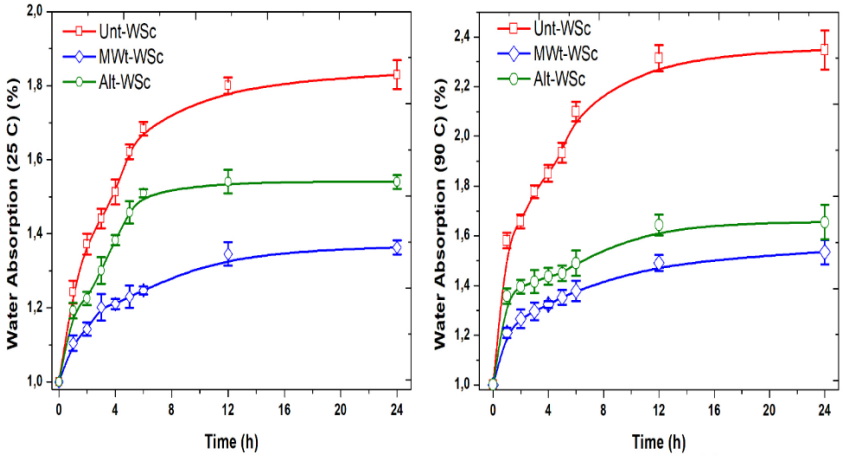

Figure 1. Water absorption results 25ºC (left) and 90ºC (right)

When the test results were analyzed, it was observed that the water absorption tendency exhibited high values in untreated wheat straw reinforced composites. In contrast, composites reinforced with alkaline and microwave-treated wheat straw displayed lower water absorption values, consistent with similar studies (Li et, 2016 and Mittal, Shishir,2017). The water absorption mechanism initially penetrates the structure through capillary action, followed by the accumulation of water molecules that bond with the reinforcement. The

alkaline treatment method prevents the aforementioned uptake and accumulation by reducing free OH groups. It can be argued that the decrease in water absorption value is attributed to the fact that alkaline treatment provides better wetting with the epoxy matrix by altering the surface topography, thereby reducing micro voids and the possible capillary effect, and subsequently reducing water transmission within the structure.

3.2 AFM and SEM results

The morphological and free surface energy changes on wheat straws after the treatment process were examined by atomic force microscopy. AFM examinations of untreated and treated interior and exterior wheat straws are shown in Figure 2 and 3.

The interior and exterior surface roughness values of untreated wheat stalks were 0.176 and 0.149, respectively. While a significant roughness change was observed on the interior surface of the wheat stalk after alkali treatment, it was determined that the roughness change efficiency was low on the exterior surface (R_a= 0.150 µm, R_{rms}=0.190 µm). This can be attributed to the difference in the chemical structure of the interior and exterior surfaces. Especially the excess of lipophilic chemical substances, cutin and wax on the exterior surface may have resisted alkaline treatment (Mohanty,2001).

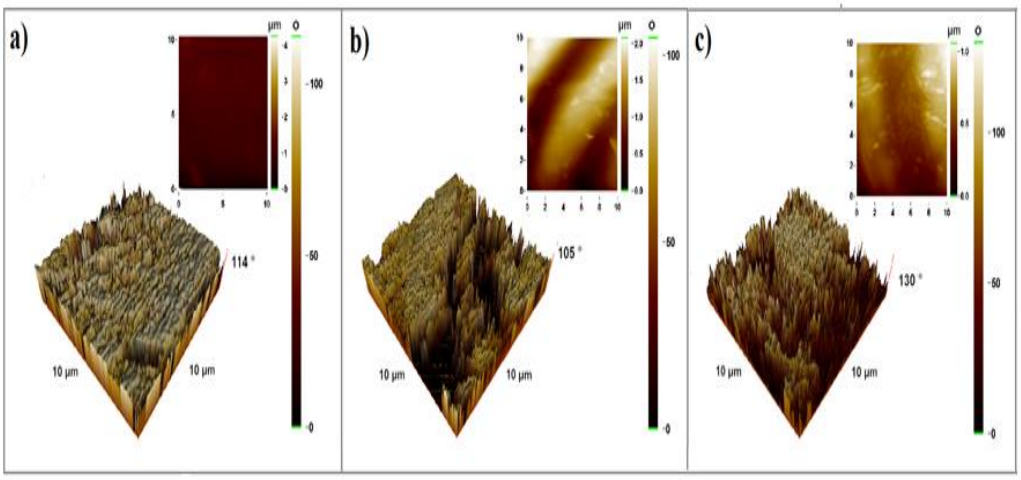

Figure 2. Exterior surfaces phase and amplitude (front view) images of the untreated (a), alkali treated (b), microwave treated (c)

Microwave treatment shows its effect on surface roughness through molecular changes such as dehydration, cristallinity change or hydrolysis by means of interaction with polar groups (-OH). A change of 65% and 182% was observed in the untreated interior and exterior surface roughness, respectively. It can be suggested that it creates more active sites in terms of wettability.

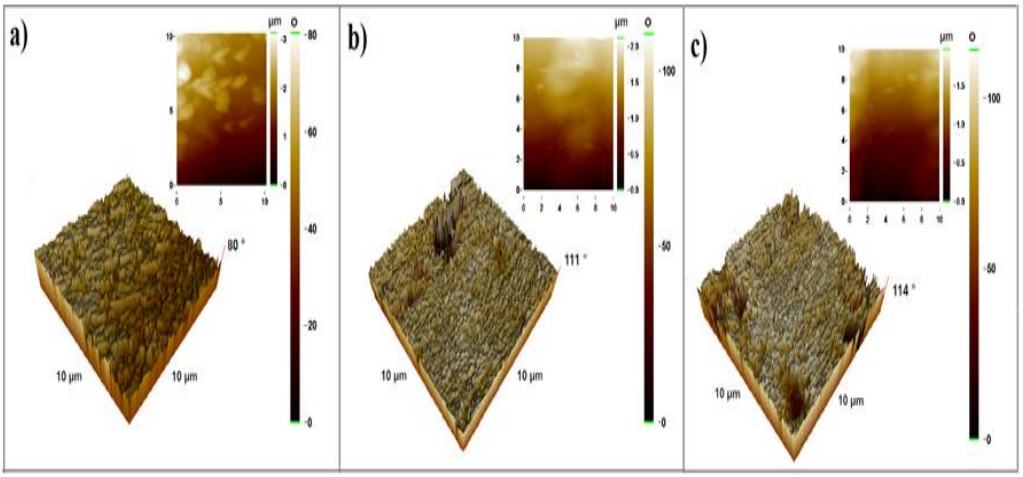

Figure 3. Interior surfaces phase and amplitude (front view) images of the untreated (a), alkali treated (b), microwave treated (c)

The existing literature has demonstrated that both alkaline and microwave treatment methods induce morphological changes on the surface of wheat straws, as well as alterations in the surface energy due to the molecular changes they elicit (Sgriccia,2007 and Li et al,2016). While alkaline treatment removes irregularities such as lignin, pectin, and wax from the wheat straw surface, it also causes a decrease in the free hydroxyl (OH) groups of cellulose in the primary wall of the stem (Li et al,2007 and Liu et al,2017). The roughness values of the interior and exterior surfaces after alkali treatment are presented in Table 3. As shown, there is a remarkable increase in the roughness values (Gadelmawla et al,2002). However, it would be cautious to also consider the skewness and kurtosis values presented in the table when evaluating the surface morphology. The skewness and kurtosis values obtained in AFM contact mode measurements are also presented in Table 3. Roughness values provide a superficial assessment of the post-treatment surface morphology. In addition, the skewness/kurtosis values, the forms of the surface shapes that occur after reclamation, i.e. the formation of peaks/valleys or sharp/oval ends, determine both the wettability and the quality of the mechanical interlocking between the matrix and the surface.

Table 3. Surface roughness parameters of untreated and APPlJ treated wheat straw

Sample	**Coefficient**			
	Average (R_a)(µm)	Root Mean Square (R_{rms})(µm)	Skewness (R_{sk})	Kurtosis (Rku)
UntIWS	0.176±0.03	0.191±0.02	-0.281±0.03	3.890±0.03
UntEWS	0.149±0.01	0.156±0.01	-0.173±0.02	3.418±0.03
5AlT-IWS	0.390±0.43	0.460±0.22	0.167±0.17	1.118±0.41
5AlT-EWS	0.150±0.21	0.190±0.24	0.155±0.19	1.614±0.33
300:20MwT-IWS	0.290±0.26	0.400±0.31	0.139±0.27	1.314±0.15
300:20MwT-EWS	0.420±0.34	0.490±0.25	0.118±0.36	1.959±0.52

Negative skewness values on the untreated wheat straw surface indicate crack-like formations, while kurtosis values greater than 3 indicate leptocurtoic-like sharp ("pointy") surface formations. It can be concluded that the skewness value turned positive after both treatment processes and the crack-like formations decreased or were filled with various substances by plastering during the process. Kurtosis values were observed to be below 3 (Gadelmawla et al,2002. This indicates platykurtic surface formations, i.e. valley-like shape formations with reduced number of sharp edges.

AFM surface examinations suggest that the treatment process is beneficial for wettability and the resulting surface shapes are shaped in a way that helps the mechanical interlocking with the matrix.

SEM images to examine the surface roughness are shown in Figure 4 and 5. On the surface of the untreated wheat straw, the roughness ratio and the wax, pectin, etc. substances on the surface were clearly observed (Figure 4a, 5a).

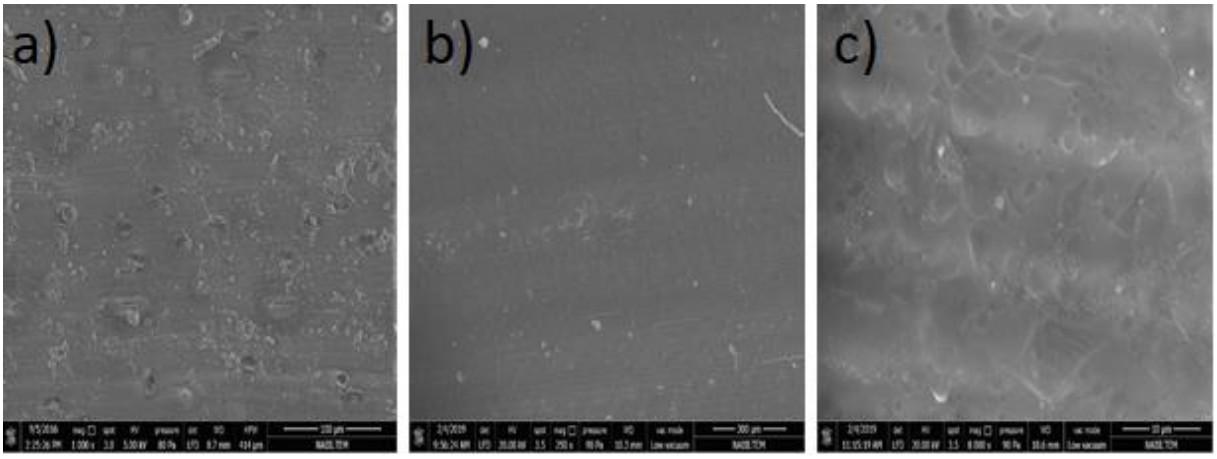

Figure 4. Exterior surface of untreated (a), alkali treated (b), microwave treated (c) wheat straws

Morphological differences between the interior and exterior surface are also evident. A clean structure was observed on the exterior surface after alkali treatment. On the interior surface, more pronounced surface contours appeared.

Microwave treatment, on the other hand, caused a rougher "shrunken" structure on the exterior surface compared to the alkaline one. On the interior surface, it caused a more distinct surface as in alkaline.

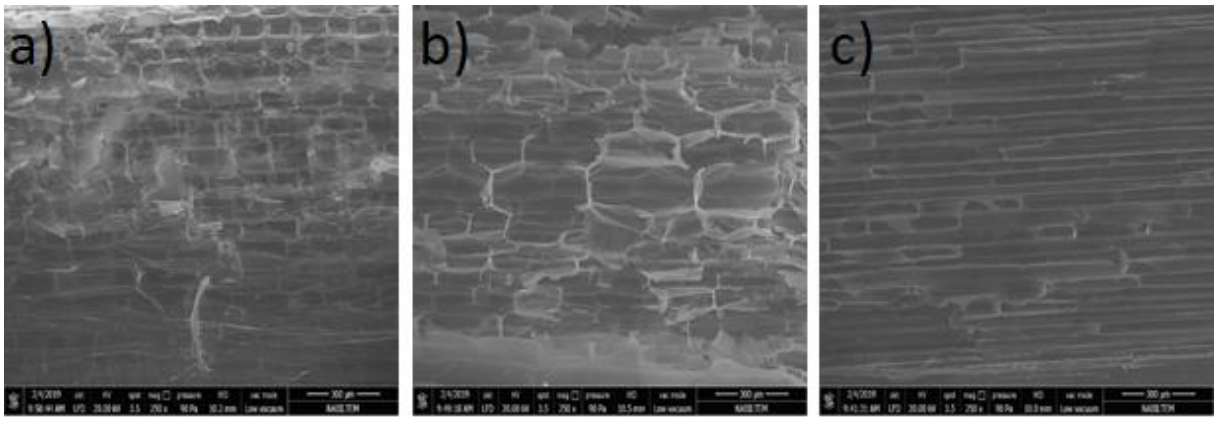

Figure 5. Interior surface of untreated (a), alkali treated(b), microwave treated (c) wheat straws

3.3 FTIR results

The results of the FTIR analysis to investigate the effect of the treatment on the molecular structure of the interior and exterior surface of the wheat straw are shown in Figure 6.

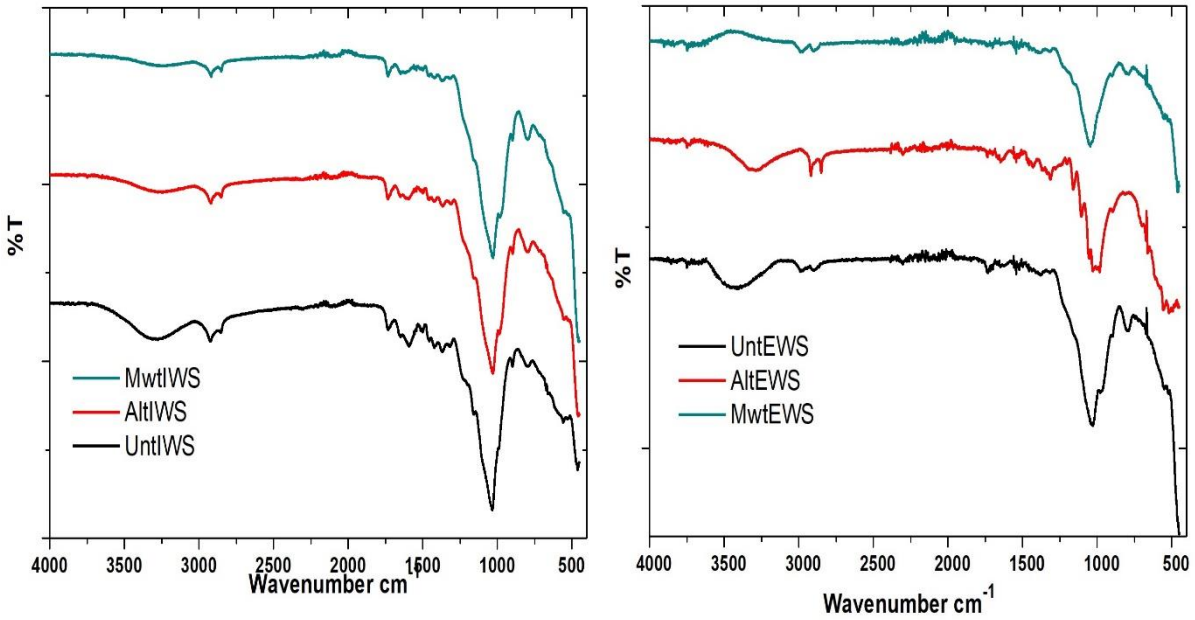

Figure 6. FITR results of interior (left) and exterior (right) surfaces of wheat straws

The stretching vibration absorption peak located around 3400 cm^{-1} of the inner and outer surface corresponds to the aliphatic components of cellulose, lignin and wax of the -OH group present in the structure (Kabir et al, 2012). While the intensity of this peak decreases after alkali treatment on the interior surface, it can be stated that the effectiveness is more limited on the exterior surface. On the other hand, it can be claimed from the changes of the mentioned peak of the interior and exterior surfaces that microwave treatment plays a more effective role in the removal of -OH groups.

The peak located at 2920 cm^{-1} is a characteristic peak originating from the stretching vibration CH group in hemicellulose and cellulose (li et al ,2007; Talebnia et al, 2010 and Li et al, 2016). The C=C peak located at 1507 cm^{-1} is the stretching of the aromatic rings of lignin. Partial fragmentation of lignin after reclamation caused a change in this peak. Peaks located around 1000 -1300 $cm^{-}1$ are due to Si-O and O-Si-O stretching. Especially on the exterior surface, the intensity of the peaks in this region decreased or disappeared after treatment, which can be attributed to the degradation of the silicon layer.

At 870 cm, the C-O peak typical of cellulose has decreased in intensity or disappeared, especially on the outer surface. In particular, the alkali treatment caused a change in the molecular bonds of the cellulose on the outer surface.

As a general evaluation, it can be suggested that both alkali and microwave partially/completely removed some components from the interior and exterior surfaces, and the effects on the interior and exterior surfaces varied depending on the difference in structural components. Surface roughness as well as possible molecular changes affect the wettability and bonding abilities between the matrix and the reinforcement, which in turn determine the overall physical/mechanical properties of the composite.

3.4 Mechanical test results

Tensile and flexure tests were carried out to investigate the effect of the treatment process on the mechanical properties of the epoxy composites produced and Figure 7 shows the pre and post-test images of the samples. The results of tensile and flexural tests are shown as bar graphs in Figure 8.

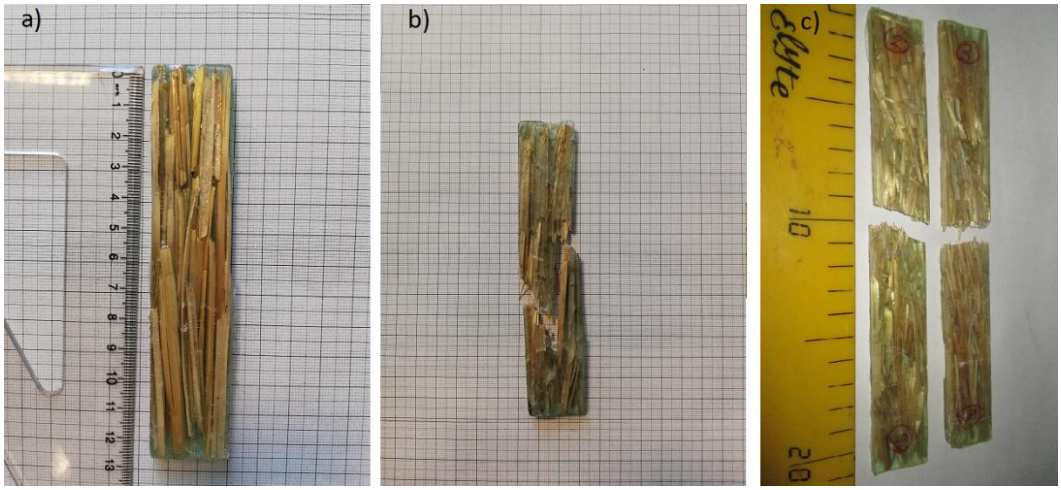

Figure 7. Wheat straw reinforced composites a) tensile test sample, b) broken tensile test sample, c) flexural test samples

A tensile strength value of approximately 19 ± 3.15 MPa was observed in composites containing untreated wheat straw. Alkali treated specimens showed an improvement of 15% and microwave treated specimens showed an improvement of 37%. This was attributed to surface treatment leading to better wetting and increased mechanical interlocking between the reinforcement and the matrix, which is in line with similar studies (bolcu et al,2022). Considering the tensile modulus, it can be argued that alkaline treatment causes embrittlement on the straw and although it shows an increase in strength, its ability to absorb energy decreases.

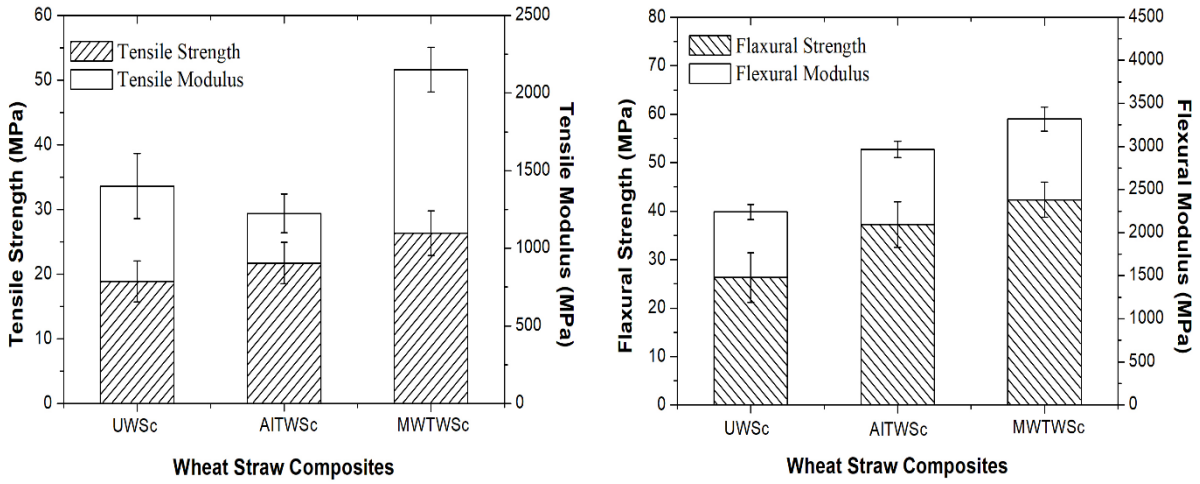

Figure 8. Tensile test results of wheat straw composites (left), Flexural test results (right)

The flexural strength and modulus of the composites containing untreated wheat straw were determined as 26 and 2240 MPa, respectively. While the flexural strength of the composites with alkali treated wheat straw increased by 42%, the increase in flexural strength in the composites with microwave treated wheat straw was 62%.

The increase in flexural modulus in alkali treated samples was measured as 32%. This increase was 48% in microwave treated samples. (Bolcu et al,2022 and mittal et al ,2017) When the flexural test results are compared with similar studies, the differences can be attributed to the physical form of the wheat straw used in the composites or the differences in parameters such as processing time and chemical ratio in the treatment process.

4. Conclusions

Untreated and alkali and microwave treated wheat straws were used in the production of composites using epoxy matrix.

When the effect of alkali treatment on the surface was examined, it was determined that the effectiveness was less on the outer surface. It caused a roughness change of approximately 162% on the inner surface.

Microwave treatment caused both roughness change and the resulting surface forms were found to be more appropriate in terms of wettability and mechanical interlocking.

At the molecular level, it was revealed with the help of FTIR that both treatment methods removed the free -OH groups in the wheat straw structure. It can be argued that microwave only helps more wettability with its effect on surface energy change and molecular bonding.

Mechanical test results revealed that both treatment processes were effective. Considering the strength values, microwave-treated wheat straw reinforced composites performed better than alkaline-treated composites.

It can be argued that the effectiveness of the microwave treatment process contributes more to the process when it is desired to increase the wettability and mechanical bonding performance of the reinforcement without weight loss and without deteriorating the structural strength of the reinforcement during the treatment process.

Conflict of Interest

Author declare that there are no conflicts of interest.

References

Alemdar, Ayse, and Mohini Sain. 2008a. “Bio composites from Wheat Straw Nanofibers: Morphology, Thermal and Mechanical Properties.” Composites Science and Technology 68(2):557–65. doi: 10.1016/j.compscitech.2007.05.044.

Bolcu, Dumitru, Marius Marinel Stănescu, and Cosmin Mihai Miriţoiu. 2022. “Some Mechanical Properties of Composite Materials with Chopped Wheat Straw Reinforcer and Hybrid Matrix.” Polymers 14(15). doi: 10.3390/polym14153175.

Gadelmawla, E. S., M. M. Koura, T. M. A. Maksoud, I. M. Elewa, and H. H. Soliman. n.d. “Roughness Parameters” Journal of Materials Processing Technology 123 (2002) 133±145

Ghaffar, Seyed Hamidreza. 2016. Aggregated Understanding of Characteristics of Wheat Straw Node and Internode with Their Interfacial Bonding Mechanisms.

Ghaffar, Seyed Hamidreza, and Mizi Fan. 2017a. “An Aggregated Understanding of Physicochemical Properties and Surface Functionalities of Wheat Straw Node and Internode.” Industrial Crops and

Products 95:207–15. doi: 10.1016/j.indcrop.2016.10.045.

Kabir, M. M., H. Wang, K. T. Lau, and F. Cardona. 2012a. "Chemical Treatments on Plant-Based Natural Fibre Reinforced Polymer Composites: An Overview." Composites Part B: Engineering 43(7):2883–92. doi: 10.1016/j.compositesb.2012.04.053.

Li, Hongqiang, Yongshui Qu, Yongqing Yang, Senlin Chang, and Jian Xu. 2016. "Microwave Irradiation - A Green and Efficient Way to Pretreat Biomass." Bioresource Technology 199:34–41.

Li, Xue, Lope G. Tabil, and Satyanarayan Panigrahi. 2007. "Chemical Treatments of Natural Fiber for Use in Natural Fiber-Reinforced Composites: A Review." Journal of Polymers and the Environment 15(1):25–33.

Liu, Qi, Yun Lu, Mario Aguedo, Nicolas Jacquet, Canbin Ouyang, Wenqing He, Changrong Yan, Wenbo Bai, Rui Guo, Dorothée Goffin, Jiqing Song, and Aurore Richel. 2017. "Isolation of High-Purity Cellulose Nanofibers from Wheat Straw through the Combined Environmentally Friendly Methods of Steam Explosion, Microwave-Assisted Hydrolysis, and Microfluidization." ACS Sustainable Chemistry and Engineering 5(7):6183–91. doi: 10.1021/acssuschemeng.7b01108.

Mengeloglu, Fatih, and Kadir Karakus. 2008. "Thermal Degradation, Mechanical Properties and Morphology of Wheat Straw Flour Filled Recycled Thermoplastic Composites." Sensors 8:500–519.

Mittal, Varun, and Shishir Sinha. 2017. "Study the Effect of Fiber Loading and Alkali Treatment on the Mechanical and Water Absorption Properties of Wheat Straw Fiber-Reinforced Epoxy Composites." Science and Engineering of Composite Materials 24(5):731–38. doi: 10.1515/secm-2015-0441.

Mohanty, A. K., M. Misra, and L. T. Drzal. 2001. "Surface Modifications of Natural Fibers and Performance of the Resulting Biocomposites: An Overview." Composite Interfaces 8(5):313–43. doi: 10.1163/156855401753255422.

Satpathy, Sangram Kishor, Lope G. Tabil, Venkatesh Meda, Satya Narayana Naik, and Rajendra Prasad. 2014. "Torrefaction of Wheat and Barley Straw after Microwave Heating." Fuel 124:269–78. doi: 10.1016/j.fuel.2014.01.102.

Sgriccia, Nikki, and M. C. Hawley. 2007. "Thermal, Morphological, and Electrical Characterization of Microwave Processed Natural Fiber Composites." Composites Science and Technology 67(9):1986–91. doi: 10.1016/j.compscitech.2006.07.031.

Talebnia, Farid, Dimitar Karakashev, and Irini Angelidaki. 2010. "Production of Bioethanol from Wheat Straw: An Overview on Pretreatment, Hydrolysis and Fermentation." Bioresource Technology 101(13):4744–53. doi: 10.1016/j.biortech.2009.11.080.

Väisänen, Taneli, Antti Haapala, Reijo Lappalainen, and Laura Tomppo. 2016. "Utilization of Agricultural and Forest Industry Waste and Residues in Natural Fiber-Polymer Composites: A Review." Waste Management 54:62–73.

Zou, Yi, Shah Huda, and Yiqi Yang. 2010. "Lightweight Composites from Long Wheat Straw and Polypropylene Web." Bioresource Technology 101(6):2026–33. doi: 10.1016/j.biortech.2009.10.042.

Trakya University Journal of Engineering Sciences
http://dergipark.org.tr/tujes
ISSN 2147–0308

Research Article / Araştırma Makalesi
DOI:10.59314/tujes.1422282

BİR KAMU BİNASINDAKİ SICAK SU KAZANINA UYGULANAN ATIK ISI GERİ KAZANIMININ ENERJİ VERİMLİLİĞİ ANALİZİ

Hacer AKHAN[1]*, Özgür ÖZAYDIN[1], Samet ÖZDEMİR[1]

[1]*Trakya Üniversitesi Mühendislik Fakültesi Makine Müh. Bölümü, Ahmet Karadeniz Yerleşkesi, Edirne, Türkiye*

Makale Künye Bilgisi: Akhan, H., Özaydın, Ö., Özdemir, S. (2024). Bir Kamu Binasındaki Sıcak Su Kazanına Uygulanan Atık Isı Geri Kazanımının Enerji Verimliliği Analizi, *Trakya Üniversitesi Mühendislik Bilimleri Dergisi*. 25(1), 53-64.

Öne Çıkanlar

- Enerji atıklarının değerlendirilmesi, enerji verimliliğinin artırılması ve mevcut enerji kayıplarının önlenmesi.
- Tüketilen enerji miktarının kalite ve performansı düşürmeden en aza indirilmesi.
- Isıtma sisteminde kullanılan kazanın enerji verimliliği incelemesi yapılmıştır.
- Geri kazanılan enerjinin karşılığı kadar yakıt kullanılmayarak tasarruf sağlanmaktadır.

Makale Bilgileri

Makale Tarihçesi:

Geliş:
31 Ocak 2024

Kabul:
28 Haziran 2024

Anahtar Kelimeler:

Kazanlarda enerji verimliliği;

Enerji tasarrufu;

Atık ısı geri kazanımı

Öz

Endüstriyel tesislerde birçok uygulama sonucunda ve kamu binalarında mekanik sistemlerde atık ısı meydana gelir ve bu atık ısının atmosfere atılmadan önce işletmede farklı faydalı amaçlar için kullanılması ile önemli miktarlarda enerji ve para tasarrufu sağlanabilir. Bu çalışmada kamu binasının ısıtma sisteminde kullanılan sıcak su kazanının enerji verimliliği incelemesi yapılmıştır. Verim arttırıcı uygulamalar kapsamında atık ısıdan faydalanarak hangi oranlarda tasarruf sağlanacağı belirlenmiştir. Yüksek sıcaklıkta baca gazlarını bir ısı eşanjöründe kullanılıp atık ısı değerlendirilerek, kazanda kullanılan yakma havasının veya besleme suyunun ısıtılması sağlanabilir. İncelenen sıcak su kazanı sisteminin bacası ısı geri kazanımı yapılacak şekilde, ekonomizerli olarak önerilmektedir. Geri kazanılan enerjinin karşılığı kadar yakıt kullanılmayarak tasarruf sağlanmaktadır. Kazanda yapılan iyileştirmeler sonucunda yakıt tasarrufu 138 Nm^3/h, kazan verimi artışı %3,87 olarak belirlenmiştir. Maliyet analizi geri ödeme süresi yöntemi kullanılarak hesaplanmıştır. Ekonomizerli sistemde yıllık $29.049,0/yıl parasal tasarruf hesaplanmıştır. Eğer incelenen kamu binasında ekonomizerli kazan kullanılırsa, iyileştirmelerin geri ödeme süresi 0,13 yıl olacaktır.

Energy Efficiency Analysis of Waste Heat Recovery Applied to a Hot Water Boiler in a Public Building

Article Info

Article Info:

Received:
January 31, 2024

Accepted:
June 28, 2024

Keywords:

Energy efficiency in boilers;

Energy saving;

Waste heat recovery

Abstract

As a result of many applications in industrial plants and mechanical systems in public buildings, waste heat is generated, and significant amounts of energy and money can be saved by using this waste heat for different useful purposes in the enterprise before it is discharged into the atmosphere. In this study, the energy efficiency of the hot water boiler used in the heating system of the public building has been investigated. Within the scope of efficiency-enhancing applications, it has been determined at which rates savings will be achieved by utilising waste heat. The exhaust gases leaving the boiler at high temperature can be used in a heat exchanger and the waste heat can be utilised to heat the combustion air or feed water used in the boiler. The chimney of the hot water boiler system examined is proposed as economiser for heat recovery. Savings are achieved by not using fuel equivalent to the recovered energy. As a result of the improvements made in the boiler, fuel saving was determined as 138 Nm^3/h and boiler efficiency increase as 3.87%. The cost analysis was calculated using the payback period method. Annual monetary savings of $29,049.0/year were calculated in the economiser system. If economiser boiler is used in the public building, the payback period of the improvements will be 0.13 years.

*Sorumlu Yazar: hacera@trakya.edu.tr

1. Giriş

Enerji verimliliği, enerji kaynaklarının üretimden, iletim-dağıtım ve tüketime kadar tüm aşamalarda en yüksek etkinlikte değerlendirilmesidir. Enerji verimliliği, binalarda yaşam standardı ve hizmet kalitesinin, endüstriyel işletmelerde ise üretim kalitesi ve miktarının düşüşüne yol açmadan birim hizmet veya ürün miktarı başına enerji tüketiminin azaltılmasıdır. Temel hedef, birim milli gelir başına tüketilen enerjiyi azaltmaktır. Enerji tasarrufu, enerji atıklarının değerlendirilmesi, enerji verimliliğinin artırılması ve mevcut enerji kayıplarının önlenmesi yoluyla tüketilen enerji miktarının ekonomik kalkınmayı ve sosyal refahı engellemeden, kalite ve performansı düşürmeden en aza indirilmesi olarak tanımlanmaktadır (T.C. Enerji ve tabii Kaynaklar Bakanlığı Enerji Verimliliği ve Çevre Dairesi Başkanlığına, 2021).

Enerji, hayatımızın her alanında ihtiyaç duyduğumuz bir kaynaktır. Enerji üretimi ve ısıtma için yaygın olarak kullanılan cihazlardan biri de kazanlardır. Kazanlar, yakıtın yanmasıyla oluşan ısı enerjisini suya veya başka bir akışkana aktararak buhar veya sıcak su üretirler. Bu buhar veya sıcak su, daha sonra ısıtma, soğutma, elektrik üretimi veya endüstriyel süreçler gibi farklı amaçlar için kullanılabilir.

Kazanların enerji verimliliği, işletme maliyetlerini azaltmak, enerji tasarrufunu sağlamak ve çevreyi korumak için önemlidir. Enerji verimliliği ve tasarrufu sağlamak için birçok farklı yöntem mevcuttur ve son teknolojilerin kullanımı ile kazanların daha verimli çalışması mümkündür.

Kazanların enerji verimliliğini artırmak için dikkat edilmesi gereken bazı faktörler şunlardır:

• İyi izolasyon: Kazanların çevresinde iyi bir şekilde izole edilmesi, ısı kaybını önler ve enerji tasarrufu sağlamaktadır. Isı kaybı kazanın verimini düşürmekte ve daha fazla yakıt tüketimine neden olmaktadır. Bu nedenle, kazanların izolasyon malzemesi, kalınlığı ve durumu önemli olmaktadır.

• Düzenli bakım: Kazanların düzenli olarak yapılan bakım işleri, kazanın verimli çalışmasını sağlamaktadır. Bakım işlerini, kazanın temizliği, ayarı, kontrolü ve onarımı gibi işlemleri içermektedir. Bakımsız kazanlar, performans kaybına, arızalara, emisyon artışına ve güvenlik risklerine yol açabilmektedir.

• Geri kazanım sistemleri: Kazandan çıkan atık sıcak baca gazının veya buharının başka bir süreçte tekrar kullanılmasına olanak sağlamaktadır. Bu şekilde, kazanın verimliliği artar ve enerji tasarrufu sağlamaktadır. Örneğin, atık ısı geri kazanım sistemi, baca gazından ısıyı geri kazanarak giriş suyunu ısıtmaktadır. Buhar geri kazanım sistemi ise, buharı yoğuşturarak ısıyı geri kazanıp kazana geri göndermektedir. Ekonomizer gaz çıkış sıcaklığı, fuel oil yakıtlı kazanlarda 180ºC, motorin yakıtlı kazanlarda 150ºC, doğal gaz ve LPG yakıtlı kazanlarda 110ºC'ye kadar düşürülebilir. Her 20 °C baca gazı sıcaklık düşümü, verimde %1 artışa neden olmaktadır (Enerji Yöneticisi Eğitimi Ders Notları, 2021).

• Yüksek verimli kazanlar: Daha az enerji tüketen kazanlardır. Yakıtın yanmasıyla oluşan ısı enerjisinin daha iyi değerlendirip ve daha az atık ısı üretmektedir. Yüksek verimli kazanlar, geleneksel kazanlara göre daha maliyetli olabilir, ancak uzun vadede enerji tasarrufu sağlayarak yatırım maliyetini karşılamaktadır.

Dünyanın farklı ülkeleri enerji verimliliği önlemlerinin eksikliği sorununu ele almış ve enerji yönetimi alanında çeşitli araştırmalar yürütmüştür (Cagno vd., 2013; Lozano vd., 2018). Örneğin, Çin (Zang vd., 2015), Amerika Birleşik Devletleri (Worrell vd., 2000), Etiyopya (Tesema ve Worrell, 2015), Tayland (Hasanbeigi vd., 2011) ve Türkiye'den (Ates ve Durakbasa, 2012) yapılan önceki çalışmalar, çimento

endüstrisindeki enerji verimliliği potansiyelini farklı bir perspektiften araştırmıştır. Hasan ve ark. Bangladeş endüstrisinde enerji verimliliği olasılığı üzerine önceki iki araştırmayı (Hasan vd., 2019; Hasan vd., 2019; Hossain vd., 2020) araştırdı. Andersson ve Thollander (2019), İsveç kağıt hamuru ve kağıt endüstrisinde enerjiyle ilgili temel performans göstergelerinin mevcut uygulama ve operasyonelleştirme düzeyini incelenmiştir. Backlund ve ark. (2012), yönetim faaliyetlerinden kaynaklanan enerji verimliliği potansiyelinin, enerji yoğun endüstriler için daha fazla enerji verimli teknolojinin uygulanmasından kaynaklanan potansiyelden daha büyük olduğunu tahmin etmiştir. Tollander ve Ottosson, endüstrilerdeki gerçek enerji yönetimi uygulamalarına ilişkin araştırmaların az olduğunu ileri sürmektedir (Yang vd., 2023). Daha önceki çalışmalar tarafından desteklenen bir argüman (Thollander ve Ottosson, 2010; Yin, 2009), aynı zamanda hem teorik katkılar hem de pratik vaka çalışmaları ile ilgili daha fazla araştırma yapılmasını talep etmektedir. Schulz ve Stehfest (1984) bölgesel enerji tedariği iş birliği yoluyla emisyonları azaltma olasılığını erkenden tespit etmiştir. Daha sonra, farklı şirketler arasında enerji konularıyla ilgili bölgesel iş birliğinin hem finansal hem de çevresel açıdan faydalı olduğu ve CO_2 emisyonlarını azaltmada geniş bir potansiyele sahip olduğu ortaya çıkmıştır (Klugman vd., 2009). Bölgesel ısı piyasası iş birliğine ilişkin daha ileri çalışmalar, toplam enerji tasarrufu olanaklarını göstermektedir (Karlsson vd., 2009; Thollander vd., 2007). Son yıllarda ilgi çeken çözümlerden biri de kojenerasyon sistemleridir (Marshman vd., 2010). Rudberg ve ark. (2013), enerji yoğun proses endüstrilerinde enerji yönetimini stratejik gündeme koymak için gerekli önkoşulları araştırmıştır. Binaların en az enerji ile ısıtılmasının termodinamik birinci ve ikinci yasalarına göre değerlendirilmesi üzerine çalışılmıştır (Can, 2011).

Yang, Lin, Pan, Geng, Chen, Liu (2023), hidrojenle zenginleştirilmiş doğal gazın kullanımının yoğuşmalı kazanların enerji tasarrufu ve termal performansı üzerindeki etkilerini değerlendirmiştir. Hidrojenle zenginleştirilmiş doğal gazın yanması, baca gazındaki su içeriğini artırarak yoğuşmalı kazanların ek gizli ısıyı geri kazanmasını sağlamaktadır. 2,8 MW'lık sabit bir ısı yükünde gerçekleştirilen değerlendirmeler, H_2 zenginleştirmesinin alevin radyasyon yoğunluğunu artırdığını ve kazan verimliliğini artırarak ısı geri kazanımını sağladığını göstermektedir. H_2 fraksiyonu %0'dan %100'e çıktıkça, CO_2 emisyon yoğunluğu önemli ölçüde azalmaktadır. Çalışma, hidrojenle zenginleştirilmiş doğal gaz yoğuşmalı kazanların potansiyel uygulama alanlarını ve karbon azaltma etkilerini inceleyerek, teorik bir referans sunmaktadır (Yang vd., 2023). Chen, Ye, Shen, Wang, Deng, Yang (2021), Hunan eyaletini örnek alarak özel olarak uyarlanmış enerji verimliliği standartlarının yerel endüstriyel sistemler için kritik önem taşıdığını vurgulamıştır. Eyaletin önde gelen endüstriyel yapısına dayanarak, etkin enerji ve ekserji analiz yöntemleri kullanılarak endüstriyel kazanların verimliliği incelenmiştir. Referans standartları, analitik hiyerarşi süreci ve belirsizlik analizi sonuçlarına dayanarak bölgesel endüstriyel kazan enerji verimliliği için önerilerde bulunulmuştur. Analiz, egzoz gazı sıcaklığı, yakıt uçucu maddesi, hava katsayısı, kazan kapasitesi, soğuk hava sıcaklık, cüruf karbon içeriği ve cüruf sıcaklığı gibi endüstriyel kazan sistemini etkileyen ana faktörleri belirlemiştir. Bu 4 faktörün anlaşılması, endüstriyel kazan sistemlerinde daha fazla enerji tasarrufunu mümkün kılacak yenileme projelerinin tasarımı için teorik bir temel sağlamaktadır. Hunan'ın enerji verimliliği standartları, karşılaştırmalı çalışmalar sonucunda önerilmiştir (Chen vd., 2021). Wang, Zou, Lu, Li, Hu, ve Wang (2024) tarafından yapılan araştırmaya göre, düşük yük altında kazanın yanma kararlılığının bozulduğu ve karbon yanma katsayısının düştüğü belirlenmiştir. Bu durum, kazanın termal verimliliğini olumsuz yönde etkilemektedir. Kazanın enerji verimliliği seviyelerini anlık olarak izlemek için

çevrimiçi izleme yöntemleri kullanılabileceği belirtilmiş, ancak karbon yanma katsayısının çevrimiçi izlenmesinin zorlu bir meydan okuma olduğu vurgulanmıştır. Araştırmada, fazla hava katsayısı ile karbon yanma katsayısı arasında bir teorik model geliştirilmiş ve çevrimiçi izleme sonuçları, daha düşük karbon yanma katsayısının kazan enerji verimliliğini artırabileceğini göstermiştir. Ancak, kısmi yük altında kazanlarda gerçek hava akışındaki eksikliklerin bu çalışma modunu etkileyebileceği belirtilmiştir. Ayrıca, karbon tükenmişlik katsayısının birim yük arttıkça yükseldiği, birim yük düştükçe azaldığı tespit edilmiştir. Düşük yük altında kazanın yanma kararlılığı ve veriminin önemli ölçüde azaldığına dikkat çekilmiş ve çevrimiçi izleme yöntemlerinin, bu koşullarda kazan enerji verimliliğini iyileştirmek için temel bir araç sağlayabileceği ifade edilmiştir (Wang vd., 2024). Satyavada ve Baldi'nin (2018) çalışmasına göre, yoğuşmalı kazanlar, baca gazlarından gelen ısının kazan girişindeki soğuk suyu ön ısıtarak çalışmaktadır, bu da enerji verimliliğini geleneksel kazanlara göre %10-12 artırmaktadır (Satyavada ve Baldi, 2018).

Bu çalışmada, kamu binasının ısıtma sisteminde kullanılan kazanın verimlilik açısından incelenmiştir. Ölçme, analiz etme ve değerlendirme aşamalarından sonra sistem iyileştirmeleri, verimlilik arttırıcı yöntemler önerilmiştir. Isıtma sisteminde kullanılan kazanın atık ısıdan faydalanarak hangi oranlarda tasarruf sağlanacağı incelenmiştir. Yüksek sıcaklıktaki baca gazları kullanılıp atık ısı değerlendirilerek, enerji, yakıt tasarrufu ve ekonomik kazanç sağlanmaktadır.

Hedefler:

-Mevcut kazan sisteminin performansının belirlenmesi,

- Mevcut sistemde yapılabilecek iyileştirmelerin tespit edilip uygulanabilirliğinin ortaya konulması,

- Atık enerjiyi faydalı enerjiye dönüştürerek, enerji, yakıt tasarrufu ve ekonomik kazanç sağlanmasıdır.

2. Materyal ve Yöntem

2.1. Deney Tesisatı

2.1.1. Sistem Özellikleri

Proje kapsamında incelenen sıcak su kazanı, gaz yakıtlıdır. Kazan 2011 yılında üretilmiştir. Kazanda yakıt olarak doğalgaz kullanılmaktadır. Maksimum çalışma basıncı 3 bar, maksimum çalışma sıcaklığı 100ºC, hidrostatik basıncı 4 bar'dır. Kazan dış yüzey izolasyonu 100'lük rapis telli taş yünü üzeri 0,60 gofrajlı alüminyum sac ile kaplanmıştır. Sıcak su kazanı teknik özellikleri **Tablo 1**'de verilmiştir.

Kazan dairesinde 3 sıcak su kazanı yer almaktadır, ancak 1 tanesi aktif olarak çalıştırılmaktadır. **Şekil 1**'de incelenen sıcak su kazanın bulunduğu kazan dairesi görüntüsü yer almaktadır. İncelenen sıcak su kazanı şekilde en sağdaki kazandır. Mevcut sıcak su kazanı sisteminde ekonomizer ısı geri kazanımı sistemi kullanılmamaktadır. **Şekil 2**'de kazan çıkış kanalı ve kazanın dağıtım kanalları, **Şekil 3**'te kazanının kumanda panosu ve doğalgaz sayacı görülmektedir.

Tablo 1. İncelenen kazanın teknik özellikleri

Özellik	Değer
Kazan cinsi	Gaz/Sıvı yakıtlı sıcak su kazanı
Kazan tipi	TR P 814
Üretim tarihi	2011
Kapasite	814
Maksimum çalışma basıncı	3 bar
Maksimum çalışma sıcaklığı	100 ºC
Su hacmi	1040 lt
Hidrostatik test basıncı	4 bar

Şekil 1. İncelenen sıcak su kazanın bulunduğu kazan dairesi görüntüsü (En sağdaki incelenen kazan)

Şekil 2. İncelenen kazanının sıcak su dağıtım kanalları

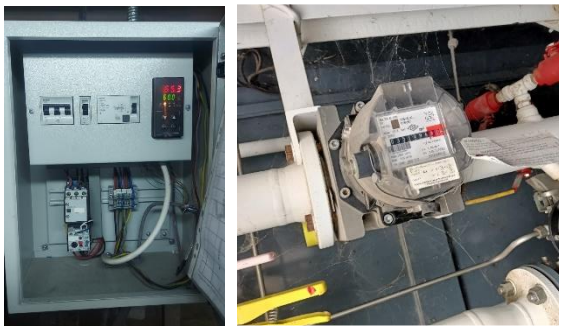

Şekil 3. Sıcak su kazanının kumanda panosu ve doğalgaz sayacı

2.1.2. Ölçüm Cihazları

Çalışmada, akredite olmuş ulusal kuruluşlar tarafından kalibrasyonu yapılmış ve etiketlenmiş ölçüm cihazları kullanılmıştır. Çalışma süresince termal kamera, baca gazı emisyon ve sıcaklık ölçüm cihazı, sistem üzerine sabit montajlı basınç, debi ve sıcaklık ölçerlerden faydalanılmıştır.

Şekil 4'te görülen termal kamera kazan yüzey sıcaklıklarını belirlemek için kullanılmıştır. Enerji israflarını, yapısal kusurları tespit edebilmekte ve AR-GE ürün kalitesi için kolaylıkla, hızlı ve güvenilir sonuçlar elde edebilmektedir. (-20 +1200 C) yüksek çalışma sıcaklık aralığı ve 0.045° hassasiyet ile rahatlıkla kullanabilmektedir. 8X zoom özelliği, Led ışık, Lazer işaretleyici ve değiştirilebilir lensler sayesinde problemli alanı görebilir, işaretleme yapabilir ve aynı anda 5 farklı noktayı görüntüleye bilir ve sıcaklık değerlerini incelenebilmektedir. Ayrıca minimum, maksimum ve ortalama değer alınabilmektedir.

Şekil 5'te görülen baca gazı ölçüm cihazı, Oksijen(O_2), Karbonmonoksit (CO), Azotoksit (NO), Sülfür (SO_2) veya Azotdioksit (NO_2), Hidrokarbon (CxHy), Hidrojen (H_2) ve Hidrojen sülfür (H_2S), Amonyak (NH_3) ve Hidroklorikasit (HCı) ölçümü yapmaktadır. Baca gazı ölçüm cihazı, 2.60 L/dk pompa çekiş gücüne sahiptir.

Şekil 4. Ölçümlerde kullanılan termal kamera

Şekil 5. Ölçümlerde kullanılan baca gazı ölçüm cihazı

2.2. Yapılan Ölçümler ve Alınan Değerler

Sıcak su kazanı sisteminde doğalgaz tüketimi ve basıncı, baca gazı çıkış sıcaklığı ve emisyon değerleri, kazan yüzey sıcaklıkları ve ortam koşulları değerleri ölçülen başlıca parametrelerdir. **Tablo 2**'de kazan sisteminde yapılan ölçümler ve alınan değerler yer almaktadır. Mevcut sistemde ekonomizer bulunmamaktadır, tablodaki "Eko dahil" verileri tasarım değerleridir.

Ölçülen veriler değerlendirildiğinde, kazanda baca gazı sıcaklıkları 120-150 °C aralığında bulunması normal kabul edilmektedir. O_2, CO_2 ve CO değerleri kabul edilebilir düzeydedir.

Şekil 6'da kazan ön yüzey sıcaklık dağılımı, Şekil 7'de kazan sağ yüzey ve Şekil 8'de sol yüzey sıcaklık dağılımı yer almaktadır. Termal görüntülerde kazan dış yüzey malzemesi emisivite değeri 0,79 'dır.

Tablo 2. Kazan sisteminde yapılan ölçümler ve alınan değerler

Tarih		03.01.2024			
Ekonomizer Durumu		**Eko Hariç**		**Eko Dahil**	
Yanma Havası Damper Açıklığı		**100%**		**100%**	
Data Toplama Zamanı		0	15 dakika	0	15 dakika
Doğalgaz Değeri	m^3	3.510.000,9	3.510.094,9	3.510.094.9	3.510.157,6
Doğal Gaz Basıncı	mbar	280.0	280.0	280.0	280.0
Doğal Gaz Sıcaklığı	°C	26.0	26.0	26.0	26.0
Doğal Gaz Sayaç Değeri	Nm^3	3.861.001,0	3.861.104,4	3.861.104,4	3.861.173,3
Çıkış Basıncı	bar	1,70	1,70	1,70	1,70
Su Sayaç Değeri	kg	65	65	65	65
Baca gazı Sıcaklığı					
Ekonomizer Öncesi	°C	172,60	186,90	172,60	186,90
Ekonomizer Sonrası	°C	172,60	186,90	100,21	108,28
Baca gazında O_2 Oranı	%	4,10	4,10	4,10	4,10
CO Oranı	ppm				
Ortam Sıcaklığı	°C	23,1	23,1	23,1	23,1
Bağıl Nem Miktarı	%	55,0	55,0	55,0	55,0
Besi Suyu İletkenliği	ppm	150,0	150,0	150,0	150,0
	mS/cm	234,0	234,0	234,0	234,0
İletkenlik Ölçülen Sıcaklıklar	°C	21,0	21,0	21,0	21,0
Kazan Yüzey Sıcaklıkları					
Ön Yüzey	°C	40,00	41,10	40,00	41.10
Arka Yüzey	°C	28,00	28,00	29,00	29.00
Sol Yan Yüzey	ºC	27,40	27,50	27,00	27,00
Sağ Yan Yüzey	ºC	30,00	30,10	30,00	30,00

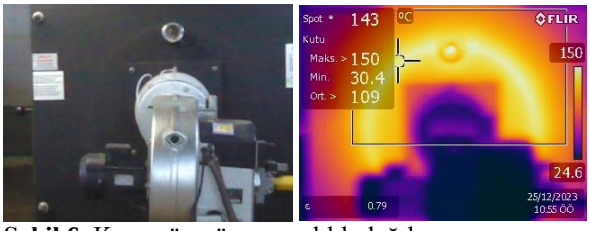

Şekil 6. Kazan ön yüzey sıcaklık dağılımı

Şekil 7. Kazan sağ yüzey sıcaklık dağılımı

Şekil 8. Kazan sol yüzey sıcaklık dağılımı

2.3. Analiz ve Hesaplamalar

Kazanlarda verimlilik hesaplaması doğrudan yöntem ve ısı kaybıyla dolaylı yöntem olarak iki yol ile hesaplanabilmektedir (Enerji Yöneticisi Eğitimi Ders Notları, 2021). Bu çalışmada kayıpların hesaplanması

yöntemi kullanılarak, kazan verimi hesaplanmıştır. Kayıpları belirleyip azaltarak, verimi artırmak hedeflendiği için kayıp yöntemi seçilmiştir. Tüm kayıpları toplayıp aşağıdaki denklemini kullanarak verimlilik hesabı yapılmıştır.

$$Kazan\ verimi\ (\%\eta) = 100 - L_{Toplam} \quad (1)$$

L_{Toplam} ısı kayıpları toplamıdır ve aşağıdaki denklem ile hesaplanmaktadır.

$$L_{Toplam} = L_{KBG} + L_{NBG} + L_{COBG} + L_{RK} + L_B \quad (2)$$

Tablo 3. Kazandan kaynaklanan başlıca ısı kayıpları (Enerji Yöneticisi Eğitimi Ders Notları, 2021)

Isı Kaybı	**Denklem**
1. Kuru Baca Gazı Yoluyla Olan Isı Kaybı **(L KBG)**	$L_{KBG} = \frac{K\ x\ (T_{BG} - T_0)}{CO_2}\ x\ \frac{Yakıt\ üst\ ısıl\ değeri}{Yakıt\ alt\ ısıl\ değeri}$ (3) $K = \frac{69{,}7\ x\ C_{yakıt}\ x\ (Yakıtın\ alt\ ısıl\ değeri)^2}{(Yakıtın\ üst\ ısıl\ değeri)^3}$ (4) $CO_2 = \left\{1 - \left[\frac{O_2}{21}\right]\right\} x\ (CO_2)_{max}$ (5) $(CO_2)_{max} =$ %11,74 (6)
2. Baca Gazındaki Nem Nedeniyle Olan Isı Kaybı **(LNBG)**	$L_{NBG} = \frac{(9 x H_{yakıt}) x (50 - T_0 + (0{,}5\ x\ T_{BG}))}{Yakıt\ üst\ ısıl\ değeri}\ x\ \frac{Yakıt\ üst\ ısıl\ değeri}{Yakıt\ alt\ ısıl\ değeri}$ (7)
3. Baca gazındaki Yanmamış Karbonmonoksit Nedeniyle Olan Isı Kaybı **(L COBG)**	$L_{COBG} = \frac{K\ x\ CO_{BG}}{CO_2 + CO_{BG}}\ x\ \frac{Yakıt\ üst\ ısıl\ değeri}{Yakıt\ alt\ ısıl\ değeri}$ (8) $Doğal\ Gaz\ için\ K\ değeri = 32$ (9)
4. Blöf Nedeniyle Olan Isı Kaybı **(L B)**	$L_B = \frac{(T_B - T_{H2O})\ x\ BM\ x\ (100 - L)}{((T_B - T_{H2O})\ xBM) + ((100 - BM) x\ (660 - T_{H2O}))}\ x\ \frac{Yakıt\ üst\ ısıl\ değeri}{Yakıt\ alt\ ısıl\ değeri}$ (10) Denklemde T_B blöf suyu sıcaklığı, T_{H2O} besi suyu sıcaklığı ve BM blöf miktarıdır. $BM = \frac{Besi\ suyu\ iletkenliği}{KAzan\ suyu\ iletkenliği}\ x\ 100$ (11)
5. Kazan Yüzeyinden Radyasyon ve Konveksiyonla Olan Isı Kaybı **(L RK)**	$L_{RK'} = (U_r + U_C)\ x\ A\ x\ (T_y - T_0)$ (12) $U_r = \frac{E\ x\ 5{,}67}{(T_y - T_0)} x [(\frac{T_y}{100})^4 - (\frac{T_0}{100})^4]$ (13) Denklemde E yüzey malzemesine ve işleme şekline bağlı Emissivite katsayısı, T_y yüzey sıcaklığı ve T_0 ortam sıcaklığıdır. $U_c = B\ x\ (T_y - T_0)^{0{,}25}$ (14) B değeri, yukarıya bakan yatay yüzeyler için 1,7 , dikey yüzeyler ve geniş silindirler için 1,45 ve yatay silindirler için 1,2 alınmaktadır. $L_{RK} = \frac{L_{RK'}}{Yakut\ tarafından\ verilen\ ısı}$ (15)
Toplam (L_{Toplam})	$L_{Toplam} = L_{KBG} + L_{NBG} + L_{COBG} + L_{RK} + L_B$ (2)

Tablo 3'teki denklemler ve ölçülen değerler kullanılarak, ekonomizerli ve ekonomizersiz durum için kazanda oluşan ısı kayıpları hesaplanmıştır. Isı kayıplarıyla dolaylı yöntem kullanılarak her bir durum için verim belirlenmiştir. **Tablo 4**'te ekonomizerli ve ekonomizersiz durum için sıcak su kazanı sistemi kayıpları ve kazan verimi değerleri görülmektedir. Kazanda yapılan iyileştirmeler sonucunda kazan verimi artışı %3,87 olarak belirlenmiştir. **Şekil 9 ve Şekil 10'**da ekonomizerli ve ekonomizersiz durum için sıcak su kazanı sistemi kayıpları yüzdelik olarak verilmektedir. Baca gazı analizinde ölçülen O_2 değerleri dikkate alınarak fazla hava oranı şu formül kullanılarak hesaplanabilmektedir.

$$Fazla\ Hava\ Oranı\ (\%) = \frac{O_2}{21-O_2} * 100 \qquad (16)$$

Tablo 4. Ekonomizerli ve ekonomizersiz durum için sıcak su kazanı sistemi ısı kayıpları (IK) ve kazan verimi

	Ekonomizersiz	Ekonomizerli
Kuru Baca Gazından IK (%)	5,98	3,11
Nem Nedeniyle IK (%)	2,19	1,48
CO Kaybı (%)	0,01	0,01
Kazan Yüzeyinden IK (%)	0,08	0,12
Blöf Nedeniyle IK (%)	1,23	1,26
Toplam Kayıp (%)	9,48	5,97
Kazan Verimi (%)	90,52	94,03
Fazla hava (%)	24,26	24,26

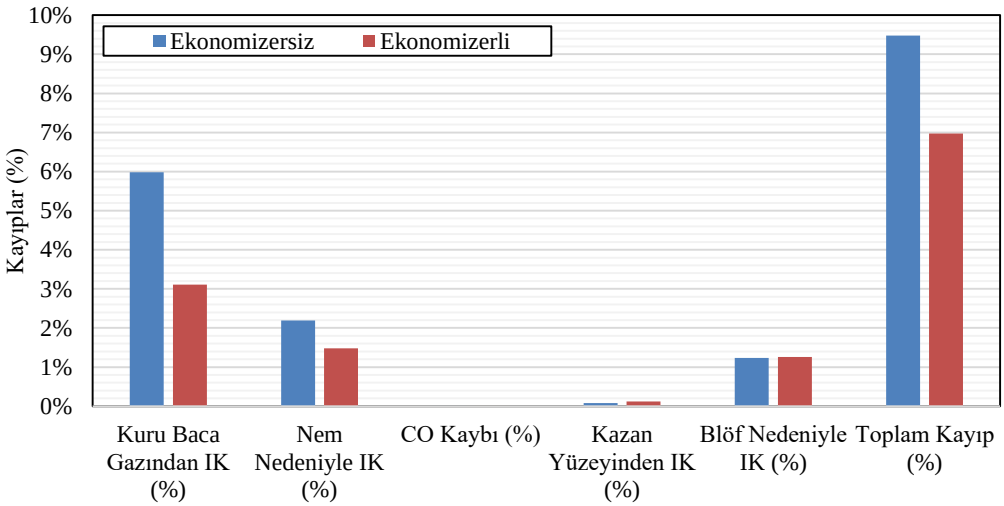

Şekil 9. Ekonomizerli ve ekonomizersiz durum için sıcak su kazanı sistemi kayıpları

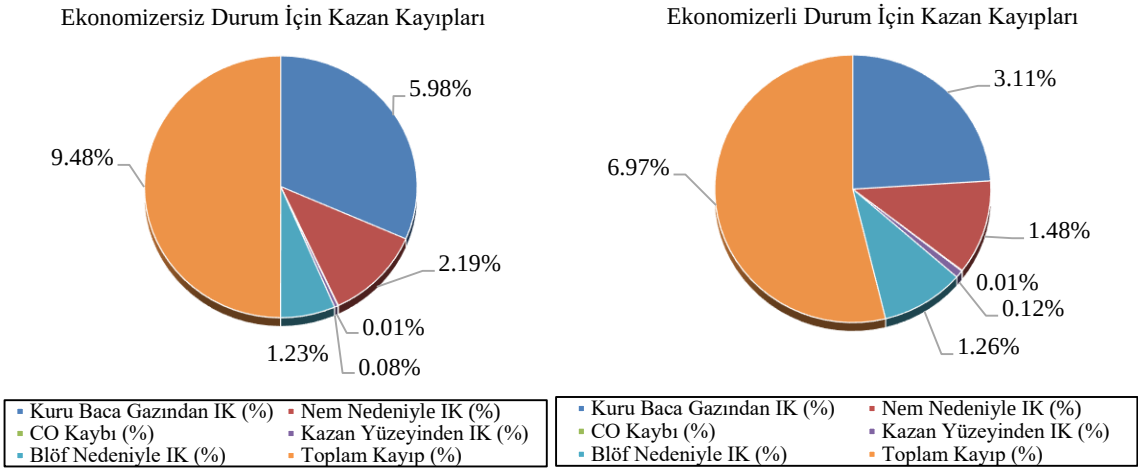

Şekil 10. Kazan ünitesi ekonomizerli ve ekonomizersiz durum için enerji kayıpları

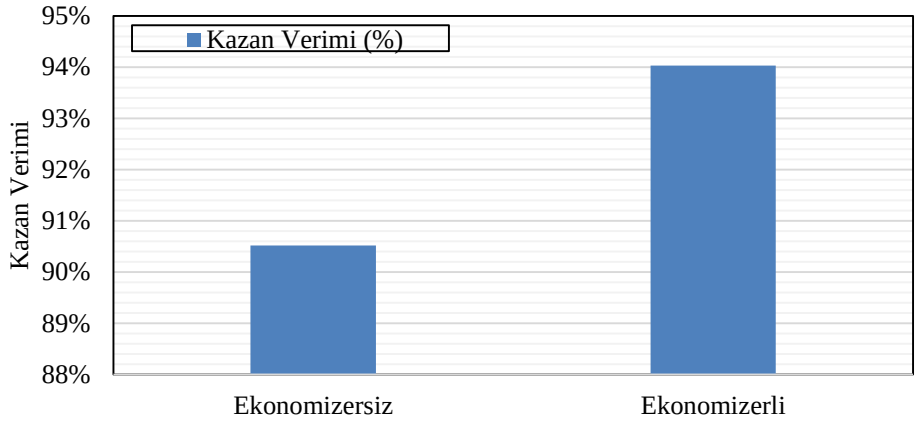

Şekil 11. Ekonomizerli ve ekonomizersiz durum sıcak su kazanı verimleri

3. Ekonomik Analiz

İncelenen sıcak su kazanı sistemi bacasında ısı geri kazanımı (ekonomizer-reküperatör) kullanıldığında sağlanacak tasarruf hesaplanmıştır. Reküperatörde iç içe geçmiş iki boru vasıtasıyla baca gazındaki ısı, yanma havasına transfer edilir ve ısı geri kazanımı ile verim artırılır. **Tablo 5**'te kazan ünitesi tasarrufu ve ekonomik analiz sonuçları yer almaktadır. Kazanda yapılan iyileştirmeler sonucunda yakıt tasarrufu 138 Nm^3/h olarak belirlenmiştir. Maliyet analizi geri ödeme süresi yöntemi kullanılarak hesaplanmıştır. Ekonomizerli sistemde yıllık **$**29.049 /yıl parasal tasarruf hesaplanmıştır. Eğer endüstriyel tesis ekonomizerli kazan kullanılırsa, geri ödeme süresi 0,13 yıl olacaktır.

Tablo 5. Kazan ünitesi tasarrufu ve ekonomik analiz sonuçları

Parametre	**Değer**
Yakıt tasarrufu (Nm^3/h)	138
Doğalgaz fiyatı (**$**/$Nm^3$)	0,16
Yıllık çalışma süresi (h)	1320
Tasarruf (**($**/Yıl)	29.049,0
Ekonomizer fiyatı + İşçilik (**($**)	3.821,0

3.1. Yakıt Ekonomisi

Tablo 6 ve **Şekil 12**'de 1 ton sıcak su üretimi için yakıt maliyetleri yer almaktadır. Yakıt maliyetini hesaplamada kullanılan denklemler aşağıda verilmiştir.

$$\text{Üretilecek Enerji} = \text{Yakıt Tüketimi x Alt Isıl Değer x Verim} \quad (17)$$

$$\text{Yakıt Tüketimi} = \frac{\text{Üretilecek Enerji Miktarı}}{\text{Alt Isıl Değer x Verim}} \quad (18)$$

$$\text{Toplam Maliyet} = \text{Yakıt Maliyeti} + \text{İşçilik Maliyeti} \quad (19)$$

Tablo 6. 1 ton sıcak su üretimi için yakıt maliyetleri.

Yakıt Türü	**Yakıt Miktarı**	**Yakıt Maliyeti ($)**
Fuel Oil No:6	73,5 (kg)	61,61
LNG	80,8 (m^3)	48,71
Doğalgaz	80,8 (m^3)	15,24
0-10mm toz Kömür	235,29 (kg)	62,73

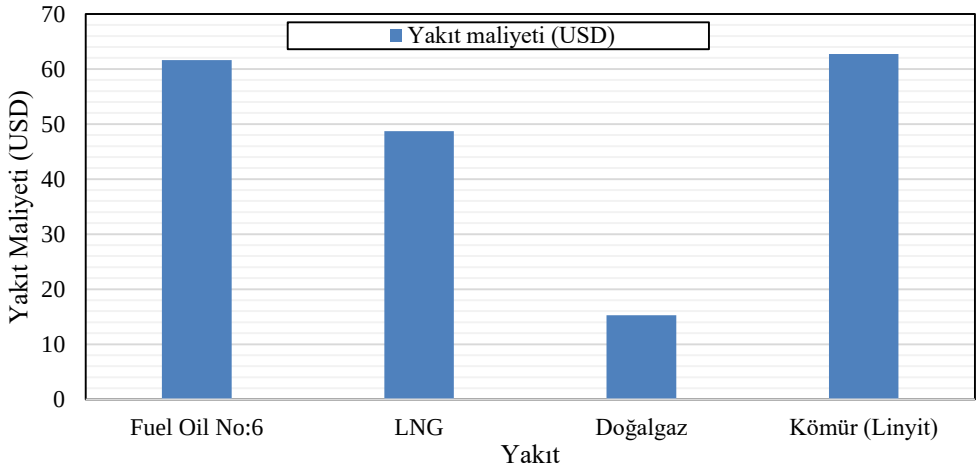

Şekil 12. 1 ton sıcak su için yakıt maliyetleri

3.2. Bulgular ve Tartışma

İncelenen sıcak sıcak su kazanı sistemi bacası ısı geri kazanımı yapacak şekilde, ekonomizerli (reküperatörlü) olarak önerilmektedir. Reküperatörde iç içe geçmiş iki boru vasıtasıyla baca gazındaki ısı, yanma havasına transfer edilir ve ısı geri kazanımı ile verim artırılır. İç içe geçmiş iki boru aracılığı ile sıcak baca gazından enerjiyi yanma havasına transfer edilmektedir. İçteki borudan sıcak baca gazı, dıştaki borudan yanma havası ters istikamette gönderilmektedir. Yanma havası baca gazından geri kazanılan ısı enerjisi kazan beslene sıcak suyuna transfer edilmektedir. Geri kazanılan enerjinin karşılığı kadar yakıt kullanılmayarak tasarruf sağlanmaktadır. Kazanda yapılan iyileştirmeler sonucunda yakıt tasarrufu 138 Nm^3/h, kazan verimi artışı %3,87 olarak belirlenmiştir. Maliyet analizi geri ödeme süresi yöntemi kullanılarak hesaplanmıştır. Ekonomizerli sistemde yıllık $29.049,0/yıl parasal tasarruf hesaplanmıştır. Eğer endüstriyel tesis ekonomizerli kazan kullanılırsa, geri ödeme süresi 0,13 yıl olacaktır.

Teşekkür

Bu çalışma, Trakya Üniversitesi Bilimsel Araştırma Projeleri Birimi (TÜBAP) tarafından Öğrenci Bilimsel Araştırma Desteği ile finanse edilmiştir (Proje No: TÜBAP-2023/175).

Çıkar Çatışması Beyanı

Çıkar çatışması bulunmamaktadır.

Kaynaklar

Andersson, E., Thollander, P. (2019). Key performance indicators for energy management in the Swedish pulp and paper industry, Energy Strategy Reviews, 24, 229-235.

Ates, S.A., Durakbasa, N.M. (2012). Evaluation of corporate energy management practices of energy intensive industries in Turkey. Energy, 45, 81-91.

Backlund, S., Broberg, S., Ottosson, M., Thollander, P. (2012). Energy efficiency potentials and energy management practices in Swedish firms (5-055-12), ECEEE Ind. Sıcak summer Study, 669–677.

Can, A. (2011). Binaların En Az Enerji İle Isıtılmasının veya Soğutulmasının Termodinamik Birinci ve İkinci Yasalarına Göre Değerlendirilmesi. X. Ulusal Tesisat Mühendisliği Kongresi – 13/16 Nisan 2011/İzmir.

Cagno, E., Worrel,l E., Trianni, A., Pugliese, G. (2013). A novel approach for barriers to industrial energy efficiency. Renew Sıcak sustain Energy Rev., 19, 290-308.

Chen, B., Ye, X., Shen, J., Wang, S., Deng, S., & Yang, J. (2021). Investigations on the energy efficiency limits for industrial boiler operation and technical requirements—taking China's Hunan province as an example. Energy, 220, 119672.

Enerji Yöneticisi Ders Notları, T.C. Enerji ve tabii Kaynaklar Bakanlığı Enerji Verimliliği ve Çevre Dairesi Başkanlığına, 2021.

Hasanbeigi, A., Menke, C., Therdyothin, A. (2011). Technical and cost assessment of energy efficiency improvement and greenhouse gas emission reduction potentials in Thai cement industry. Energy Efficiency, 4, 93-113

Hasan, A.M., Hoq, M.T., Thollander, P. (2018). Energy management practices in Bangladesh's iron and steel industries. Energy strategy reviews, 22, 230-236.

Hasan, A., Rokonuzzaman, M., Tuhin, R.A., Salimullah, S.M., Ullah, M., Sakib, T.H. (2019). Drivers and barriers to industrial energy efficiency in textile industries of Bangladesh. Energies, 12, 1775.

Hossain, S.R., Istiak, A., Ferdous, S., Azad, A.S.M., Monjurul, H. (2020). Empirical investigation of energy management practices in cement industries of Bangladesh, Energy, 212, 118741.

IEA - International Energy Agency. (2018). Energy Efficiency 2018: Analysis and Outlooks to 2040. in: Market Report Series. IEA/OECD. Ingarao, G., 2017.

Karlsson, M., Gebremedhin, A., Klugman, S., Henning, D., Moshfegh, B. (2009). Regional energy system optimization – potential for a regional heat market. Appl Energy, 86(4):441–451.

Klugman. S., Karlsson, M., Moshfegh, B. (2009). A Swedish integrated pulp and paper mill – energy optimisation and local heat cooperation. Energy Pol, 37(7):2514–24.

Lozano, F.J., Lozano, R., Freire, P., Jimenez-Gonzalez, C., Sakao, T., Ortiz, M.G. (2018). New perspectives for green and sıcak sustainable chemistry and engineering: approaches from sıcak sustainable resource and energy use, management, and transformation. J Clean Prod, 172, 227-232.

Marshman, D.J., Chmelyk, T., Sidhu, M.S., Dumont, G.A. (2010). Energy optimization in a pulp and paper mill cogeneration facility. Appl Energy, 87, 3514–3525.

Rudberg, M., Waldemarsson, M., Lidestam, H. (2013). Strategic perspectives on energy management: A case study in the process industry, Applied Energy, 104, 487-496.

Satyavada, H., & Baldi, S. (2018). Monitoring energy efficiency of condensing boilers via hybrid first-principle modelling and estimation. Energy, 142, 121-129.

Schulz, V., Stehfest, H. (1984). Regional energy sıcak supply optimization with multiple objectives. Eur J Operat Res. 17(3):302–12.

Tesema, G., Worrell, E. (2015). Energy efficiency improvement potentials for the cement industry in Ethiopia. Energy, 93, 2042-2052.

Thollander, P., Ottosson, M. (2010). Energy management practices in Swedish energyintensive industries. J Clean Prod., 18, 1125-1133.

Thollander, P., Danestig, M., Rohdin, P. (2007). Energy policies for increased industrial energy efficiency: evaluation of a local energy programme

for manufacturing SMEs. Energy Pol., 35(11):5774–5783.

Wang, Y., Zou, Z., Lu, K., Li, Q., Hu, P., & Wang, D. (2024). Modeling for on-line monitoring of carbon burnout coefficient in boiler under partial load. Energy, 288, 129859.

Worrell, E., Martin, N., Price, L. (2000). Potentials for energy efficiency improvement in the US cement industry. Energy, 25, 1189-1214.

Worrell, E., Bernstein, L., Roy, J., Price, L., Harnisch, J. (2009). Industrial energy efficiency and climate change mitigation. Energy Eff., 2, 109–123.

Yang, H., Lin, X., Pan, H., Geng, S., Chen, Z., & Liu, Y. (2023). Energy saving analysis and thermal performance evaluation of a hydrogen-enriched natural gas-fired condensing boiler. International Journal of Hydrogen Energy, 48(50), 19279-19296.

Yin, R.K. (2009). Case study research: design and methods. 4th ed. Thousand Oaks, CA: SAGE Inc.

Zhang, S., Worrell, E., Crijns-Graus, W. (2015). Evaluating co-benefits of energy efficiency and air pollution abatement in China’s cement industry. Appl Energy, 147, 192-213.